



This is to certify that the

thesis entitled

COLLOIDAL PROCESSING OF SiC_(w)/Si₃N₄ CERAMIC COMPOSITES BY SLIP CASTING

presented by

Zhengmao Yeh

has been accepted towards fulfillment of the requirements for

Master's degree in Materials Science

Major professor

Date February 14, 1996

O-7639

MSU is an Affirmative Action/Equal Opportunity Institution



PLACE IN RETURN BOX to remove this checkout from your record. TO AVOID FINES return on or before date due.

DATE DUE	DATE DUE	DATE DUE
AUN 1 1999	ACC 1 6 578	

MSU Is An Affirmative Action/Equal Opportunity Institution

COLLOIDAL PROCESSING OF SiC_(w)/Si₃N₄ CERAMIC COMPOSITES BY SLIP CASTING

Ву

Zhengmao Yeh

A THESIS

Submitted to
Michigan State University
in partial fulfillment of the requirements
for the degree of

MASTER OF SCIENCE

Department of Materials Science and Mechanics

1996

ABSTRACT

COLLOIDAL PROCESSING OF Si₃N₄/SiC_(w) CERAMIC COMPOSITES BY SLIP CASTING

By

Zhengmao Yeh

Si₃N₄/SiC_(w) ceramic composites show improvements in both strength and wear resistance over their monolithic constituents. These improvements, however, cannot be realized without a homogeneous mixture of the individual powders. Optimized colloidal processing can be used to control the homogeneity of composite ceramic slips, avoiding matrix- and reinforcement-rich zones in slip cast parts which act to destroy improvements in mechanical properties expected from whisker reinforced CMCs. The effects of ultrasonic dispersion and ball milling on the slip casting of Si₃N₄/SiC_(w) composites will be presented in this thesis. A method combining both ball milling and ultrasonication was found to consistently achieve the highest green and sintered densities, while providing a maximum in distribution for each component. Additions of SiC whiskers were found to not only inhibit the densification, but also the final grain size and the α - to β-Si₃N₄ transformation, especially at high whisker content. The reduction in aspect ratio of SiC whiskers can improve sinterability and the α - to β -Si₃N₄ transformation. Less than 20 $^{\rm v}/_{\rm o}$ of whisker additions result in an increase in fracture toughness. The highest fracture toughness value of 10 MPa^{1/2} was found in composites with 20 vol% whisker.

To my Mom and Hong, the girl I love

ACKNOWLEDGMENTS

This study was made possible by grants from the State of Michigan Research Excellence Funds.

I would like to express my sincere thanks to Dr. M. J. Crimp for her guidance, support and inspiration throughout the course of this research. I would like to thank Dr. M. A. Crimp for his instructive opinions on my TEM results. I wish to express my thanks to Pat Sneary for the assistance and coorporation on this project. Special thanks to my other lab colleagues and Chinese friends for their support and friendships.

TABLE OF CONTENTS

LIST OF TABLES	ix
LIST OF FIGURES	x
INTRODUCTION	1
1. LITERATURE REVIEW	3
1.1 Colloid Theories	3
1.1.1 Surface Charge of Particles	3
1.1.2 Potential Determining Ion	4
1.1.3 Electric Double Layer	6
1.1.4 Stern Layer	6
1.1.5 DLVO Theory	9
1.1.6 HHF Theory	11
1.1.7 Stability of Colloidal System	12
1.2 Deagglomeration of Ceramic Suspension	16
1.3 Silicon Nitride Matrix Ceramic Composites	17
1.3.1 General	17
1.3.2 Whisker Toughening	19
1.3.3 Processing of SiC _(w) /Si ₃ N ₄ Composites and Related Problems	21
1.4 Monolithic Si ₃ N ₄	25

	1.4.1 Crystal Structure of Si ₃ N ₄	26
	1.4.2 Thermodynamic Properties and Stability	27
	1.4.3 Processing of Si ₃ N ₄ ceramics	31
	1.4.4 Microstructural Evolution in Si ₃ N ₄	35
	1.4.5 Fracture Toughness	40
	1.4.6 Development	42
2	. EXPERIMENTAL PROCEDURE	43
	2.1 About Starting Powder	43
	2.1.1 Si ₃ N ₄ Powder	43
	2.1.2 SiC Whisker	44
	2.1.3 Y ₂ O ₃ Powder	44
	2.1.4 Al ₂ O ₃ Powder	44
	2.2 TEM Observation of SiC Whiskers	44
	2.3 ESA Measurement	44
	2.4 Particle Sizing	48
	2.5 Sedimentation Observation	50
	2.6 Slip Preparation	50
	2.6.1 Ball Milling	51
	2.6.2 Ultrasonication	51
	2.7 Viscosity Measurement	52
	2.8 Slip Casting	52
	2.8.1 Making Plaster Molds	53

	2.8.2 Casting	53
	2.9 Cold Isostatic Pressing	53
	2.10 Pressureless Sintering	54
	2.11 Density Measurement	54
	2.11.1 Green Density Measurement	54
	2.11.2 Sintered Density Measurement	54
	2.11.3 Theoretical Density Calculation	55
	2.12 Cutting and Polishing	56
	2.13 SEM	56
	2.14 X-ray Diffraction (XRD) and Phase Content (F_{α}) Calculation	56
	2.15 Microhardness and Toughness Measurement	57
3.	RESULTS AND DISCUSSIONS	58
	3.1 TEM Observation of SiC Whiskers	58
	3.2 Properties of SiC _(w) /Si ₃ N ₄ Suspension System	58
	3.2.1 Zeta Potential (ζ) and Stability Ratio (W)	58
	3.2.2 Sedimentation Density	63
	3.2.3 Effect of pH on Green Density	65
	3.2.4 Viscosity	69
	3.3 Deagglomeration of SiC _(w) /Si ₃ N ₄ System	69
	3.3.1 Effect of Ultrasonication Time	69
	3.3.2 Effect of Ball Milling	74
	3.3.3 Effects of Ultrasonication and Ball Milling on SiC _{6.3.7} /Si ₂ N ₄ System	78

	3.3.4 Effect of Whisker Loading on Green Density	78
	3.3.5 Effect of Reducing Whisker Aspect Ratio	82
	3.4 Sintering Additives	86
	3.5 Sintered Density	86
	3.6 Microstructure of the Composites	92
	3.7 Mechanical Properties of SiC _(w) /Si ₃ N ₄ composites	106
	3.8 X-ray Diffraction Analysis	112
1.	CONCLUSIONS	123
RI	EFERENCES	125

LIST OF TABLES

Table 1.1	Equilibrium Reactions in Si-C-N-O System.	30
Table 2.1	Typical Characteristics of UBE SN-E10 Powder Supplied by the Manufacturer.	43
Table 2.2	Typical Characteristics of TWS-100 SiC Whisker as Supplied by the Manufacturer.	45
Table 2.3	Typical Characteristics of AKP-50 Al ₂ O ₃ Powder as Supplied by the Manufacturer.	46

LIST OF FIGURES

Eigure		Page
1.1	Illustration of a electric double layer.	5
1.2	Schematic representation of the structure of the electric double layer according to Stern's theory.	8
1.3	Total interaction energy curves, $V(1)$ and $V(2)$, obtained by the summation of an attraction curve, V_A , with different repulsion curves, $V_R(1)$ and $V_R(2)$.	14
1.4	Silicon vapor pressure in equilibrium with silicon nitride as a function of nitrogen pressure and temperature.	29
1.5	Phase relationships in the Si-C-N-O system as a function of oxygen partial pressures and temperature at a_c =1, p_{N2} =1 atm (0.10 MPa), and p_{N2} =10 atm (1.01 Mpa).	32
3.1	Some SiC whisker are bent and have irregular surface.	59
3.2	SiC whisker with several branches.	59
3.3	<011> zone selected area diffraction pattern of the SiC whisker.	60
3.4	(a) TEM bright field image of SiC whisker.(b) Selected area diffraction pattern of SiC whisker.	61
3.5	Zeta potential plot of SiC whisker and Si ₃ N ₄ powder.	62
3.6	Stability ratio of SiC _{(w} /Si ₃ N ₄ suspension system.	64
3.7	Sedimentation density of Si ₃ N ₄ powder as a function of pH. Suspensions remained undisturbed for 4 weeks.	66
3.8	Sedimentation density of SiC whisker as a function of pH. Suspensions remained undisturbed for 1 week.	67

3.9	Effect of pH on green density. Slip prepared without ball milling.	68
3.10	Effect of pH on viscosity of composite suspension. Slip prepared with 35 wt% solids with 20 vol% whiskers.	70
3.11	Effect of SiC whisker content on viscosity of composite suspension. Slip prepared at pH=11 with 35 wt% solids.	71
3.12	Effect of ultrasonication time on Si ₃ N ₄ particle size. Suspensions at pH=11 used for ultrasonication were composed of 5g powder and 300 ml DI water with a electrolyte concentration of 10 ⁻⁴ M.	72
3.13	Ultrasonication time effect on slip casting green density of Si ₃ N ₄ .	73
3.14	Effect of ultrasonication and ball milling on slip casting green density of Si_3N_4 .	75
3.15	 (a) SEM micrograph of Si₃N₄ composite green compact with 30 vol% SiC whiskers. Both materials were not ball milled. (b) SEM micrograph of Si₃N₄ composite green compact with 30 vol% SiC whiskers. Both materials were ball milled. 	76-77
3.16	SEM micrograph of diluted SiC whisker suspension.	79
3.17	Flow chart of the method combining ball milling and ultrasonication.	80
3.18	Slip cast green density as a function of whisker loading.	81
3.19	 (a) SEM micrograph of Si₃N₄ composite green compact with 30 vol% SiC whisker. Both materials were prepared without ball milling. (b) SEM micrograph of Si₃N₄ composite green compact with 30 vol% SiC whisker. Both materials were ball milled. 	83-84
3.20	Effect of ball milling SiC whiskers on slip cast green density.	85
3.21	Al ₂ O ₃ -Y ₂ O ₃ -SiO ₂ phase diagram. P denotes the grain boundary phase composition.	87
3.22	Effect of ball milling Si ₃ N ₄ on the sintered density. Whiskers were added to the suspensions after ball milling.	88

3.24	Sintered density as a function of whisker loading. Whiskers were ball milled.	91
3.25	 (a) Fracture surface of monolithic Si₃N₄. Ultrasonicated only. Sintered at 1800°C for 2 hours. (b) Fracture surface of monolithic Si₃N₄. Ball milled only. Sintered at 1800°C for 2 hours. (c) Fracture surface of monolithic Si₃N₄. Ultrasonicated and ball milled. Sintered at 1800°C for 2 hours. 	93-95
3.26	Fracture surface of Si ₃ N ₄ composite with 10 vol% non-ball-milled SiC whiskers. Sintered at 1750°C for 2 hours.	96
3.27	Fracture surface of monolithic $\mathrm{Si_3N_4}$. Ultrasonicated only. Sintered at $1800^{\circ}\mathrm{C}$ for 4 hours.	97
3.28	 (a) Fracture surface of Si₃N₄ composite with 10 vol% non-ball-milled SiC whiskers. Sintered at 1800°C for 2 hours. (b) Fracture surface of Si₃N₄ composite with 10 vol% ball-milled SiC whiskers. Sintered at 1800°C for 2 hours. 	98-99
3.29	 (a) Fracture surface of Si₃N₄ composite with 20 vol% non-ball-milled SiC whiskers. Sintered at 1800°C for 2 hours. (b) Fracture surface of Si₃N₄ composite with 20 vol% ball-milled SiC whiskers. Sintered at 1800°C for 2 hours. 	101-102
3.30	 (a) Fracture surface of Si₃N₄ composite with 30 vol% non-ball-milled SiC whiskers. Sintered at 1800°C for 2 hours. (b) Fracture surface of Si₃N₄ composite with 10 vol% ball-milled SiC whiskers. Sintered at 1800°C for 2 hours. 	103-104
3.31	Fracture surface of monolithic $\mathrm{Si_3N_4}$ having 4Y2A additive. Sintered at $1800^{\circ}\mathrm{C}$ for 2 hours.	105
3.32	Crack like void was observed in fracture surface of $\mathrm{Si_3N_4/SiC_{(w)}}$ composite.	107
3.33	The effect of ultrasonication and ball milling on the mechanical properties of monolithic Si ₃ N ₄ . Sintered at 1800°C for 2 hours.	108
3.34	Fracture toughness as a function of whisker loading. Sintered at 1800°C, 2 hours.	109
3 35	Hardness as a function of whisker loading Sintered at 1800°C 2 hours	111

3.36	The effect of sintering temperature and time on the fracture toughness of composites.	113
3.37	The effect of sintering temperature and time on the hardness of composites.	114
3.38	Diffraction pattern of SiC whiskers.	115
3.39	Diffraction pattern of silicon nitride starting powder.	116
3.40	Diffraction pattern of monolithic silicon nitride ceramic.	117
3.41	Diffraction pattern of silicon nitride composite with 10 vol% ball-milled SiC whiskers.	118
3.42	Diffraction pattern of silicon nitride composite with 20 vol% ball-milled whiskers.	119
3.43	Diffraction pattern of silicon nitride composite with 20 vol% non-ball-milled SiC whiskers.	120
3.44	Diffraction pattern of silicon nitride composite with 30 vol% ball-milled SiC whiskers.	121
3.45	Diffraction pattern of silicon nitride composite with 30 vol%	122

INTRODUCTION

Ceramic processing has been regarded as a conventional production procedure that involves the preparation and mixing of particulate components followed by consolidation. However, particle preparation and characterization, dispersion and mixing of powders in liquids, the rheology of the resulting slurry, and packing of powders are all governed by basic surface properties. Colloidal processing gives control and allows manipulation of the interparticle forces existing between particles in suspension, which enhances homogeneity and improves sinterability.

The lack of toughness of many monolithic ceramics is well known [1]. Si₃N₄ matrix ceramics are receiving a great deal of recent attention because of their mechanical properties at both ambient and high temperatures, thermal shock resistance and high resistance to wear [2]. Additions of reinforcement materials such as whiskers, particles, and fibers thereby forming a ceramic matrix composite (CMC) are required to improve the toughness. However, inhomogenous distribution of the reinforcement materials will lead to defects in the sintered product and degrade the mechanical properties of the composite. It was reported that powder processing through colloidal suspensions increases the mechanical properties and the reliability of advanced ceramics and ceramic matrix composites [3,4]. It is the intention of this study to examine the links

between the surface chemistry and the rheological behavior of SiC/Si_3N_4 CMCs with regard to the resulting fracture toughness of the consolidated samples. Variables in this study are the states of agglomeration between the SiC and Si_3N_4 , the electrolyte concentration and the slip casting parameters. Results will correlate processing pH to slurry viscosity and toughness of the sintered samples. The colloidal processing of SiC whisker reinforced Si_3N_4 CMCs will be studied in detail in this thesis.

1. LITERATURE REVIEW

1.1 Colloid Theories

A dispersion is defined as a two-phase system in which one phase, called the dispersed phase, is distributed as small particles throughout the second phase, called the continuous phase. When the size of the small particles is much larger than the size of the molecules of the solvent, such systems are referred to as colloidal dispersions [5]. The lower limit of particle size is around 1nm. Smaller particles would ultimately become indistinguishable from the liquid, forming a true solution. The upper particle size limit is normally set at a radius of 1 µm but there is no clear distinction between the behavior of particles of 1 µm and the somewhat larger particles [5].

1.1.1 Surface Charge of Particles

The state of electric charge of the particles of a colloidal dispersion is always an important factor governing the stability of the system, which is the ability to maintain its singular state. The redistribution of charge which is implied by the formation of an electric double layer when electrically neutral particles are placed in a solution which is itself electrically neutral will be governed by the following factors [6]. (i) The dissociation of any inorganic groups at the particle surface. (ii) Dipolar molecules at the particle surface. (iii) The unequal adsorption by the particle of oppositely charged ions in the solution. (iv) The unequal dissolution of oppositely charged ions of which the particle may be composed. Such dipoles will not directly contribute to the net charge of the particle but they may have an important effect on the electric double layer.

The particle surface attracts ions of opposite charge which are initially physically adsorbed to the surface. These ions are termed counter-ions since they are of opposite charge to the surface and counter the charge of the surface. The concentration of counterions is very high close to the surface as shown in Figures 1.1 (a) and 1.1 (b), but their concentration decreases as the distance from the surface is increased until the concentration is eventually the same as the concentration of the ions in the bulk liquid [7]. The ions having the same charge as the surface, called co-ions, have a very low concentration at the surface, but their concentration increases as the distance from the surface is increased until the concentration eventually becomes the same as that in the bulk liquid [7]. The distance where the co-ions and counter-ions reach the bulk concentration is of the order of tens of nanometers [5]. The phenomenon above is shown in Figure 1.1, in which the particle surface is illustrated as a flat surface because of the extremely small size of the ions (on the order of a few tenths of a nanometer or less) compared to the radius of the particles. The distance $1/\kappa$ in the figure is known as the Debye length which is used to characterize the size of the layer of adsorbed ions.

1.1.2 Potential Determining Ion

A potential determining ion determines the potential of a particle surface or as in (iii) mentioned above generates charge on the particle surface. For particles with surface charge generation resulting from the interaction of ionic surface groups with H⁺ and OH⁻ ions, the potential determining ions are H⁺ and OH⁻. In this case adding more H⁺ and

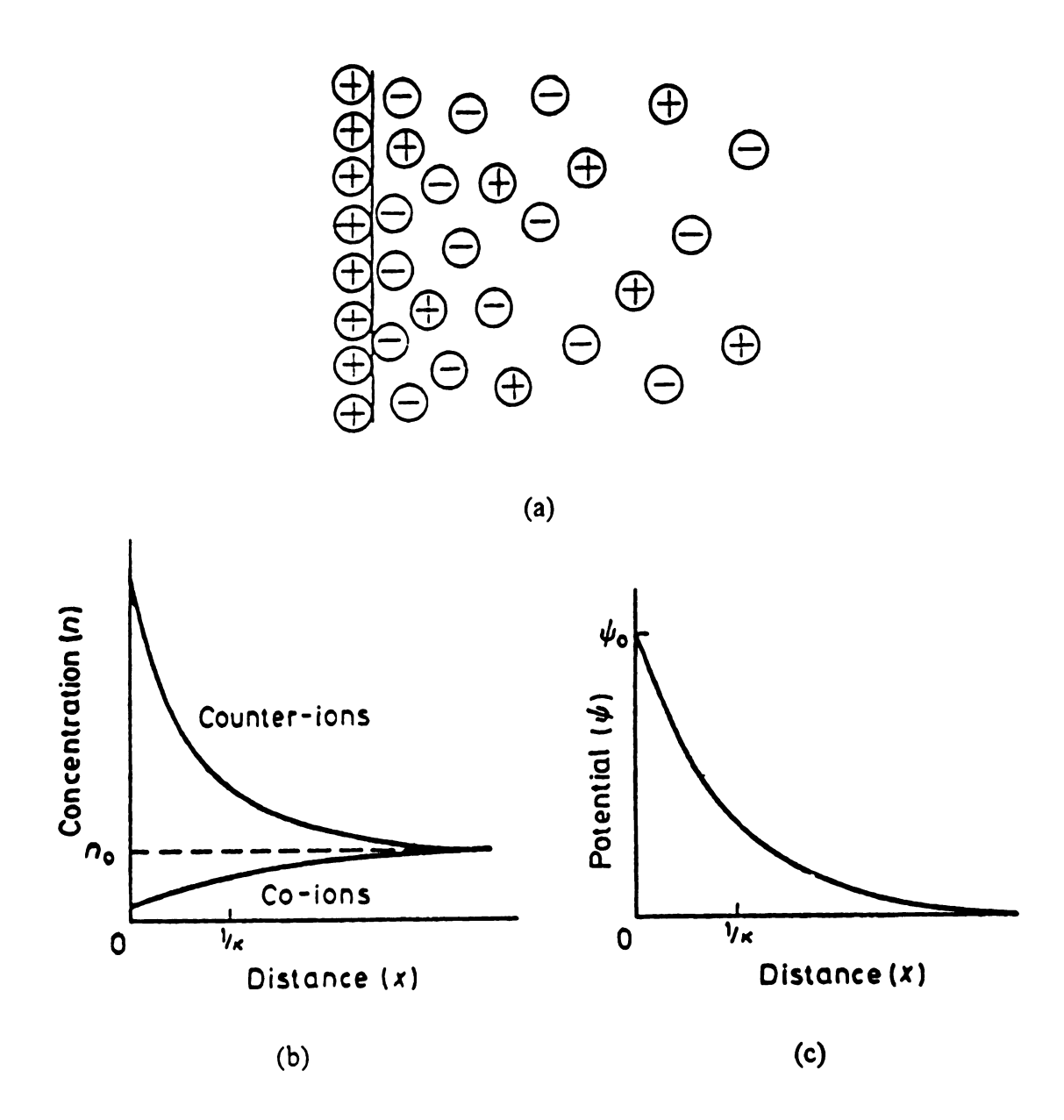


Figure 1.1 Illustration of a electric double layer (taken from [7]).

OH through the addition of an acid or base will change the concentration of potential determining ions which will change the degree of interaction of the potential determining ions with the ionic surface groups and consequently will change the charge on the particle surface. Similarly, changing the concentration of any potential determining ion will result in a net change of surface charge.

1.1.3 Electric Double Layer

Gouy [8] and Chapman [9] pointed out that the electric double layer can be regarded as consisting of two regions: an inner region which may include adsorbed ions, and a diffuse region in which ions are distributed according to the influence of electrical forces and random thermal motion. This diffuse distribution of ions is associated with a smooth variation of potential from its value φ_0 at the phase surface to zero in the bulk of the solution as illustrated in Figure 1.1 (c), assuming that the ions in the diffuse part of the double layer are point charges distributed according to the Bolzmann distribution. However, the finite size of the ions will limit the inner boundary of the diffuse part of the double layer, since the center of an ion can only approach the surface to within its hydrated radius without becoming specifically adsorbed.

1.1.4 Stern Layer

Stern [10] proposed a model in which the double layer is divided into two parts separated by a plane (the Stern plane) located a hydrated ion radius from the surface, and also considered the possibility of specific ion adsorption. Accordingly, the ions forming the

diffuse double layer are distributed not only under the influence of the electric field, but also under the influence of the intermolecular forces between them and the outer phase. The forces of attraction between ions in solution and the outer phase can be quite considerable, and can give rise to the formation and adsorption of ions of a certain type. This is equivalent to the accumulation of a certain amount of electricity at the interface, so that the potential near the surface will be changed. Stern's theory is schematically illustrated in Figure 1.2. There are three layers whose potential is of particular interest. One is at the surface of the particle itself and measures the total potential of the double layer, ψ_0 . Another is the boundary between the Stern and the Gouy (diffuse) part of the double layer, ψ_d . The third layer is formed by the boundary between the solvent adhering to the particle in its' motion and that which can move with respect to it. The potential of this plane is called the zeta potential (ζ). Electrokinetic phenomena depend on the relative motion of the surface and the diffuse double layer. Hence electrokinetic experiments can give us information only about ζ potential, and say nothing directly about ψ_0 and ψ_d . The shear plane is usually located at a small distance further out from the surface than the Stern plane and that ζ is, in general, marginally smaller in magnitude than ψ_d . In tests of double-layer theory it is customary to assume that ψ_d and ζ are approximately equivalent. The bulk of experimental evidence suggests that errors introduced through this assumption are usually small [7].

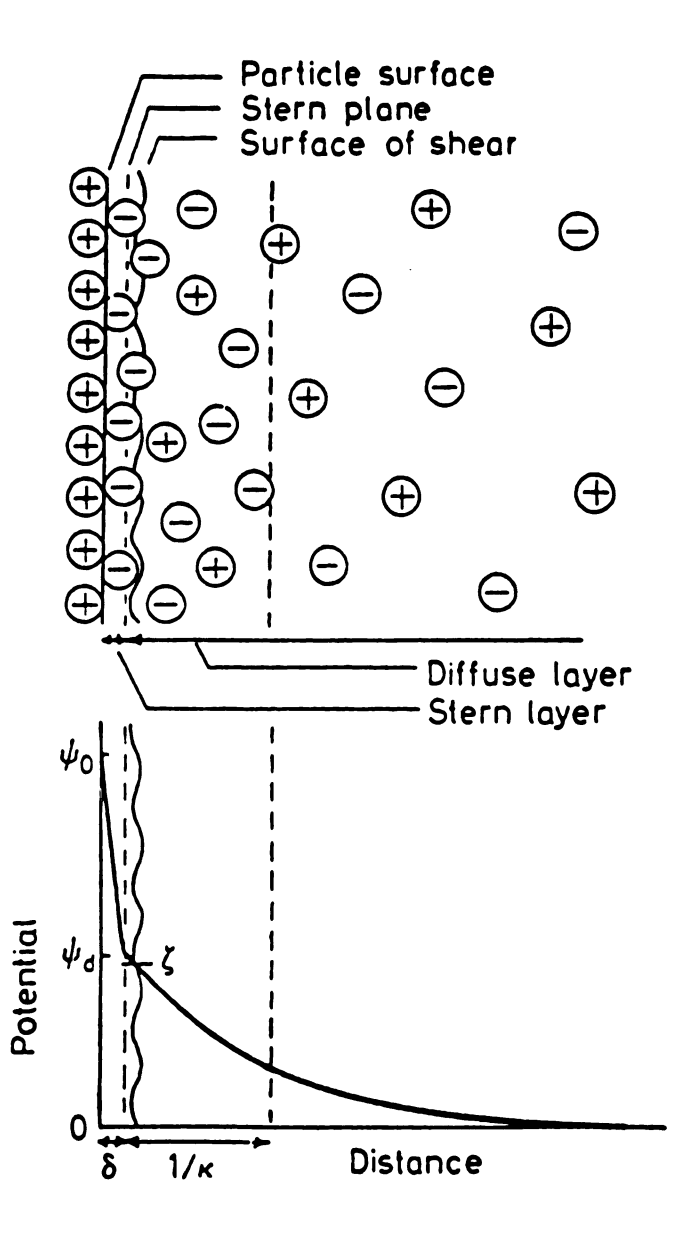


Figure 1.2 Schematic representation of the structure of the electric double layer according to Stern's theory (taken from [7]).

1.1.5 DLVO Theory

At least three major types of interactions are involved in the aproach of colloidal particles, namely: (i) the London-van der Waals force of attraction, (ii) the Coulombic force (repulsive and attractive) associated with charged particles, and (iii) the repulsive force arising from solvation, adsorbed layers, etc.. The interplay of (i) and (ii) form the basis of the classical theory of flocculation of lyophobic dispersions, first proposed by Deryagin and Landau [11] and Verwey and Overbeek[12], and known as the DLVO theory. The force (iii) is less well defined and will not be discussed hereafter. DLVO theory provided the quantitative explanation of coagulation by equating the total interaction potential equation, V_T , as the summation of the dispersion attraction, V_A , and the electrostatic repulsion, V_R :

$$V_T = V_A + V_B. \tag{1.1}$$

To calculate V_A , the intermolecular attractive forces must be taken into consideration.

Originally, three types of molecular attractive forces were postulated by van der Waals.

- (1) Two molecules with permanent dipoles mutually orientate each other in such a way that, on average, attraction results.
- (2) Dipolar molecules induce dipoles in other molecules so that attraction results.
- (3) Universal attractive forces between non-polar molecules were first explained by

 London and are due to the polarization of one molecule by fluctuation in the charge

 distribution in a second molecule, and vice versa.

London forces are the dominant attractive forces in suspensions unless the materials are highly polar [7]. Hamaker [13] calculated the force due to van der Waals attraction which results from London forces with the potential decreasing as the inverse of the sixth power of separation distance [14]. Van der Waals attraction without retardation for two different interacting particles of radius, a_i and a_j , separated in a vacuum by a distance, H, can be represented by [13]:

$$V_A = -\frac{A}{12} \left[\frac{y}{x^2 + xy + x} + \frac{y}{x^2 + xy + x + y} + 2\log \frac{x^2 + xy + x}{x^2 + xy + x + y} \right],$$
 (1.2)

where

$$x = \frac{H}{a_i + a_j}$$
 and $y = \frac{a_i}{a_j}$,

The Hamaker constant in a vacuum, A, can be calculated using a simplified Lifshitz method [15]:

$$A_i(kT) \approx 113.7 \frac{(\varepsilon_i - 1)^2}{(\varepsilon_i + 1)^{3/2} (\varepsilon_i + 2)^{1/2}},$$
 (1.3)

where

 A_i =Hamaker constant of material 'i' in a vacuum k=Boltzmann's constant (1.381E-23 (J/K)) T=temperature (K), and ϵ_i =dielectric constant of material 'i' in a vacuum.

The presence of a liquid dispersion medium, rather than a vacuum, between the particles notably lowers the van der Waals interaction energy. The constant A in equation (1.2) must be replaced by an effective Hamaker constant. Therefore, for two different particles in a medium an effective Hamaker constant A_{eff} is calculated as:

$$A_{eff} = \left(A_i^{1/2} - A_m^{1/2}\right) \left(A_j^{1/2} - A_m^{1/2}\right), \tag{1.4}$$

where

 A_i =Hamaker constant of material 'i' in a vacuum

 A_i =Hamaker constant of material 'j' in a vacuum, and

 A_m =Hamaker constant of medium 'm' in a vacuum.

The calculation of the interaction energy, V_R , which results from the overlapping of the diffuse parts of the electric double layers around two spheres is complex. It is assumed that ion adsorption equilibrium is maintained as two charged particles approach each other and their double layers overlap, two well-defined situations can be recognized. If the surface charge is the result of the adsorption of potential determining ions, the surface potential remains constant and the surface charge density adjusts accordingly; but if the surface charge is the result of ionization, the surface charge density remains constant and the surface potential adjusts accordingly.

1.1.6 HHF Theory

In the mid 1960's, Hogg, Healy, and Fuerstenau (HHF) built upon DLVO theory to develop a quantitative theory which described the kinetics of coagulation of colloidal systems containing more than one dispersed species [21]. Attraction energy, V_A , is calculated by equation (1.2) and repulsive energy, V_R , is derived using Derjaguin's method [16-17]. For two spherical particles of radii a_i and a_j , having a constant potential, V_R is expressed as

$$V_{R} = \varepsilon_{o} \varepsilon_{R} \pi \left(\frac{a_{i} a_{j}}{a_{i} + a_{j}} \right) \left(\psi_{o_{i}}^{2} + \psi_{o_{j}}^{2} \right) \left(\psi_{o_{i}}^{2} + \psi_{o_{j}}^{2} \right) \ln \left(\frac{1 + \exp(-\kappa H)}{1 - \exp(-\kappa H)} \right) + \ln(1 - \exp(-2\kappa H)) \right),$$
......(1.5)

where

 $\varepsilon_o = \text{permitivity in a vacuum}$

 ε_R = relative permittivity

 ψ_{o} = total double layer potential of particle i

 ψ_{o_i} = total double layer potential of particle j

H =distance between two particles, and

 κ = Debye-Hückel reciprocal length parameter.

This relationship only holds for low potential and for solution conditions such that the double layer "thickness" is small compared to the particle size. Wiese and Healy later derived an energy of repulsion solution similar to the HHF solution for systems with particle charges which remain constant [18]:

$$V_{R} = \varepsilon_{o} \varepsilon_{R} \pi \left(\frac{a_{i} a_{j}}{a_{i} + a_{j}} \right) \left(\psi_{o_{i}}^{2} + \psi_{o_{j}}^{2} \right) \left(\frac{2 \psi_{o_{i}} \psi_{o_{j}}}{\psi_{o_{i}}^{2} + \psi_{o_{j}}^{2}} \ln \left(\frac{1 + \exp(-\kappa H)}{1 - \exp(-\kappa H)} \right) - \ln(1 - \exp(-2\kappa H)) \right).$$
......(1.6)

1.1.7 Stability of Colloidal System

The stability of any system, including a colloidal system, is understood to mean its ability to maintain its singular state and in particular full homogeneity throughout its volume.

Unlike molecularly dispersed systems, lyophobic suspensions have only limited stability. Suspensions of coarse particles are unstable mainly because their particles settle at an appreciable rate owing to the force of gravity. In systems with higher degrees of

dispersion, in which Brownian movement is sufficiently vigorous to prevent sedimentation, the stability can be disturbed as a result of changes which occur in such systems with time and which lead to an increase in the apparent particle size. When the apparent particle size becomes sufficiently large, the dispersed phase separates from the dispersion medium by sedimentation. In ceramic colloidal systems, this coarsening process, called coagulation or flocculation, is caused by adhesion of colliding particles. The number of collisions among colloidal particles is therefore of fundamental importance for the coagulation rate. Every collision, however, does not have to be effective, i.e. not every encounter necessarily results in aggregation.

Both attraction and repulsion forces participate in the collision between a pair of particles. When the former are predominant, the effectiveness of collision is high, and the colloidal systems are unstable. When repulsion forces predominate, the effectiveness of collisions is decreased and the stability is correspondingly higher. The total energy of interaction between the particles in a lyophobic suspension is obtained by summation of the electric double layer and van der Waals energies, as illustrated in Figure 1.3. Van der Waals attraction will predominate at small and at large distances. At intermediate distances double-layer repulsion may predominate, depending on the actual values of the two forces. Two possible type of potential energy curves are shown in Figure 1.3. The total potential energy curve V(1) shows a repulsive energy maximum, whereas in curve V(2) the double-layer repulsion does not predominate over van der Waals attraction at any interparticle distance. If the potential energy maximum, at 20 kT [19] is large compared

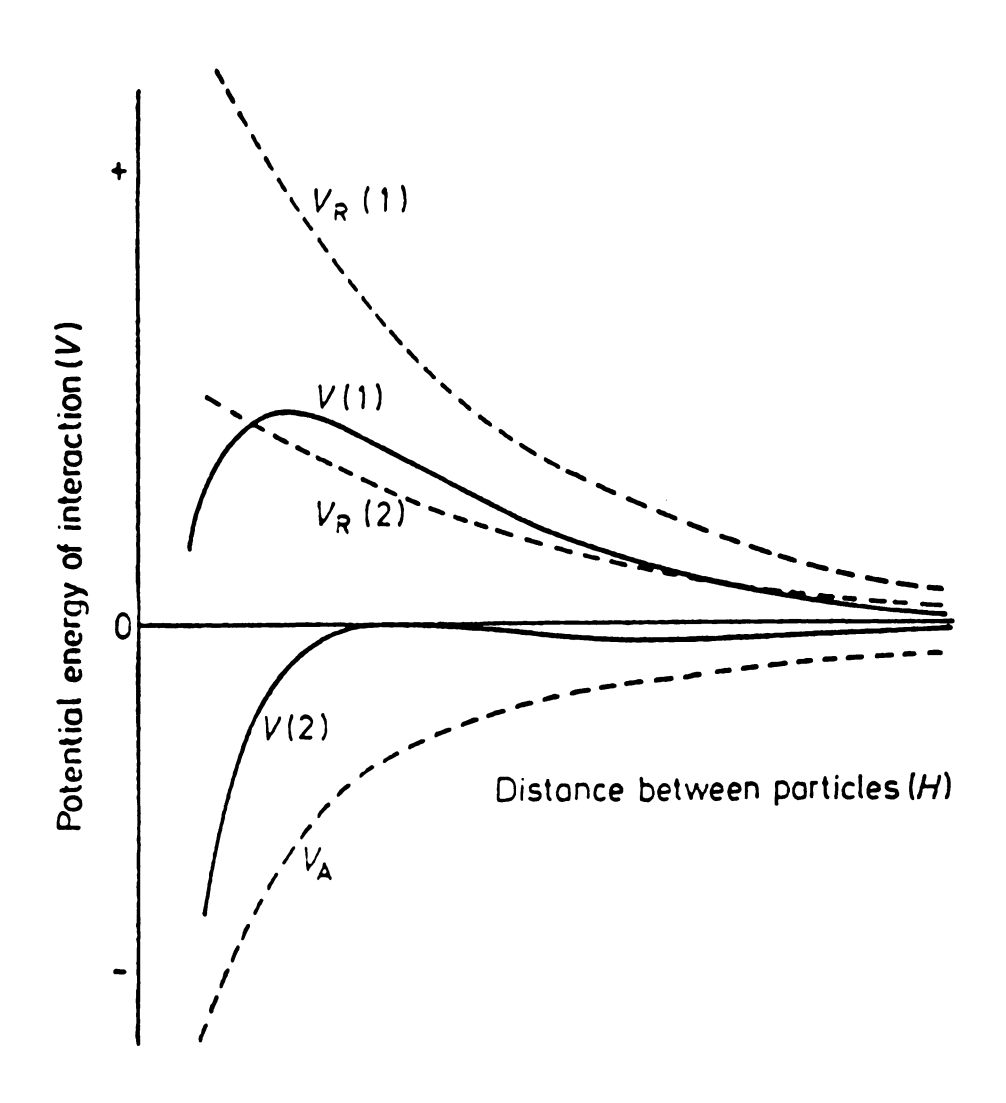


Figure 1.3 Total interaction energy curves, V(1) and V(2), obtained by the summation of an attraction curve, V_A , with different repulsion curves, $V_R(1)$ and $V_R(2)$. (taken from [7])

with the thermal energy kT of the particles, the system should be stable; otherwise, the system should coagulate.

These plots do not address the kinetic aspect of stability. In order to better describe the effects of homo- and hetercoagulation and to generate a quantitative theory for the overall kinetic stability of the system, Fuchs [20] showed that the rate of coagulation is decreased by a factor W, the stability ratio of the system. For identical particles with radius 'a', and a separation distance 'r', (measured from particle center to particle center),

$$W = 2a \int_{2a}^{\infty} \exp\left(\frac{V_T}{kT}\right) \frac{dr}{r^2}, \qquad (1.7)$$

where V_T is the total energy described in equation (1.1). For two nonidentical particles of radius, a_i and a_j , the stability ratio becomes:

$$W_{ij} = \left(a_i + a_j\right) \int_{a_i + a_j}^{\infty} \exp\left(\frac{V_T}{kT}\right) \frac{dr}{r^2}.$$
 (1.8)

For a dispersion containing two kinds of particles (i and j) there are three possible interactions which can occur between particles [21]. Since the energy of interaction may by different for each of these three possibilities, it is necessary to define three separate stability ratios W_{ii} , W_{jj} , and W_{ij} . An overall stability ratio W_i , which was defined by Hogg and his co-workers, to describe the overall stability of a colloidal system with two components, is written as [21]

$$\frac{1}{W_{i}} = \frac{n^{2}}{W_{ii}} + \frac{(1-n)^{2}}{W_{ii}} + \frac{2n(1-n)}{W_{ii}},$$
(1.9)

where 'n' is the overall proportion in terms of numbers of particles of component 'i' in the system.

A study by Wilson and Crimp [22] has developed a computer program (Suspension Stability, ©) which calculates the stability of ceramic composite systems based upon information about the materials' surface potential, particle size, the electrolyte and its concentration, pH, and temperature. The program, which will be used for SiC_(w)/Si₃N₄ system, allows the degree of homostability and heterostability to be determined and controlled in order to optimize composite suspension conditions, and hence reduces the defects and improves the composite properties.

1.2 Deagglomeration of Ceramic Suspension

Slip casting has been the most economic shape forming method to fabricate ceramic green bodies. However, deagglomeration of the slip is critical for the densification processes because agglomerates in the slip will reduce the packing efficiency of the particles and produce large voids in green bodies [23]. This leads to low sintered densities and an increased number of internal flaws [24] which decreases the strength of the material.

Colloidal processing methods, including control over suspension pH, type and concentration of electrolyte, surfactants, dispersants, etc., can be effective in reducing agglomeration in ceramic slips like we discussed before. However, in as-received

ceramic powders, agglomeration can not be removed by simply adjusting the surface potential of the particles in suspension. Mechanical energy is required to break up the agglomerates into single particles. Ball milling and ultrasonic dispersion have been widely used to deagglomerate ceramic slips, and ultrasonication is especially effective in dispersing submicron ceramic particles [25]. Ultrasonication is known to break up the agglomerates by creating small bubbles, called "cavities", which collapse violently and produce local, high velocity jets and pressure gradients. The resulting mechanical forces on the agglomerates are strong enough to break up weakly bonded particles [26]. However, the effects of ball milling and ultrasonication on a $SiC_{(w)}/Si_3N_4$ composite system have rarely been reported. The influences of both techniques on the consolidation of $Si_3N_4/SiC_{(w)}$ composites will be discussed in detail.

1.3 Silicon Nitride Matrix Ceramic Composites

1.3.1 General

Applications of silicon nitride ceramics have considerably widened since the mid-1980's, ranging from engine components such as turbocharger rotors and glow plugs to industrial parts such as bearing materials and cutting tools. These applications have various requirements among which light weight, heat resistance, wear resistance and thermal shock resistance are important characteristics. The properties of silicon nitride ceramics are well balanced compared with other ceramic materials. For instance, toughened ZrO₂ can exhibit much higher strength and toughness, but its' higher temperature properties and thermal shock resistance are poor. SiC has excellent heat resistance, but its'

toughness and thermal shock resistance are low. For Si_3N_4 , the highly covalent Si-N bonds provide a favorable combination of chemical, mechanical and thermomechanical properties: hardness, high strength at high temperature ($\sigma_f = 600 \sim 700$ MPa at 1400° C), low density (3.2 g/cm³), low thermal expansion (3.0×10^{-6} K⁻¹) and good oxidation resistance. These features make them the prime candidate materials for a gas turbine and other heat engine applications.

Numerous investigations in the US, Japan and Germany have resulted in significant improvements in the properties of Si₃N₄ materials such as strength, creep, oxidation, thermal shock and fracture toughness. Average room temperature flexure strengths (4point bend) ranging between 1000-1100 MPa and high temperature (1400°C) strength ranging between 600-700 MPa was achieved [27], but a critical factor still limits the widespread application of these ceramics in heat engines. They are highly sensitive to microstructural flaws which result in catastrophic (brittle) failure. Toughening is expected to improve reliability, because for most of the loading conditions, the stress required to propagate a crack is directly proportional to the fracture toughness, K_{IC}. Considerable work, including particulates and transformation toughening, whisker toughening and continuous fiber reinforced toughening, are underway to improve the toughening of the matrix. Particulate toughening of Si₃N₄ did not result in noticeable improvements in toughness, while toughness values ranging between 6-9 MPa·m^{1/2} were routinely achieved in SiC whisker reinforced Si₃N₄ matrix composites [28-30]. Whisker reinforced composites have the additional advantage that they can be produced by

conventional processing methods, i.e. as a two-step preparation by compaction and heat treatment. The whiskers are short enough to be mixed as a conventional powder and being monocrystals, can sustain high sintering temperatures.

1.3.2 Whisker Toughening

Reinforcement of ceramics by high strength whiskers can improve the fracture toughness and other mechanical properties as compared with unreinforced ceramics [31-32]. It has been reported that the toughness of Si₃N₄ can be increased by 50% when reinforced with 40 vol% SiC whiskers [33]. However, there have been some inconsistencies concerning SiC whisker-reinforced Si₃N₄ composites. Some researchers reported a decrease in strength and toughness of Si₃N₄ with additions of SiC whiskers [31,34], whereas others reported a small increase in strength and a much larger increase in toughness with the same whisker additions [32-33]. These inconsistencies have been thought to result from the differences in raw materials and processing.

It is well known that increased toughness in brittle composite materials is due to increases in fracture energy and Young's modulus. A material containing 20 vol% of randomly distributed whisker phase exhibits a Young's modulus about 5% higher than that of the matrix. This means that the contribution due to modulus toughening is very small, and the toughness can be discussed in terms of energy dissipation related to the interaction between the main crack and the secondary phase. The toughening of ceramics by whiskers typically includes contributions from debonding, crack bridging, pullout, and

crack deflection [35-37]. Each mechanism predicts very different dependencies of toughness upon microstructure. Crack deflection is ostensibly governed only by whisker shape and volume fraction [38], albeit that the relative elastic moduli and thermal expansion coefficients may have implicit effects on the deflection path. The other contributions depend sensitively upon the mechanical properties of the interface, the whisker strength, the whisker radius, and the volume fraction. Toughening by crack bridging is induced by debonding along whisker/matrix interfaces [35]. This energydissipation process in the crack wake requires that the energy necessary for crack propagation along the interface be lower than the work required to fracture the matrix grains and whiskers. The debonding allows the whiskers to remain intact within a small bridging zone behind the crack [35]. This phenomenon was observed by Angelini et al. [39] indicating that matrix cracks propagate past the whiskers and result in bridging whiskers in the wake of the crack tip. The magnitude of the toughening involves a consideration of the extent of debonding and the mode of reinforcement failure, as well as of residual stress effects [35]. If the whiskers are strongly bonded, cracks can propagate through the whiskers without deflection and the composite fails in a brittle manner.

The mechanical behaviour improvement conferred by the whiskers is very different for the two matrices, Al_2O_3 and Si_3N_4 . A very significant increase is generally reported, both in strength and toughness for the SiC-Al₂O₃ composites. Results for a Si_3N_4 matrix are less significant and this is in part attributed to the much higher performance of the

monolithic Si₃N₄ material [40]. Another significant factor relates to the activation of the theoretical models for toughening by matrix-whisker debonding, and crack deflection, or pull out. The SiC-Si₃N₄ bond is stronger than for SiC- Al₂O₃ and often precludes debonding, and therefore the operation of these models.

1.3.3 Processing of SiC_{(w}/Si₃N₄ Composites and Related Problems

Reinforcement of silicon nitride ceramics by SiC whiskers has ben studied extensively. It has been shown that the densification of whisker reinforced ceramics is fairly difficult, even in Al₂O₃ matrix composites when whisker content exceeds 10 wt% [41]. Therefore, hot pressing (HP) or hot isostatic pressing (HIP) has been employed to fabricated high density Si₃N₄ composites, in order to overcome densification difficulties that arise from the introduction of reinforcement in the powder. However, hot pressing is limited to relatively simple shapes, and the orientation of whiskers in hot pressed whisker reinforced ceramic composites will result in anisotropic mechanical properties [42]. Appropriate HIP conditions can produce fully densified (>99.5%) monolithic Si₃N₄ and SiC_(w)/Si₃N₄ composites even without sintering aids [43], but is costly. There is a big economic advantage to be gained by fabricating such composites by pressureless or low pressure sintering. In this respect, a dispersion of fine particles of narrow size distribution has been recognized as facilitating sinterability allowing a relatively high densification rate, even to high densities [44]. Pressureless sintering of the composites have good thermal shock resistance and have been applied as ceramic parts for aluminium die casting [45]. Olagnon *et al.* [45] have succeeded in sintering composites of Si₃N₄ reinforced with up to 20 wt% SiC whiskers using low pressure sintering.

Cold isostatic pressing and slip casting are shaping methods of particular interest for composite ceramics. Uniform distribution of the whisker in the matrix, high green densities, no whisker damage during shaping, and the possibility of obtaining preferred whisker orientations are attractive advantages of the slip casting process. Consolidation by slip casting was shown to bring the double advantage of leading to nearly dense material containing up to 15 wt% whiskers, with a highly homogeneous whisker dispersion free from agglomeration bundles [46]. During casting, the viscous flow of the water through the consolidating layer caused an alignment of the whiskers parallel to the mold surface. This will cause anisotropic properties in the composite. Mitomo et al. [47] have succeeded in sintering highly oriented whisker composites through a combination of slip casting and pressureless sintering techniques. They reported that linear shrinkage perpendicular to the mould surface was larger and that along the slip flow was smaller than that in a monolithic compact, but only a slight anisotropy in fracture toughness when a crack propagated perpendicular to the slip direction. Optical microscopy of polished surfaces indicated alignment of whiskers in the slip direction. However, considering the apparent anisotropy of the microstructure, no proportional and clear effect on the material toughness could be observed [47].

It has been reported that owing to their needle-like shape, whiskers tend to form clumps [48] that lead to flaw sources limiting the final component properties. Whisker enrichment or whisker agglomeration is the main characteristic of inhomogeneous whisker dispersion [42]. When the dispersion of whiskers is inhomogeneous, the densification of whisker enriched areas can be seriously retarded by the whisker agglomerates [49]. First, whisker agglomeration will prevent the matrix powders filling the void space during the mixing process. Then, if there is insufficient liquid phase to infiltrate this space, the voids remain.

Addition of SiC whiskers to Si₃N₄ makes it difficult to obtain high densities by pressureless sintering [50]. Compositions that provide excellent monolithic sinterability do not completely sinter when used as matrix material in whisker reinforced composites. They can be densified by pressure approaches [51]. Lange [52] and Scherer [53] suggest that the whiskers form a touching network at a relatively low whisker loading. The network would inhibit densification of the composite. Bordia and Raj [54] propose that the constraint imposed by the whiskers generates a shear stress in the matrix and a tensile hoop stress at the whisker-matrix interface would reduce the sintering rate. Another possible reason for the failure to achieve complete densification by pressureless sintering is attributed to the use of compositions which result in a "glass deficit" [55]. The glass grain boundary phase influences the rates of dissolution, diffusion, and redeposition of Si₃N₄ during liquid phase sintering. During sintering of whisker reinforced composites, an adequate glass amount is necessary for the rearrangement of both SiC whiskers and Si₃N₄

grains. Freedman et al. [55] presented a simple two-dimensional model which predicts a larger glass requirement for sintering a whisker reinforced composites compared to an analogous monolithic material. The additional glass improves the wetting of the whiskers, aids in pore removal, and provides the whiskers with a medium for rearrangement during sintering. It is also suggested [55] that this glass amount should not be detrimental to the high temperature properties of the material.

The incorporation of SiC whiskers to a Si₃N₄ matrix allows dissipative mechanisms, such as crack bridging and crack deflection, to operate and increase the work of fracture. The efficiency of these mechanisms is strongly dependent upon (1) the size and the aspect ratio of the reinforcing whiskers, and (2) the strength of the whisker-matrix interface. It has been reported that inhibition to particle rearrangement and composite shrinkage is reduced as the whisker aspect ratio is lowered [50]. Yasuda et al. [56] have constructed a model, based on the energy balance of crack propagation and frictional energy during whisker pull-out, to analyze the influence of whiskers' shape and size on mechanical properties of SiC whisker-reinforced Al₂O₃. It was shown that $\Delta(K_{IC}^2)$ and $\Delta\gamma_{eff}$ changed in proportion to r^2/l_w (K_{IC} : fracture toughness, γ_{eff} : effective fracture energy, r: whisker radius and l_w : whisker length), and $\Delta (K_{IC}^2)$ and $\Delta \gamma_{eff}$ were also in proportion to $V_f(V_f)$. volume fraction of the whiskers in the composite) [56]. Coatings on whiskers can modify the strength of whisker-matrix interface. Matsui et al. [57] have reported that C-coating of whiskers increased the chances of interfacial peeling, while Al₂O₃ coating enhanced whisker bridging during crack propagation.

There is a very high probability that the incorporated whisker not only slows down the matrix sintering rate but also retards the $\alpha \rightarrow \beta$ transformation. The observed fracture toughness of whisker reinforced composite, K_C^C , can be determined by the matrix fracture toughness, K_C^M , and the toughness increment by the whisker incorporation, dK^w [58].

$$K_C^{\ C} = K_C^{\ M} + dK^{\mathbf{w}} \tag{1.10}$$

The toughness of the matrix is a function of the matrix microstructure, which is seriously influenced by the sintering process. For Si_3N_4 , elongated β grains are formed during sintering when α type powder is used as starting material, resulting in a reasonably high fracture toughness through a self-reinforced mechanism by these β grains. If the addition of SiC whiskers inhibits the formation of β grains, this results in a lower matrix toughness, K_C^M . Even though the dispersed whiskers contribute to the total composite toughness by dK^W , the degradation in K_C^M will offset it, and there will be no net improvement in the composite toughnesss, K_C^C . Therefore, for the fabrication of whisker reinforced matrix composites, it is necessary to find the best sintering conditions that will realize not only a fully densified composite body but also the optimum matrix microstructure with the highest amount of β grains, to utilize the self-reinforcing mechanism effectively.

1.4 Monolithic Si₃N₄

The properties of Si₃N₄ composites do not only depend on the reinforcement phases, but also the microstructures of the Si₃N₄ matrices. It is anticipated that the Si₃N₄ powder

characteristics and sintering behavior of Si_3N_4 matrix will influence the mechanical properties of $SiC_{(w)}/Si_3N_4$ composites.

 Si_3N_4 is a highly covalent material and requires the use of sintering additives to reach full densification. During sintering, the silica on the silicon nitride surface reacts with sintering additives to form a oxynitride glass. The α -Si₃N₄ dissolves into the glass and precipitates in the form of β -Si₃N₄ at high temperatures. The morphology of the β phase varies from equiaxed to highly elongated grains depending on the characteristics of the glass, as well as on other factors such as characteristics of starting powder and sintering additives, and processing conditions.

In 1979, Lange reported an improvement in flexure strength and fracture toughness (up to 6 MPa·m^{1/2}) when β-Si₃N₄ grains with high aspect ratios were formed during sintering [59]. Matsuhiro and Takahashi [60] produced Si₃N₄ specimens with fracture toughness of 9.7 MPa·m^{1/2} and flexure strengths of 900 MPa.

1.4.1 Crystal Structure of Si₃N₄

 Si_3N_4 crystallizes in two hexagonal modifications, α and β , which differ in that the lattice distance in the direction of the crystallographic c-axis for α - Si_3N_4 is about twice as large as for the β modification [61]. Both phases are built up of SiN_4 tetrahedra joined in a three-dimensional network by sharing corners. The silicon atoms are located in the center of irregular nitrogen tetrahedra, each nitrogen atom belonging to three tetrahedra. The β

structure consists of Si_3N_4 layers which alternate in the sequence AB, forming hexagonal tunnels in the direction of the crystallographic c-axis [62]. In the unit cell of the α -phase, the layers alternate with mirror-inverted layers in the sequence ABCD, resulting in a c-direction lattice distance which is about twice as large as for the β modification.

With increasing temperature, the α -phase becomes unstable with respect to β -phase. The transformation is reconstructive and can occur with solution-precipitation by means of a liquid phase. The significance of this transformation is that the β -phase has a tendency to form a rod-like morphology, which can by interpreted by relating the hexagonal crystal structure of β -Si₃N₄ to an anisotropic boundary energy [63]. β -Si₃N₄ is a highly covalent ceramic with stacking arrangements of the nitrogen atoms that differ in the a- and c-directions. This difference in the stacking arrangement results in a lower boundary energy in the c-direction than in the a-direction of the hexagonal crystal. The nucleation on the surface of the basal plane is more energetically favorable resulting in a higher growth rate in the c-direction and the formation of the enlonged grains. The activation energy for grain growth was attributed to Si diffusion in silicate glasses.

1.4.2 Thermodynamic Properties and Stability

 Si_3N_4 does not have a real melting point but decomposes under 0.1 MPa $N_2(g)$ at 2173 K. The reaction during decomposition according to the formula [64]

$$Si_3N_4(s) \leftrightarrow 3Si(l) + 2N_2(g)$$
 (1.11)

is of increasing importance above 1500°C. The liquid silicon has an equilibrium with silicon vapor:

$$Si(I) = Si(v). (1.12)$$

For the vapor pressures over Si₃N₄, the following equation is obtained [64]

$$p_{N}^{3} \times p_{N}^{2} = K, \qquad (1.13)$$

where K is the equilibrium constant. This relationship is illustrated in Figure 1.4, which implies that Si₃N₄ will also decompose at high nitrogen pressures if silicon vapor is not prevented from escaping from the system. An increased nitrogen pressure can cause the silicon equilibrium pressure according to equation (1.12) to fall below the equilibrium pressure value over liquid silicon and that a spontaneous decomposition of Si₃N₄ is thus suppressed.

The decomposition of Si_3N_4 is important, because very high sintering temperatures must be selected due to the high degree of covalent bonding in silicon nitride. This extensive covalent bonding means great bonding strength and hence low self-diffusion coefficients. Diffusion of nitrogen in α - and β -Si₃N₄ is about four orders of magnitude below the self-diffusion coefficients of oxygen and aluminum in polycrystalline Al_2O_3 [65]. As a consequence, Si_3N_4 can not be highly densified without sintering aids or high pressure.

Carbon activity (a_c) is also of important since the sintering of Si_3N_4 is usually performed in a graphite crucible a furnace with graphite heating element. Wada *et al.* [66] calculated the phase stability in the Si-C-N-O system and a phase stability diagram

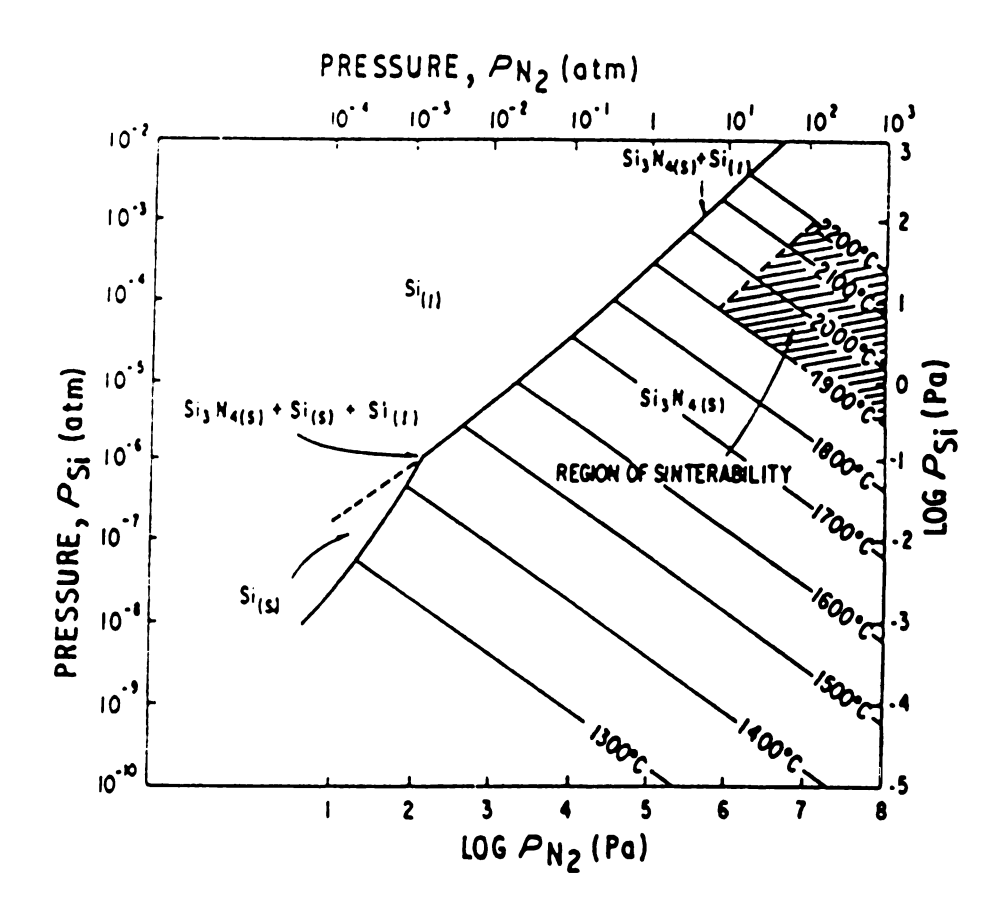


Figure 1.4 Silicon vapor pressure in equilibrium with silicon nitride as a function of nitrogen pressure and temperature (taken from [64]).

 Table 1.1
 Equilibrium Reactions in Si-C-N-O System (taken from [66]).

Reaction			
(1)	$\beta - \text{Si}_3 \text{N}_4 + 3\text{C}(s) = 3\beta - \text{SiC} + 2\text{N}_2(g)$		
(2)	$4\beta - Si_3N_4 + 3O_2(g) = 6Si_2N_2O(s) + 2N_2(g)$		
(3)	$\beta - \text{Si}_3 \text{N}_4 + 3\text{O}_2(g) = 3\text{SiO}_2(c) + 2\text{N}_2(g)$		
(4)	$2Si_2N_2O(s) + 4C(s) = 4\beta - SiC + O_2(g) + 2N_2(g)$		
(5)	$2Si_2N_2O(s) + 3O_2(g) = 4SiO_2(c) + 2N_2(g)$		
(6)	$SiO_2(c) + C(s) = \beta - SiC + O_2(g)$		
(7)	$3Si(l)$ or $(s) + 2N_2(g) = \beta - Si_3N_4$		
(8)	$4Si(l)$ or $(s) + 2N_2(g) + O_2(g) = 2Si_2N_2O(s)$		
(9)	$\operatorname{Si}(l) \text{ or } (s) + \operatorname{O}_2(g) = \operatorname{SiO}_2(c)$		

plotted as a function of partial pressures of nitrogen and oxygen. Carbon activity is referenced to solid graphite as a standard state. When a graphite crucible or furnace is used for Si₃N₄ sintering, the carbon activity would be unity or very close to unity.

Figure 1.5 shows that β -Si₃N₄ can react and form β -SiC when the nitrogen pressure is low, or β -Si₃N₄ can form SiO₂ when the oxygen pressure is high enough. Therefore, flowing nitrogen gas is commonly used for Si₃N₄ sintering. This plot can be applied as a guideline to sintering both Si₃N₄ and SiC/Si₃N₄ composites. For a nitrogen pressure of 1 atm, Si₃N₄ cannot be sintered without forming β -SiC at temperatures higher than 1374°C, even if the oxygen pressure is kept below 10⁻²⁰ atm. However, if the nitrogen pressure is increased to 10 atm, the sintering temperature of Si₃N₄ increases to 1536°C without SiC formation.

1.4.3 Processing of Si₃N₄ ceramics

Classical sintering is not applicable to produce pure, dense Si₃N₄ ceramics because of the high degree of covalent bonding. Alternative techniques have been developed, such as nitridation of silicon compacts or the addition of sintering aids to Si₃N₄ powders to create liquid phase sintering with or without the application of pressure to assist the sintering process. Four techniques are commonly used: reaction-bonding, hot-pressing, sintering and hot-isostatic pressing.

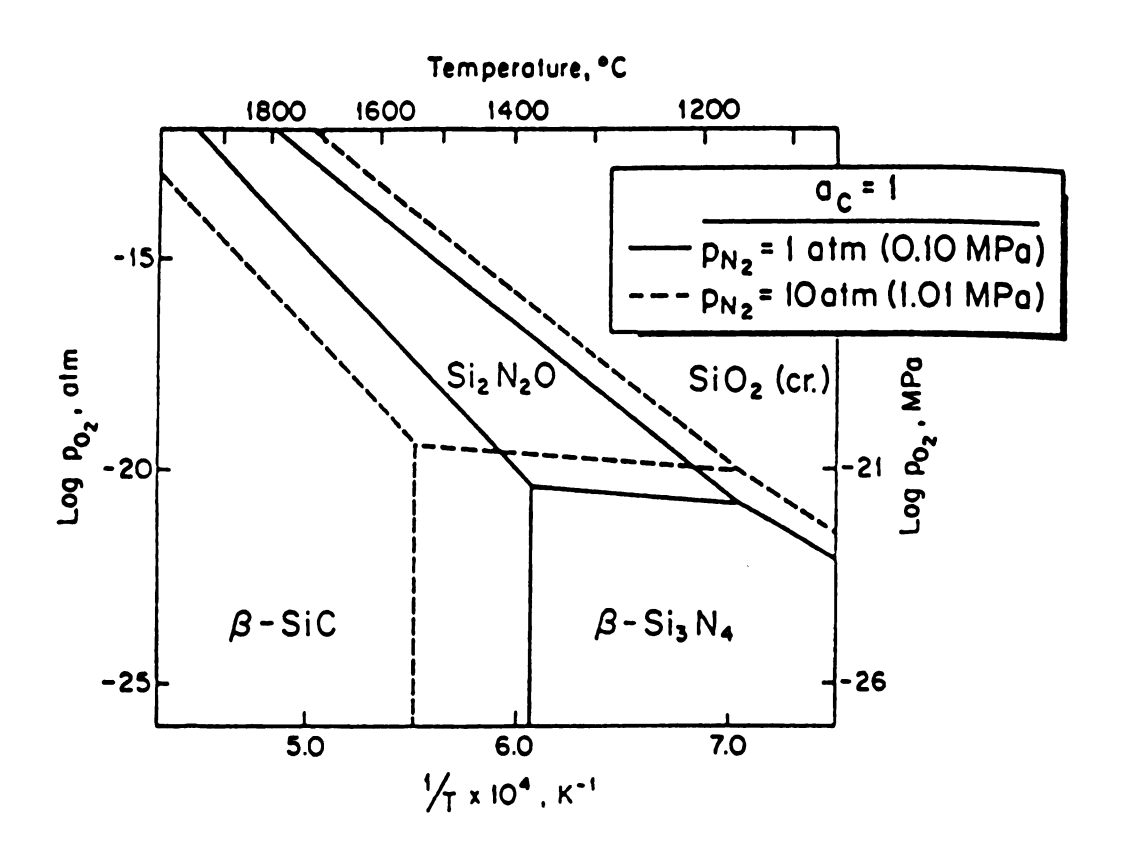


Figure 1.5 Phase relationships in the Si-C-N-O system as a function of oxygen partial pressures and temperature at $a_c=1$, $p_{N2}=1$ atm (0.10 MPa), and $p_{N2}=10$ atm (1.01 MPa) (taken from [66]).

Reaction-Bonding

The starting material is silicon powder which is usually consolidated by isostatic pressing, injection molding or slip casting. Before nitriding to convert silicon to Si_3N_4 , a pre-sintering step in an inert atmosphere is often inserted to provide sufficient strength to allow the powder compact to be machined to approximately the final required size. The nitridation process is carried out under a nitrogen atmosphere in a temperature up to 1420° C for several days [67]. Only small dimensional changes occur during the nitridation process. Reaction-bonding method is possible to produce complex components requiring no or only little subsequent machining, however, it results in a still porous material. Dense Si_3N_4 , can only be produced by hot-pressing, sintering and hot-isostatic pressing, with the use of different oxide or non-oxide sintering additives, such as MgO, Y_2O_3 or $Y_2O_3 + Al_2O_3$.

Hot Pressing

Fully dense and high strength Si₃N₄ ceramics, which are capable of being used at temperatures up to 1100°C without a decrease in strength, can be produced using hotpressing. They typically exhibit a certain amount of grain texture, i.e. a preferred orientation of the elongated β-crystals perpendicular to the hot pressing direction. The main limitation of hot-pressing is that extremely hard and strong materials are difficult to machine and the components made from this materials are rather costly [67].

Sintering

Sintered Si₃N₄ is expected to offer a good combination of high strength and the possibility of forming complex shaped components on a large scale within a reasonable cost limits. In general, variables affecting densification behavior are similar for pressureless sintering and hot pressing. They all occur by a liquid phase sintering process[59]. Nevertheless, two more factors have to be considered for the pressureless sintering process. First, the requirements for the starting powders are much higher because both the thermodynamic driving force for sintering can be increased and diffusion distances for sintering can be decreased by using ultrafine powders[68]. Second, control of the partial pressures of reactants in the sintering atmosphere can be used to avoid the dissociation of Si_3N_4 . This can be achieved by high nitrogen pressures based on thermodynamic considerations, and/or by embedding the specimens to be sintered in a powder bed with a composition similar to the compact [67]. Thus, a local gas equilibrium in the immediate surroundings of the compacts is created to minimize decomposition and vaporization. Moreover, higher sintering temperatures can be employed.

Hot-Isostatic Pressing

Another technique which combines good mechanical and thermo-mechanical properties of Si₃N₄ with the possibility of producing complex shaped components is hot-isostatic pressing (HIP). Special HIP equipment has been developed to enable HIP densification at temperatures higher than 1700°C. During HIP pressing, high pressure is applied via a

m pr oo si

1 F

a

]

S

gas to consolidate a powder compact or to remove residual porosity from pre-sintered materials. Hot-isostatic pressing has advantages in three respects compared to hot-pressing. First, the uniform way of applying the high pressure results in fully isotropic material properties. Second, the use of pressures up to 300 MPa, which are more than one order of magnitude higher than in uniaxial hot-pressing, enhances the densification of Si₃N₄. As a result, dense Si₃N₄ parts can be produced from powders of lower sintering activity and powder compositions with smaller amounts of sintering aids. Third, the use of high pressure yields a more uniform and fine grained microstructure which may lead to a further increase in strength [64,67].

1.4.4 Microstructural Evolution in Si₃N₄

Formation Mechanisms

There are four steps which can be utilized to sinter fully dense Si₃N₄ [64].

- (1) Use ultrafine powders.
- (2) Apply external pressure
- (3) Increase the sintering temperature (an increase of nitrogen pressure is necessary at the same time).
- (4) Use a powder bed.
- (5) Add sintering aids to form a liquid phase.

The last step is of the most important because the first four steps do not result in a sufficient densification. Kingery [69] described the liquid phase sintering process by a

three stages model: rearrangement, solution-diffusion-precipitation, and coalescence. These apply to Si_3N_4 in the following ways.

A liquid phase is formed by the sintering aids reacting with the oxygen, SiO₂ or oxynitride, which are always present on the particle surface of commercially available Si₃N₄ powders. If the amount of liquid phase is high enough and the viscosity at sintering temperature is sufficiently low, rearrangement processes will occur induced by capillary forces. The degree of densification in the stage is mainly depend on the particle size and the amount and viscosity of the secondary phase [64].

The solution diffusion precipitation process starts when the temperature is high enough. In this stage, the driving forces are the capillary forces and the differences in the chemical potentials between small and large particles. As a result, the densification rate of liquid phase increase compared with that of self-diffusion in Si_3N_4 , because the diffusion rate is increased about ten orders of magnitude [70]. High α starting powders are usually employed for sintering. The reason for this is that the α -phase becomes thermodynamically unstable at temperatures higher than $1400^{\circ}C$ and exhibits the tendency to transform into stable β -phase. If the starting powder contains a large number of β -particles, the fine particles start to dissolve and precipitate on the coarser original β -particles so that their surface energy is minimized. This leads to large spherical or equiaxed grains. If the starting powder contains only a low concentration of β -grains, high supersaturation in the liquid phase is created locally due to the lack of sufficient β -

nuclei, resulting in a spontaneous nucleation and crystallization of rod-like β -grains [59][70][71].

The third stage of the liquid phase sintering is coalescence basically solid state sintering, which gives nearly no contribution to further densification [72]. During cooling, the liquid silicates solidify to amorphous or partially crystalline phases.

One of the most important features of dense Si_3N_4 is the morphology of elongated β -grains structure which has a strong influence on the mechanical properties up to about 1000° C. The aspect ratio of the β -grains is mainly controlled by the phase composition of the starting materials, the characteristics of the liquid phase, and processing conditions. The optimization of all these parameters may lead to improved mechanical properties.

The Effects of Silicon Nitride Powder

 Si_3N_4 powders that are synthesized by different methods have a variety of characteristics that can affect the final microstructure of the densified parts. Characteristics such as particle size, distribution and morphology, surface chemistry and phase content can all influence the $\alpha \to \beta$ transformation.

Generally, the finer the starting powder, the higher the resulting sintered density.

Because finer powder has higher specific surface area and also higher oxygen content which results in an increasing amount of liquid phase and thus in an enhancement of the

rearrangement and diffusion processes [64]. The impurities in the starting powders such as alkali and alkaline earth metals and compounds of aluminum or iron have a positive effect on the densification process, but the formation of the low viscosity liquid phases degrade the high temperature properties of the resulting materials [67,73].

High concentrations of the α -phase enhances the densification and the formation of the rod-like β -grains. Lange [59] estimated the resulting aspect ratio, 'a', by the α/β ratio in the starting powder using $a=1+\alpha/\beta$. When the transformation occurs at high temperatures, if the starting powders are uniform in size, the presence of β -grains in the starting Si₃N₄ powder becomes critical. Hoffmann and Petzow [74] pointed out that the microstructure of Si₃N₄ was not controlled by homogeneous or heterogeneous nucleation of β -Si₃N₄, but rather by the preexisting β particles in the starting powder. Their experiments showed that the number of β grains in a dense material is always the same or lower than the number of β nuclei in starting powder. This means that β grains do not nucleate, but grow on surfaces of already existing particles. A slight variation in the amount of β-Si₃N₄ in a starting powder can have a dramatic effect on the final microstructure [74]. The Si₃N₄ powders with low amounts of residual β phase typically form coarse microstructures with elongated grains. As the amount of β - Si_3N_4 in the starting powder increases to about 5%, grain growth becomes hindered by the presence of other β-Si₃N₄ grains and results in a finer microstructure. At higher β contents in the starting powder, microstructural coarsening occurs as the smaller grains dissolve and

precipitate out onto the larger grains. This process causes the grain morphology to change from highly elongated to more equiaxed.

The Effects of Glass Chemistry

The type and amount of sintering additives determine the temperature at which densification commences and its rate during pressureless and pressure sintering, as well as the temperature and rate of the $\alpha \to \beta$ transformation. They also determine the morphology of the β -grains and the characteristics of the grain boundary phase, which control the high temperature properties [67].

The grains with highest aspect ratios have been produced in multi-component glass systems such as Y₂O₃-Al₂O₃ [75], Nd₂O₃-MgO [76], Y₂O₃-CeO₂ [77], Y₂O₃-MgO [78] etc. By mixing these components in the proper ratios, the glass chemistry can be altered to produce microstructures with varying sizes, aspect ratios, and quantities of grains. The microstructures of Si₃N₄ ceramics produced from low viscosity glass (e.g. MgO) are generally characterized by large whiskers. This is because the low viscosity glass provides rapid mass transport and low supersaturation. In high viscosity systems (e.g. Y₂O₃), the rate of mass transport in the glass is slow, which causes a reduction on grain growth, resulting in a high number of small grains with a broader size distribution. The grain morphology can be affected by glass content. In Si₃N₄-Y₂O₃-MgO-CaO system, Pyzik *et al.* [79] have shown that materials made with 15 vol% glass contained mainly large grains, while materials made with 4 vol% glass had a large number of fine grains.

Higher amounts of the glass content also improves the densification, however, the amount of a sintering aid necessary to achieve high densities can be reduced by applying external pressure, as in the case of hot-pressing and hot-isostatic pressing.

Effects of Processing Conditions

Important process parameters are temperature, time, atmosphere and pressure. Applied pressure is the most important processing parameter in hot-pressing and hot-isostatic pressing, however, increasing pressure seems to increase orientation effects in the microstructure of hot-pressed materials [67]. Generally, higher temperatures and longer times enhance densification. But the temperature is limited by the decomposition of Si₃N₄ and the vaporization of the liquid phase. This can be realized by using the powder bed technique and by applying high nitrogen pressures as we discussed before. It also has to be considered that long times and high temperatures favor grain growth and lead to a change in grain morphology towards equiaxed grains, resulting in a strength degradation although the density remains nearly constant.

1.4.5 Fracture Toughness

At room temperature, the mechanical properties of dense Si_3N_4 materials are mainly controlled by two microstructural parameters: average aspect ratio of elongated β -grains and the overall grain size.

There are still some arguments about which parameter is the most important. Mitomo and Uenosono [80] found that in Y2O3-Al2O3 system, even though the material had a smaller aspect ratio, an increase in fracture toughness was still observed because of an increased grain diameter. This suggests that the diameter of the elongated grains are more important than the aspect ratio. Higher fracture toughnesses can be obtained when the grain morphology has a large diameter with a high aspect ratio. It was explained that at larger grain sizes, residual stresses from the thermal expansion anisotropy of the Si₃N₄ grains will start to affect the glass/Si₃N₄ interface. These residual stresses will weaken the interface, thus enhancing the amount of grain bridging and pull-out, resulting in the increase of fracture toughness. But the residual stress will cause extensive microcracking of the material when the grains are large enough. However, Wötting and Ziegler [81] suggested that the major factor controlling fracture toughness up to 1000°C is the aspect ratio of the β -grains. Higher aspect ratio β -grains provide higher resistance to crack growth because of the absorption of energy, crack deflection and pull-out effects.

The formation of elongated grains is a necessary, but not sufficient condition to produce a high fracture toughness in ceramics. In addition to the formation of elongated grains, the glass chemistry and interface properties are critical, especially at high temperature.

Because of the softening of the glassy phase at higher temperatures, a decrease in strength, toughness, creep and oxidation resistance has been observed at temperatures above 1000°C [82].

1.4.6 Development

Further development of dense $\mathrm{Si}_3\mathrm{N}_4$ is mainly concentrated on the following goals:

- (a) to develop less-expensive processing techniques for complex-shaped components in order to use $\mathrm{Si}_3\mathrm{N}_4$ on a broader scale.
- (b) to improve the high-temperature properties by optimizing the grain boundary characteristics.

2.1

2.1.1

was

The

synt

(SiC

resu

μm.

part

The

2. EXPERIMENTAL PROCEDURE

2.1 About Starting Powder

2.1.1 Si₃N₄ Powder

The Si_3N_4 powder used in this project is SN-E10 by UBE Industries, LTD. of Japan. It was produced by an imide decomposition process which involed three steps [83]: (a) synthesis of silicon diimide ($Si(NH)_2$) by the ammonolysis of silicon tetrachloride ($SiCl_4$), (b) calcining $Si(NH)_2$ at about $1000^{\circ}C$ to produce amorphous Si_3N_4 , and (c) converting amorphous Si_3N_4 to α - Si_3N_4 powder by heating to a higher temperature. The resulting SN-E10 is uniformly equiaxed α - Si_3N_4 powder with average particle size of 0.2 μ m. The oxygen content of this Si_3N_4 powder was controlled by regulating the oxygen partial pressure in the nitrogen gas during calcination and crystallizing heat-treatment. The typical characteristics of an SN-E10 powder are listed in Table 2.1.

Table 2.1 Typical Characteristics of UBE SN-E10 Powder Supplied by the Manufacturer.

Chemical composition	
N (wt%)	38.6
O (wt%)	1.22
C (wt%)	~0.1
Cl (ppm)	<100
Fe (ppm)	<100
Ca (ppm)	<50
Al (ppm)	<50
β/(α+β) (wt%)	<5
Specific surface area (m ² /g)	10.7
Density (g/cm ³)	3.44

2.1.2

The

Co.,

2.1... Yttr

a m

2.1.

Che

Al₂

2.2

0.0

Αp

sus

TI)

2.3

MJ.

diff

--

2.1.2 SiC Whisker

The SiC whisker (TWS-100) used in the experiments was produced by Tokai Carbon Co., Japan. The characteristics of the SiC whiskers are shown in Table 2.2.

2.1.3 Y₂O₃ Powder

Yttria powder, supplied by Rhône-Poulenc Basic Chemicals Co., is 99.99% pure and has a manufacture's reported particle size of 1~3 µm.

2.1.4 Al₂O₃ Powder

Al₂O₃ powder used in the experiments was AKP-50, produced by the Sumitomo Chemical Co.,LTD. of Japan.

2.2 TEM Observation of SiC Whiskers

0.01 g of SiC whiskers were weighed and ultrasonically dispersed in 150 ml of ethanol. A prepared copper grid coated with carbon holey film was dipped into the SiC whisker suspension, air dried, and examined in a Hitachi 800 transmission electron microscpe (TEM).

2.3 ESA Measurement

When an alternating electric field is applied to a colloidal dispersion, the particles will move in the electric field because of their net zeta potential. If there is a density difference between the particles and the liquid, this oscillatory motion of the particles will

Table 2.2 Typical Characteristics of TWS-100 SiC Whisker as Supplied by the Manufacturer.

Impurities (wt%)	
SiO_2	0.5
Ca	0.05
Co	0.05
Fe	0.05
Cr	0.05
Mg	0.02
Al	0.08
Crystal Type	β
Diameter (µm)	0.3~0.6
Length (µm)	5~15
Aspect Ratio	10~40
Density (g/cm ³)	3.20
Bulk Density	0.06~0.12
Specific Surface Area (m ² /g)	2~4
SiC Content (wt%)	99
Particulate Content (wt%)	<1
Coefficient of Thermal	5.0
Expansion from RT to 1400° C (× 10^{-6} /°C)	

Table 2.3 Typical Characteristics of AKP-50 Al₂O₃ Powder as Supplied by the Manufacturer.

Crystal Form	α
Purity	99.995%
Particle Size	0.1~0.3
Loose Bulk Density (g/cm³)	0.6-1.1
Pack Bulk Density (g/cm ³)	0.9-1.3
Density (g/cm³)	3.98
Specific Surface Area (m²/g)	2.5-4.5
Impurity (ppm)	
Si	≤25
Na	≤10
Mg	≤10
Cu	≤10
Fe	≤20

result in

This eff

pressur

was co

ESA 8

amplit

where

and

Note

.

result in the transfer of momentum to the liquid and the development of an acoustic wave. This effect has been termed the Electrokinetic Sonic Amplitude or ESA, which is the pressure amplitude generated by the colloid per unit electric field strength. The ESA data was collected and converted to zeta potential automatically by the computer controlled ESA 8000 system from Matec Applied Sciences. The equation for converting the ESA amplitude to zeta potential is:

$$\zeta = \frac{ESA\eta}{\varepsilon \phi \Delta \rho c} G(\alpha)^{-1}, \qquad (2.1)$$

where

$$G(\alpha) = \left[1 - \frac{i\alpha\left(3 + \frac{2\Delta\rho}{\rho}\right)}{9\left(1 + \left(1 - i\right)\sqrt{\frac{\alpha}{2}}\right)}\right]^{-1},$$
 (2.2)

and

$$\alpha = \frac{\omega a^2}{v} = \frac{\omega a^2 \rho}{\eta} . \tag{2.3}$$

Note that

 ω = angular frequency c = velocity of sound in the suspension $\Delta \rho$ = density difference between the particles and the liquid ϕ = volume fraction of the particles ϕ = dynamic or high frequency electrophoretic mobility ϕ = particle radius ϕ = dielectric permittivity of the suspension ϕ = kinematic viscosity of the liquid ϕ = viscosity of the liquid, and ϕ = zeta potential of the particle.

Suspens

from pl

2.4 Pa

The par

a fixed

time 'i'

where

The pe

were c

where

Suspensions of 5 vol% solid were prepared and the titration performed automatically from pH values of 2 to 11 by addition of HNO₃ or NaOH.

2.4 Particle Sizing

The particle size of the Si_3N_4 powder was measured by the Andreson pipette method. A suspension is placed in a cylindrical vessel and samples collected of a fixed volume from a fixed distance below the surface at specific times. The size of the solids removed at a time 't', is determined from Stokes' law:

$$d = \sqrt{\frac{18h\eta}{g(D_1 - D_2)t}},$$
 (2.4)

where

d = diameter of coarsest particles which remain in suspension at a depth below h and at a time t (cm)

 η = liquid viscosity

h= height below the surface of the suspension (cm)

 $D1 = \text{density of particles (g/cm}^3)$

D2 = density of liquid (g/cm³)

 $g = acceleration of gravity = 980 cm/s^2$

t = time (sec).

The percent undersize of sample is calculated at each of the specific times that samples were drawn with the equation:

$$%Undersized = \frac{W_1 V_2}{W_2 V_1} \times 100\%,$$
 (2.5)

where

 W_I = weight of solids in sample withdrawn

 W_2 = weight of total solids in cylinder at time of sample drawing

 V_I = volume of the sample drawn, and

 V_2 = volume in the cylinder at the time of drawing.

The pro

to disp

design

glass (

all of

shake

14 hr.

pre-w

each 24 hr

perce

2.4 a

who bec The procedure of particle sizing is described as follows: 475 ml of deionized (DI) water was first adjusted to have a 10⁻⁴ N KNO₃ at pH=10.5. 300 ml of this liquid was then used to disperse 5 g Si₃N₄ powder in a glass beaker. After certain minutes (depends on the design of the experiment) of ultrasonic dispersion, the suspension was moved to a 500 ml glass cylinder. The remainder of prepared liquid was used to wash the beaker to capture all of the remaining Si₃N₄ powder and to fill the cylinder to 475 ml. This sample was shaken for 2 minutes. Samples of suspension were collected after 15 min, 40 min, 2.5 hr, 14 hr, 42 hr, 138 hr, 209 hr, 288 hr,351 hr and 479 hr. Each sample was placed into a pre-weighed 50 ml beaker, making sure the pipette was washed with distilled water after each sample was poured into the beakers. The beakers were then placed in a furnace for 24 hr. to evaporate the water and then re-weighed. The maximum particle size and percent undersized were calculated for each fixed time of sample removal using equation 2.4 and 2.5. For this experiment, equation 2.4 can be simplified as

$$d = 192\sqrt{\frac{1}{t}}\tag{2.6}$$

where maximum size 'd' in μ m and time of sample removal, 't', in seconds,

because

 $\eta_{\text{water}} = 0.0082 \text{ poise}$ h = 6 (cm) $D1 = \text{density of Si}_3\text{N}_4 = 3.44 \text{ (g/cm}^3\text{)}$ $D2 = \text{density of water} = 1.0 \text{ (g/cm}^3\text{), and}$ $g = \text{acceleration of gravity} = 980 \text{ cm/s}^2\text{.}$

SUS

aı

T

m

ca

ad

po

SU

2.5 Sedimentation Observation

The stability of the suspensions at different pHs can be directly observed by sedimentation. A suspension of 5 vol% solids was first prepared at 10⁻⁴ N KNO₃. The pH of this suspension was then adjusted from 2 to 11. At each integral number, the suspension was ultrasonicated for 2 minutes and 14 ml of suspension was removed to a test tube. After all samples from ten pHs were removed, the tubes were plugged and left undisturbed for a week or one month for SiC whisker or Si₃N₄ powder, respectively. The sedimentation densities at each pH were calculated from the known weight of the solid and the volume of sediment in each tube.

2.6 Slip Preparation

The slips for casting were prepared with 50, 55, 60, 65 wt% deionized (DI) water for monolithic Si₃N₄, 10, 20, 30 vol% whisker samples respectively. The solids were first calculated and weighted. The exact amount of DI water was measured and placed in a beaker of suitable size. Electrolyte concentration of the liquid was adjusted to 10⁻⁴ N and adjusted to the desired value by adding HNO₃ or NaOH. Then the solids were slowly poured into the liquid while the suspension was magnetically stirred. The pH of the suspension was monitered and held constant. After all solids were poured into the suspension, the whole suspension was transferred to a container for ball milling.

2.6.1

Ball

size a

close its ax

the m

broke

for ba

2.6.2

The s

for 5

suspe

Was 1

cerar

calle

press

enou

ultra

supp

2.6.1 Ball Milling

Ball milling is the most common method used in the ceramic industry to reduce particle size and deagglomerate. Ball milling consists of placing the particles to be ground in a closed cylindrical container with grinding media and rotating the cylinder horizontally on its axis so that the media cascade. The ceramic particles or agglomerates move between the much larger grinding media and between the media and the wall of the mill and are broken into successively smaller particles. In this experiment, a nalgene bottle was used for ball milling with Al₂O₃ grinding media. The slips were adjusted to pH 11 and ball milled for 48 hours.

2.6.2 Ultrasonication

The slip was then transferred from the ball mill to a beaker and ultrasonically dispersed for 5 periods of 4 minutes each (a total of 20 minutes) in an ice bath in order to keep the suspension cool during ultrasonication. Following the ultrasonication, the suspension was ready for slip casting. Ultrasonication is effective in dispersing submicron size ceramic particles [25]. It is known to break up agglomerates by creating small bubbles, called "cavities", which collapse violently and produce local, high velocity jets and pressure gradients. The resulting mechanical forces on the agglomerates are strong enough to break up weakly bonded particles [26]. The device used to perform ultrasonication in this experiment is a Branson Sonifier 250 which consists of a power supply, a converter and a horn. With the tip of the horn immersed at about 6 to 13 mm in

the sus

suspen

2.7 V

The v

II. Th

spind

spring

flow.

A sus

centi

Visco

2.8

Slip

has I

geor

 m_0

Wall

the suspension, an output of 120 W with 20 kHz ultrasonic waves was applied to the suspension.

2.7 Viscosity Measurement

The viscosity of the slip was measured using a Brookfield Digital Viscometer Model DV-II. The viscometer measures the torque required to rotate an immersed element (the spindle) in a fluid. The spindle is driven by a synchronous motor through a calibrated spring. For a given spindle geometry and speed, an increase in viscosity, or resistance to flow, will be indicated by an increase in the deflection of the spring.

A suspension of at least 250 ml was used in a 400 ml beaker to immerse the spindle of viscometer. Slips were prepared following the method described above. Five readings in centipoise (cps) were taken for each data point using spindle #1 at a speed of 100 rpm. Viscosities of slips at varying pHs and SiC whisker content, were measured.

2.8 Slip Casting

Slip casting is one of the oldest shape-forming techniques used in traditional ceramics. It has been introduced to advanced ceramics because it permits the formation of complex geometries. During slip casting, a slip or suspension, is poured into a plaster mold. The mold extracts the fluid and forms a compact of close-packed particles along the mold walls due to capillary forces present within the pores, causing a partial vacuum.

2.8.1

250 g ; was st

was le

minute mold

one da

castin

2.8.2

Two o

poure

This I

The s

2.9

Cold

geom

Thus

specia

used

2.8.1 Making Plaster Molds

250 g plaster of Paris powder were weighed and poured into 165 ml water. The mixture was stirred completly to make sure that all the powder were wetted and no agglomerate was left. The plaster was then poured into a weighing dishes with a wait for about 5 minutes. A negative mold was inserted before the plaster got thickenned, and the negative mold was kept at about 5 mm from the bottom of the weighing dish. After air drying for one day, the negative mold was removed and the plaster mold was cut into half for slip casting.

2.8.2 Casting

Two different slip casting methods may by distinguished: drain-casting and solid casting. The specimens used for this experiment were prepared by solid casting. The slip is poured into the mold and water is sucked out where the slip is in contact with the mold. This leaves a close-packed layer of particles growing into the slip from the mold walls. The slip is continually added until a solid casting is achieved.

2.9 Cold Isostatic Pressing

Cold isostatic pressing (CIP) is one of the shape-forming methods for complex geometries. It involves application of pressure equally to the powder from all sides.

Thus, problems of non-uniformity can be overcome. The isostatic pressure acting on the specimens is transferred via a non-compressible fluid in a pressure vessel. The device used in this experiment is made by Iso-Spectrum, Inc. The slip-cast green specimens

were pl

cylinde

was pre

were th

2.10

All sar

Therma

in a B.

at a he

A cool

2.11

2.11.1

The gr

a calip

green (

Five sp

five sp

were placed in deformable rubber bag. Air in the rubber bag was removed using a cylinder before the bags were tied. Double rubber bags were used to ensure that the fluid was prevented from penetrating into the specimens during pressurization. The specimens were then immersed in the fluid and pressure was increased to 350 MPa for two minutes.

2.10 Pressureless Sintering

All samples were sintered in a high temperature graphite furnace, model 1000-4560 by Thermal Technology Inc., in a flowing N₂ gas atmosphere. The samples were embedded in a BN powder bed in a graphite crucible and heated from room temperature to 1200°C at a heating rate of 10°C/min, and from 1200°C to a designated temperature at 5°C/min. A cooling rate of 15°C/min followed each sintering cycle.

2.11 Density Measurement

2.11.1 Green Density Measurement

The green specimens were first sanded to rectangular shapes and dimensions measured by a caliper to calculate the volume of the specimens. After the specimens were weighed, green densities were obtained by dividing the weight of the specimens by its' volume. Five specimens were measured for each green density data point. At each formulation, five specimens were measured for green density.

2.11

The

to di base

wipe

At e

The

2.11

the sint

oft

Du

In t

be :

gla Y₂(

N₇0

2.11.2 Sintered Density Measurement

The sintered specimens were weighted to obtain D_{dry} , and then boiled in water for 30 min. to drive off the air in the open pores. Suspended weights D_{sus} , were measured by a set up based on Archimedi theory. Then the specimens were weighed, with the surface water wiped off, to obtain D_{wel} . The sintered densities were calculated using equation 2.7.

$$D_{\sin} = \frac{D_{dry}}{\left(D_{wet} - D_{sus}\right)}. (2.7)$$

At each formulation, three specimens were measured for sintered density.

2.11.3 Theoretical Density Calculation

Theoretical densities for green compacts were calculated directly from the proportion of the raw materials. For sintered products, because of microstructural changes during sintering, the formation of the oxynitride glass needs to be considered in the calculation of the theoretical density.

During sintering, Si₃N₄ and Al₂O₃ are believed to react as follows [84]:

$$7.9Si_3N_4 + 0.2Al_2O_3 \rightarrow 4Si_{5,9}Al_{0,1}O_{0,1}N_{7,9}(sialon) + 0.1SiO_2$$
 (2.8)

In the oxynitride glass of the Si-Al-Y-O-N system [85], nitrogen in glass was thought to be supplied by dissolution of Si_3N_4 , which corresponded to 17.5 wt% of the oxynitride glass. Based on the above estimation, the theoretical density of 8Y2A Si_3N_4 (8 wt% Y_2O_3 , 2 wt% Al_2O_3) was calculated as follows. The Si_3N_4 starting powder contained 2.5 wt% SiO_2 : $90\times(1-0.025)=87.75$ wt% Si_3N_4 and $90\times0.025=2.25$ wt% SiO_2 . Si_3N_4 reacted

with 1.0

of oxid

wt%. S

the den

the theo

3.293 a

2.12

The spe

speed c

using S

•

Al₂O_{3]}

2.13

A S-25

surface

Specim

minute

with 1.6 wt% Al_2O_3 to form 88.87 wt% sialon and released 0.48 wt% SiO_2 . The amount of oxide components of the glass was $SiO_2+Al_2O_3+Y_2O_3=(2.25+0.48)+0.4+8.0=11.13$ wt%. Si_3N_4 dissolved to form $11.13\times(1+0.175)=13.1$ wt% oxynitride glass. Assuming the density of sialon and the oxynitride glass were 3.19 and 4.00 g/cm³ [86], respectively, the theoretical density of the 8Y2A Si_3N_4 was evaluated as 3.296 g/cm³. For products with 10, 20 and 30 vol% SiC whisker, the theoretical densities were calculated as 3.295, 3.293 and 3.292 g/cm³, respectively.

2.12 Cutting and Polishing

The specimens for Vickers hardness measurements were first cut using Accutom-5, high speed diamond cutting wheel machine at a speed of 3000 rpm. They were then sanded using SiC paper in the order of 240, 320, 400 and 600 grit followed by polishing with Al_2O_3 powder in the order of 600 grit, 5.0 μ m, 0.3 μ m and 0.05 μ m.

2.13 **SEM**

A S-2500C scanning electron microscope (SEM) was used to observe the fracture surfaces of both green and sintered samples and the polished surface of sintered samples. Specimens were attached to SEM mounts by conductive carbon tapes, followed by 3 minutes of gold coating. SEM pictures were taken at an accelerating voltage of 15 kV.

2.14 X

X-ray di Scintag

accelera

was det

and Kar

The inte

case of

2.15

The har

head sp

calcula

 $\quad \text{where} \quad$

impres

Dutta e

2.14 X-ray Diffraction (XRD) and Phase Content (F_{α}) Calculation

X-ray diffraction measurements were performed using bulk specimens by XDS 200^{TM} by Scintag Inc., with Cu K_{α} radiation at a scanning rate of 2° /min. Filament current and accelerating voltage were set at 25 mA and 35 kV respectively. The α -Si₃N₄ content, F_{α} , was determined from the XRD peak intensities using equation 2.6 proposed by Suzuki and Kanno [84][85].

$$F_{\alpha} = 1.898 \frac{\left(I_{\alpha(102)} + I_{\alpha(210)}\right)}{1.898\left(I_{\alpha(102)} + I_{\alpha(210)}\right) + \left(I_{\beta(101)} + I_{\beta(210)}\right)}.$$
 (2.9)

The integrated diffraction intensity I can be approximated by using peak height in the case of $Si_3N_4[86]$.

2.15 Microhardness and Toughness Measurement

The hardness of the samples were measured by Vickers indentation method with cross head speed of 70 μ m/sec and 15 second loading time. The fracture toughness, K_{Ic} , is calculated using the following relationship:

$$K_{lc} = 0.057 H \sqrt{q} \left(\frac{E}{H}\right)^{2/5} \left(\frac{C}{q}\right)^{-3/2},$$
 (2.10)

where H is the Vickers hardness, 'q' is one-half the length of the diagonal of the Vickers impression, and C is one-half the median crack length, as proposed by Singh $et\ al.$ [87]. Dutta $et\ al.$ [88] reported that elastic modulus E has a relationship with porosity p as

$$E = E_o \cdot e^{-3.06p} \tag{2.11}$$

where E_o is the elastic modulus of fully dense materials. Desmarres *et al.* [89] have reported that the presence of 30 vol% SiC whiskers increased Young's modulus by 20%. Assuming E_o for monolithic Si₃N₄ is 310 GPa [46], and 10, 20 and 30 vol% whiskers will increase the elastic modulus by 7, 13 and 20%, the E_o of 332, 350 and 372 GPa will be used for 10, 20 and 30 vol% whisker samples. Five measurements per sample were taken for hardness and fracture toughness calculation.

3. RESULTS AND DISCUSSIONS

3.1 TEM Observation of SiC Whiskers

From TEM observations, the SiC whiskers used in this project have several types of morphological features. The diameter of the whiskers observed ranged from $0.4 \sim 0.8$ μm with a miximum length of 30 μm . The majority of the whiskers were relatively straight and had a smooth surface, but about 20 % of them were branched or bent with irregular surfaces (Figure 3.1 and 3.2). Whiskers connected with SiC aggregates were also observed.

Diffraction patterns showed that all the whiskers observed had FCC structure (Figure 3.3) with {111}growth axis. Most of the whiskers had parallel lines perpendicular to the axis of the crystal which may be an indication of high density of stacking faults (Figure 3.4a). However, the very sharp spot from (111) plane in Figure 3.4b verifies that the interplaner distance between successive close packed layers was not at all disturbed. The streaks in the same picture are further evidence of the high density stacking faults.

3.2 Properties of SiC_(w)/Si₃N₄ Suspension System

3.2.1 Zeta Potential (ζ) and Stability Ratio (W)

Zeta potentials for both the Si₃N₄ powder and SiC whiskers were collected and plotted in Figure 3.5. The suspensions were prepared with 0.5 vol% solid, at a KNO₃ concentration of 10⁻⁴ M. Generally speaking, the Si₃N₄ powder has higher absolute zeta potential than

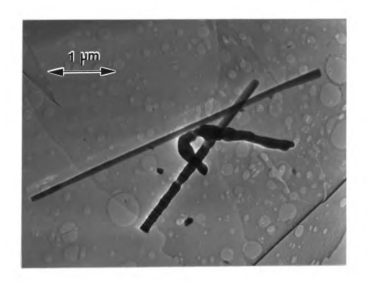


Figure 3.1 Some SiC whisker are bent and have irregular surface.



Figure 3.2 SiC whisker with several branches.

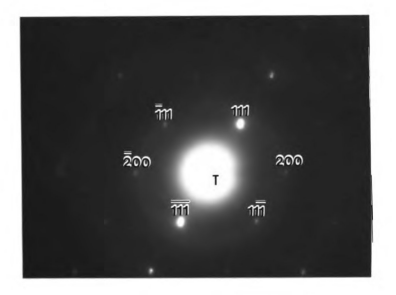
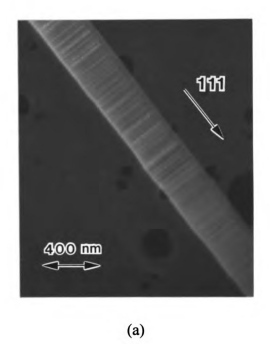


Figure 3.3 <011> zone selected area diffraction pattern of the SiC whisker.



1777 1775 - 1771 2003 - 1771 6178 - 2222 4222

Figure 3.4 (a) TEM bright field image of SiC whisker. (b) Selected area diffraction pattern of SiC whisker.

(b)

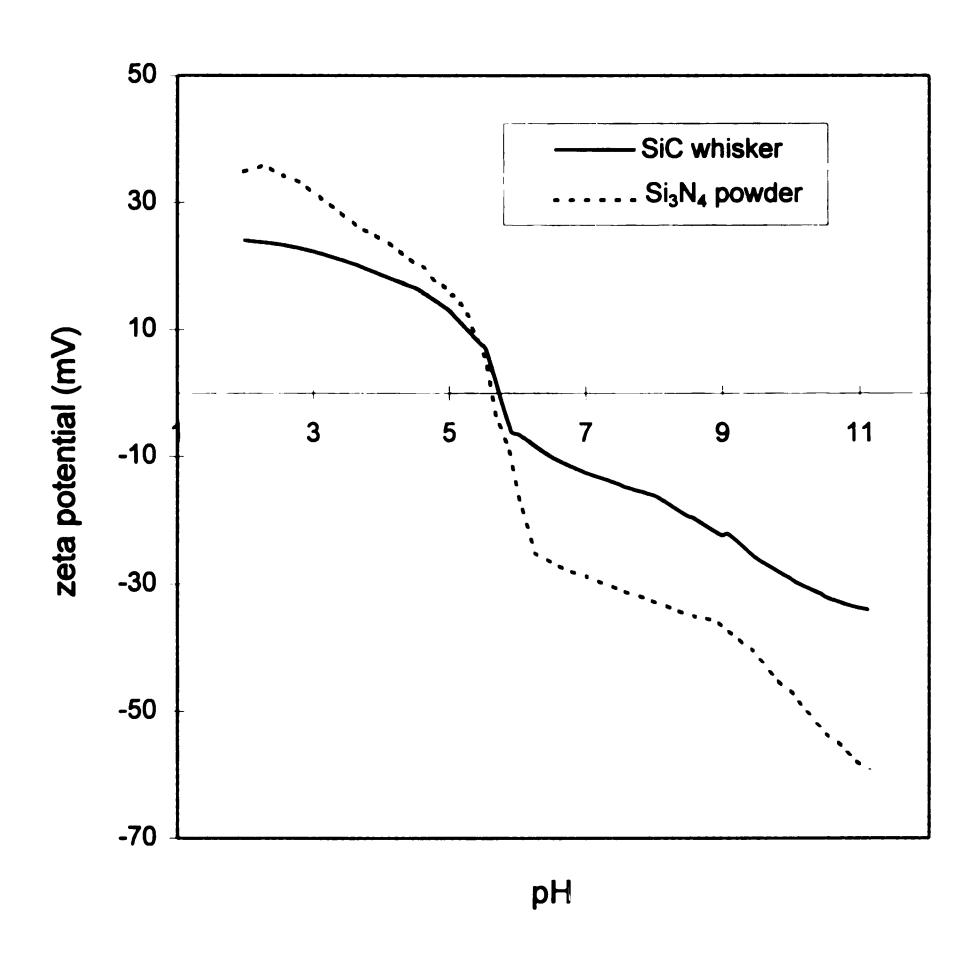


Figure 3.5 Zeta potential plot of SiC whisker and Si_3N_4 powder.

the SiC whiskers throughout the pH range tested. Both materials have positive potentials in acid solutions and negative potential value in base solutions. Further, they both have an isoelectric point (i.e.p.) [90] at a pH of about 6. The maximum potential values for both Si₃N₄ powder and SiC whiskers were found at pH=11 of 59 and 34 mV, respectively.

The stability ratio data was calculated by the previously developed computer program $Suspension\ Stability^{\odot}$ [22], based on stability calculations using the Hogg, Healy, and Fuerstenau theory [21]. Results from $Suspension\ Stability^{\odot}$ (Figure 3.6) indicate homostability for Si_3N_4/Si_3N_4 at pH 2-4.5 and pH \geq 6.5, homostability for Si_3N_4/Si_3N_4 at pH 2-4.5 and pH \geq 9.5. Therefore, at pH 11 the deagglomerated suspensions of Si_3N_4/SiC_w at pH \geq 9.5. Therefore, at pH 11 the deagglomerated suspensions of Si_3N_4 , $SiC_{(w)}$ and $Si_3N_4/SiC_{(w)}$ are each stable. Electrostatic repulsion between the particles is strong enough to set up a barrier which resists agglomeration between approaching particles. This assures that once primary agglomerates are broken apart, reagglomeration can be prevented. Thus, the optimum suspension pH value was chosen at 11. Another reseason to choose this pH is that one of the sintering additives used in this project, Y_2O_3 , is dissolvable in acids, but stable in base solutions.

3.2.2 Sedimentation Density

Sedimentation density represents the packing efficiency of the particles in suspension after undisturbed sedimentation. It is also a method to measure the dispersion efficiency

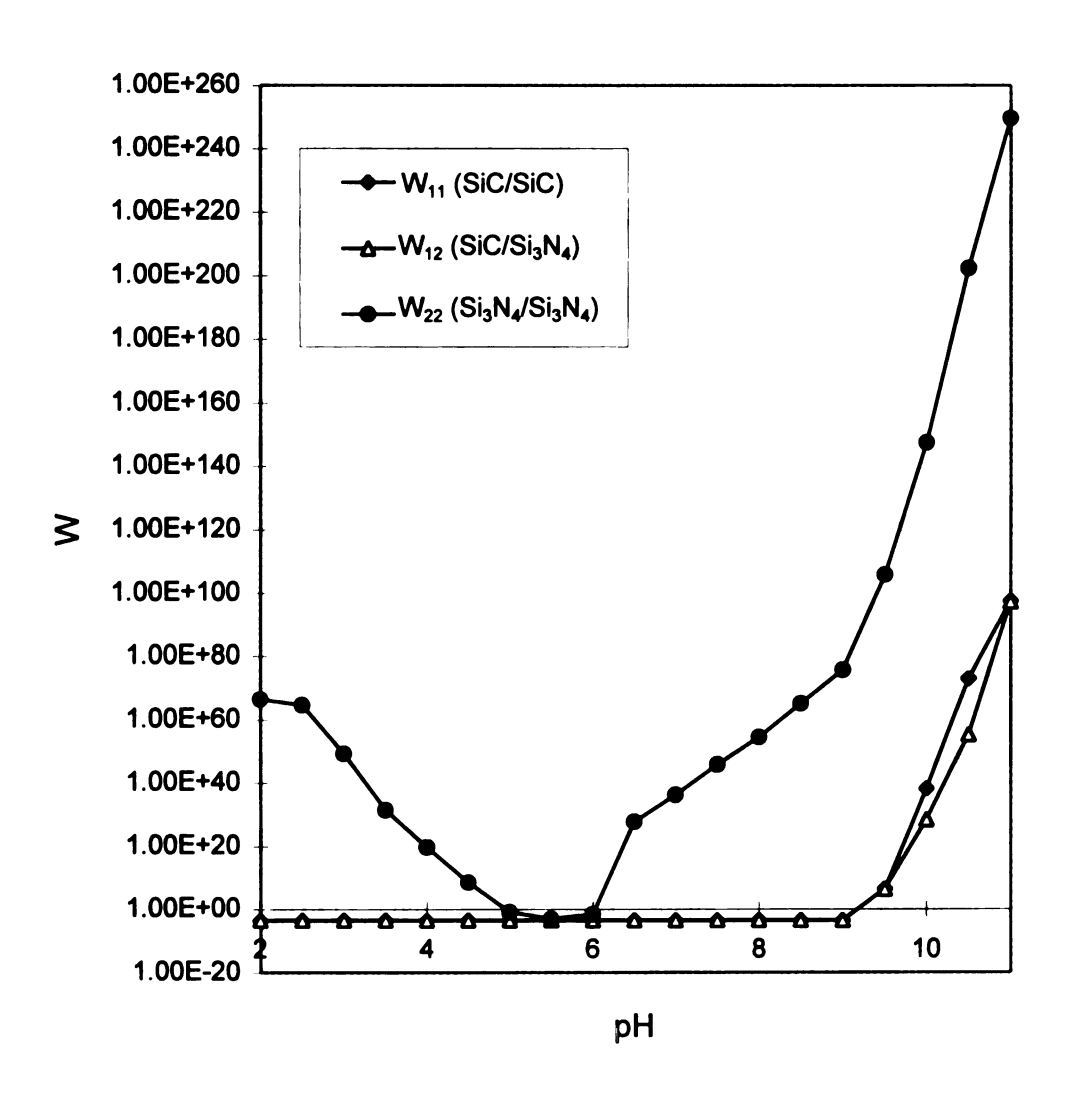


Figure 3.6 Stability ratio of $SiC_{(w)}/Si_3N_4$ suspension system.

in the suspensions. The higher the density, the more efficient the dispersion. Figure 3.7 and Figure 3.8 show the sedimentation densities of the Si₃N₄ powder and the SiC whiskers at different pHs. Both curves have shape of a bowl, which is high at the two ends and low in the middle. Also, the highest density was found at pH=11 for both materials, which matched the prediction based upon the stability ratio results. The sedimentation densities of Si₃N₄ were higher than those of the SiC whisker at all the measured pH ranges because of the aciculate shape of the whiskers.

3.2.3 Effect of pH on Green Density

The green density of ceramic compacts is very sensitive to agglomeration of ceramic powders [91]. It is known from the previous discussion of the stability ratio, that agglomerate free SiC_(w)/Si₃N₄ composite suspensions can be prepared at pH's≥9.5. There is still agglomeration existing in the acid region and strong agglomeration occurring when the pH of the suspension is close to the i.e.p.. The data in Figure 3.9 shows that specimens made at pH=11 have a higher green density than those prepared at pH=3 and 6. This is a good example of the effectiveness of the prediction by the *Suspension Stability*® program. Cold isostatic pressing can increase the density of all slip cast products, but it only reduces the density difference between specimens made at different pHs and does not change their density order.

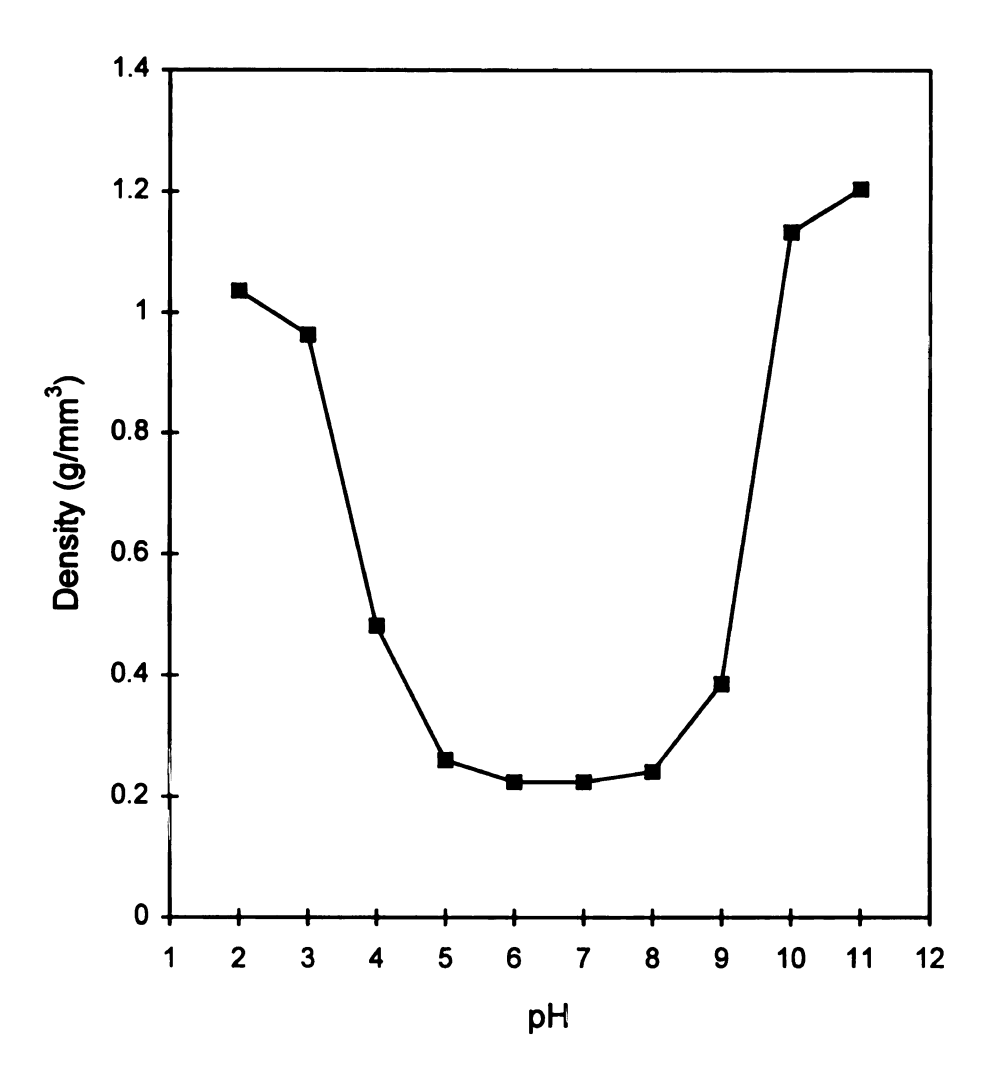


Figure 3.7 Sedimentation density of Si₃N₄ powder as a function of pH. Suspensions remained undisturbed for 4 weeks.

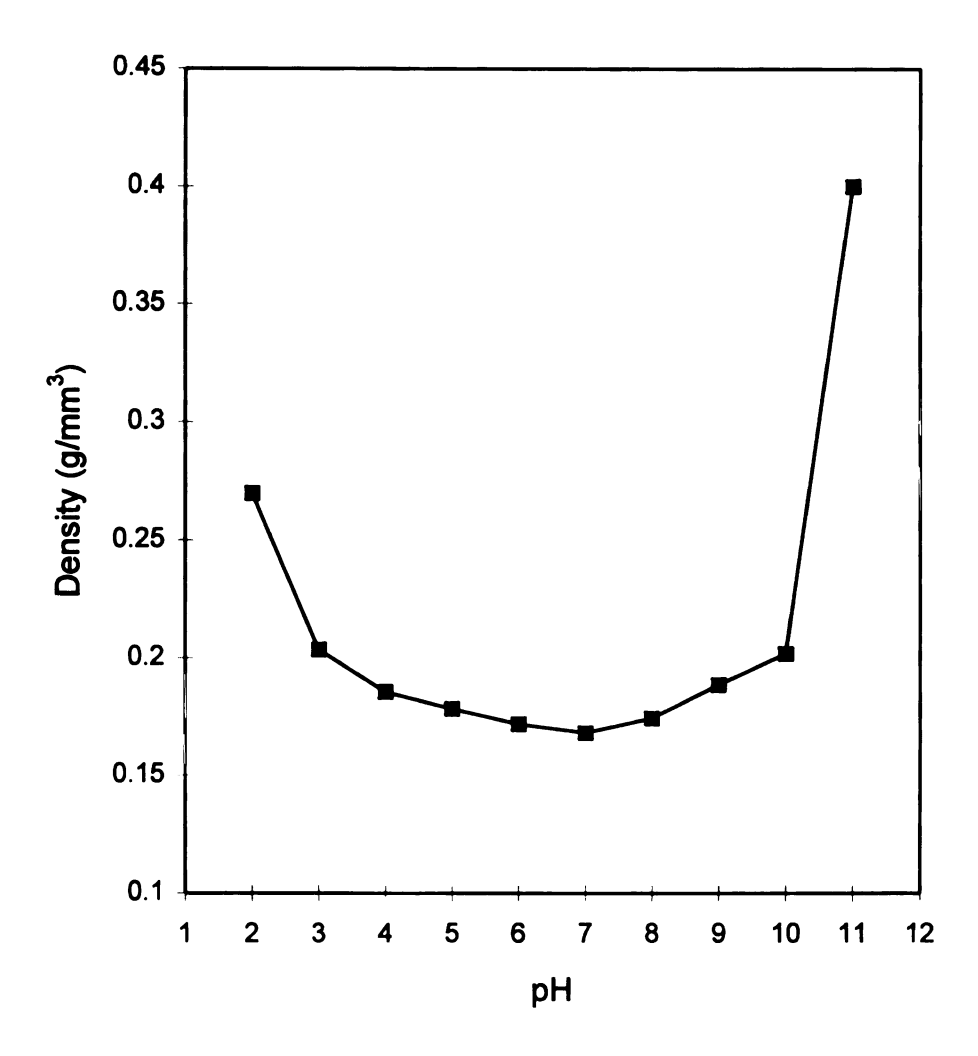


Figure 3.8 Sedimentation density of SiC whisker as a function of pH. Suspensions remained undisturbed for 1 week.

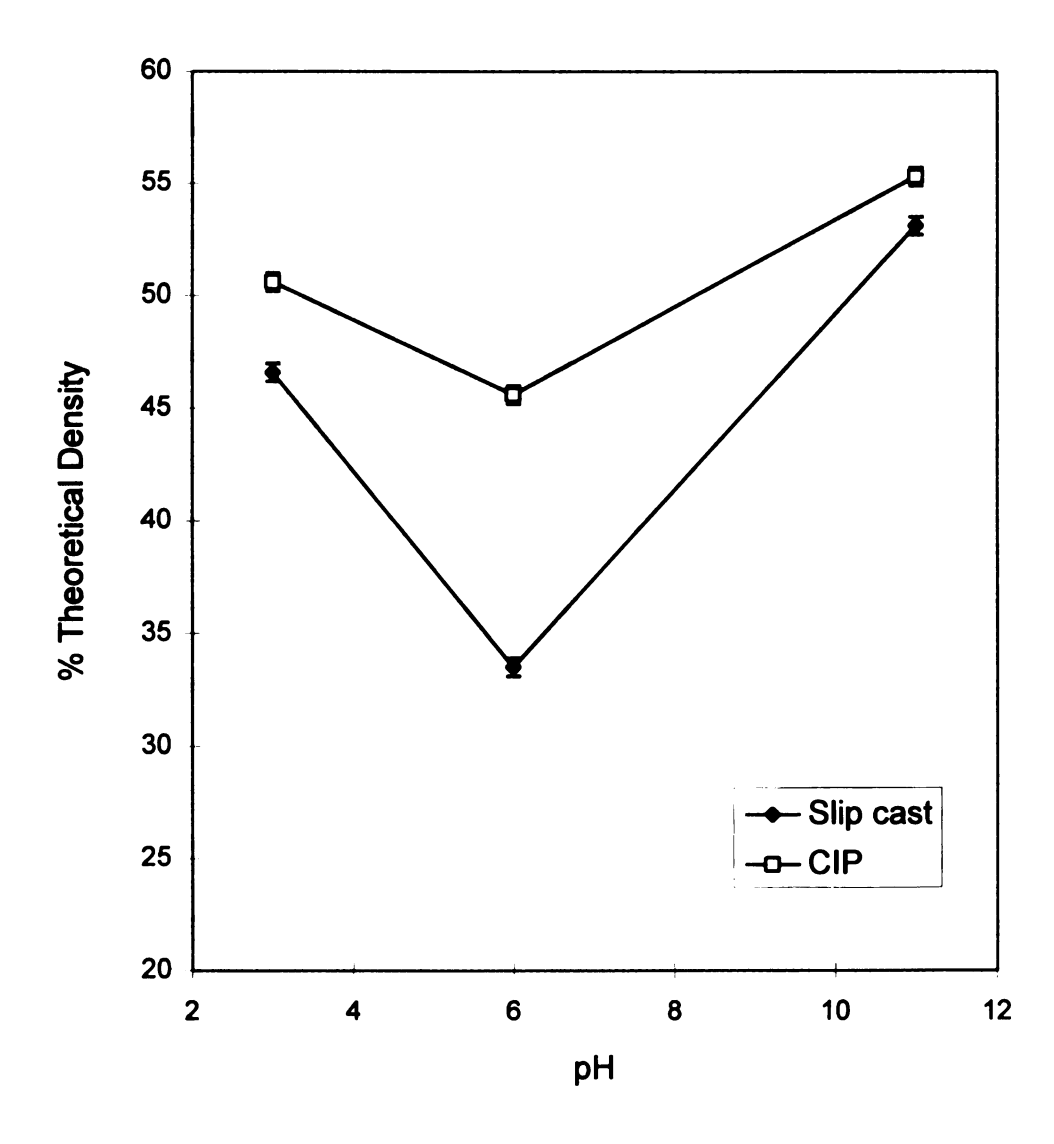


Figure 3.9 Effect of pH on green density. Slip prepared without ball milling.

3.2.4 Viscosity

The viscosity of a ceramic slip is strongly affected by agglomeration [92]. As shown in Figure 3.10, the viscosity is dramatically high at pH=6. This occurs because of the strong agglomeration compared to that of both the acid and base suspensions. Both of these suspensions have low viscosities, but the viscosity of the base suspension is the lowest.

Theoretically, SiC whiskers will have an effect on increasing the viscosity of a suspension because the acicular shape of the whiskers will increase the shear rate of the slip. But at pH=11, where the agglomeration can be prevented, SiC whiskers have not noticeably influenced the viscosity, as illustrated in Figure 3.11. The flow of the suspension is not retarded when the whisker content is increased from 10 to 30 $^{\text{v}}$ /_o.

3.3 Deagglomeration of SiC_(w)/Si₃N₄ System

3.3.1 Effect of Ultrasonication Time

Ultrasonication time is an important parameter in deagglomeration [91] as shown in Figures 3.12 and 3.13. From this data, the Si₃N₄ powder reached a finer particle size distribution as the ultrasonication time increased (Figure 3.12). It is also apparent that the slip cast green density (shown in Figure 3.13) likewise increases from 42 to 53 %TD as the ultrasonication time increases from 1 minute to 19 minutes. From this data it can be inferred that the green density increases dramatically in the first few minutes of dispersion indicating that agglomerates were broken up, while the size and number of the remaining agglomerates decreased. The density increase peaked at prolonged

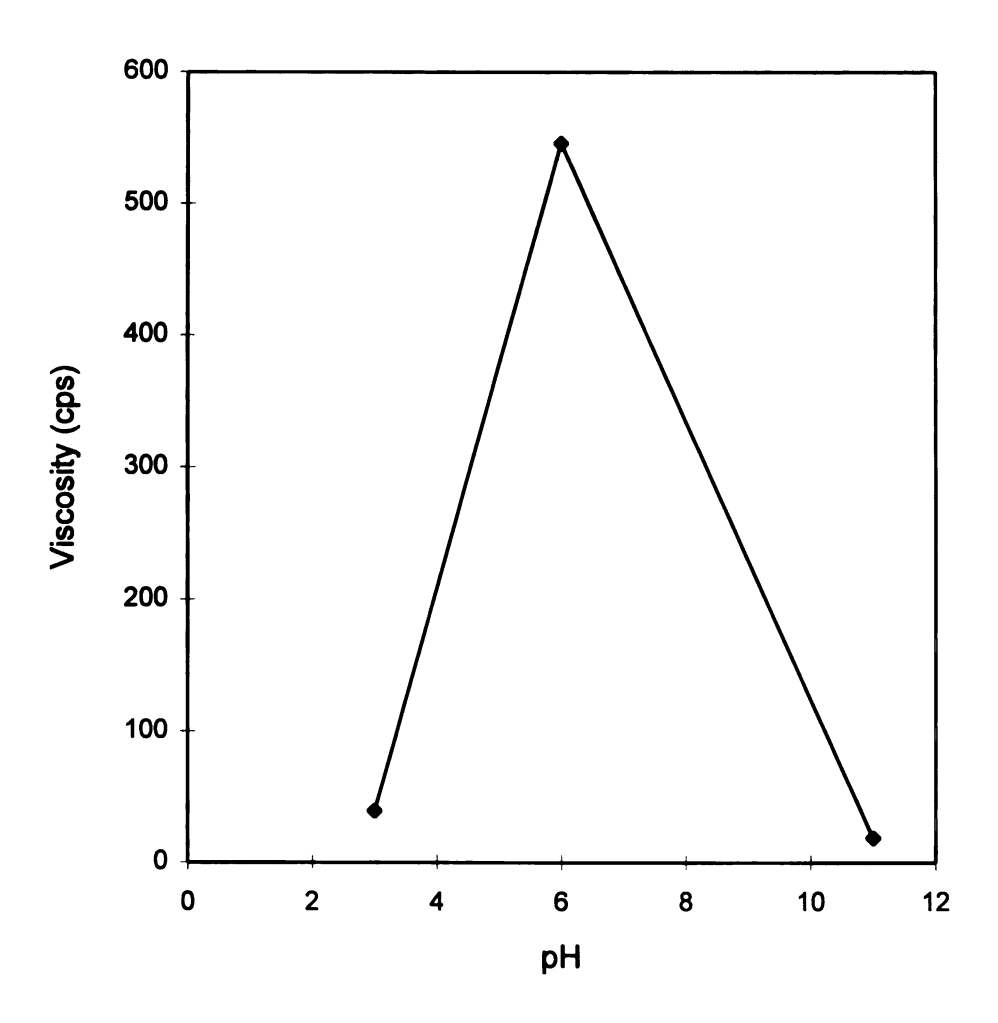


Figure 3.10 Effect of pH on viscosity of composite suspension. Slip prepared with 35 wt% solids with 20 vol% SiC whiskers.

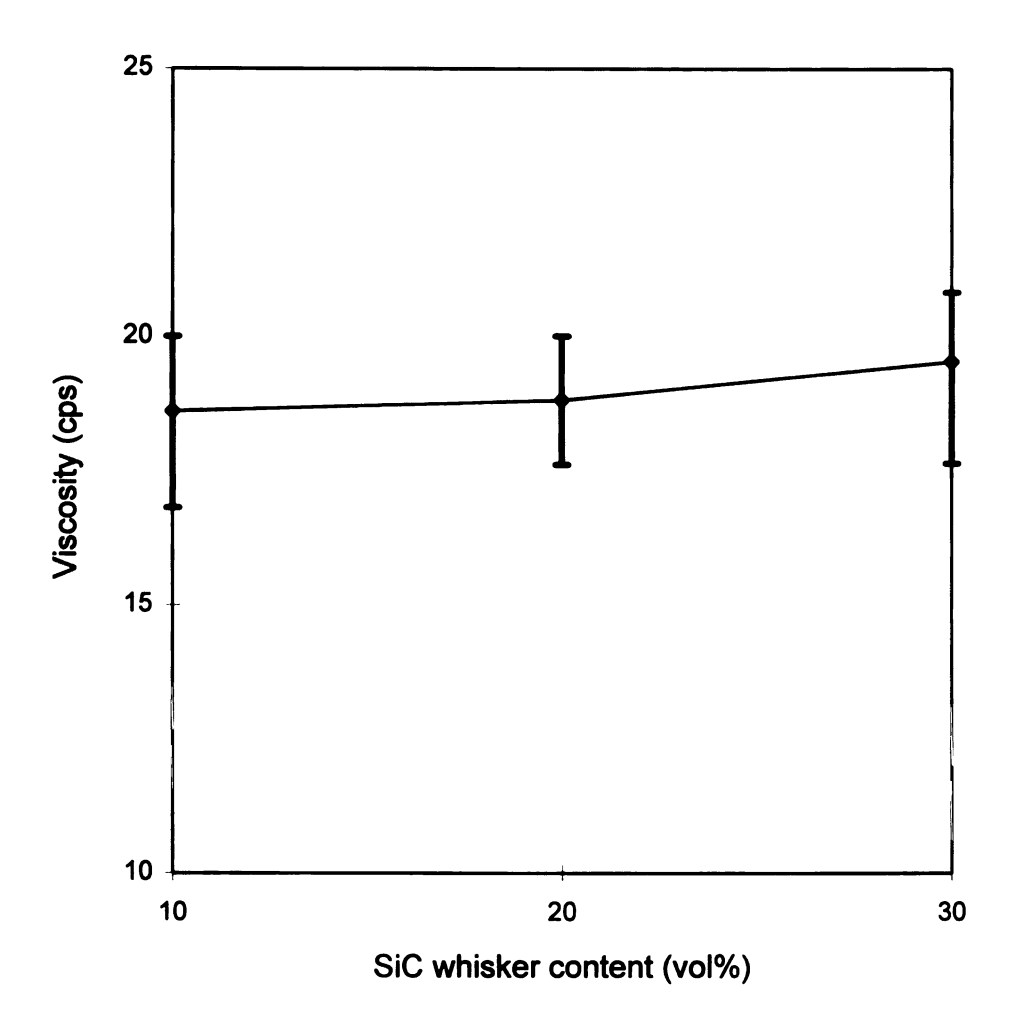


Figure 3.11 Effect of SiC whisker content on viscosity of composite suspension. Slip prepared at pH=11 with 35 wt% solids.

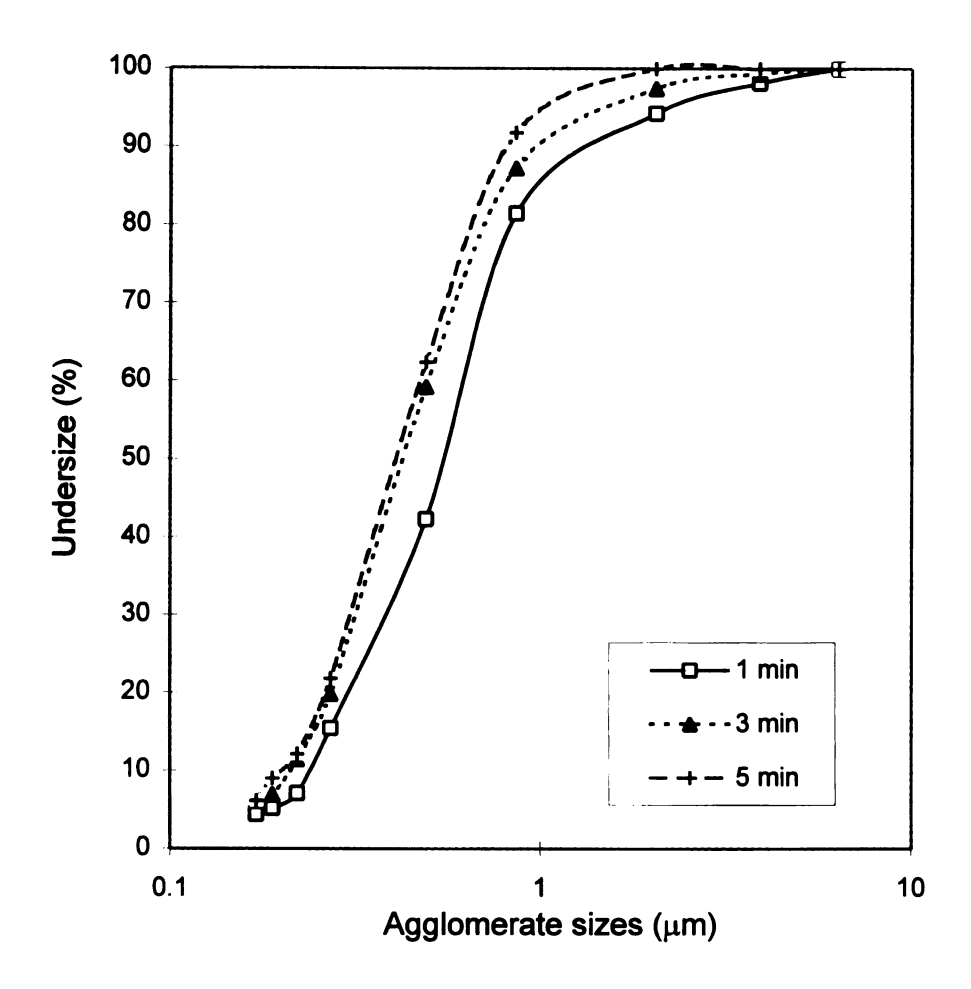


Figure 3.12 Effect of ultrasonication time on Si₃N₄ particle size.

Suspensions at pH=11 used for ultrasonication were composed of 5g powder and 300ml DI water with a electrolyte concentration of 10⁻⁴ M.

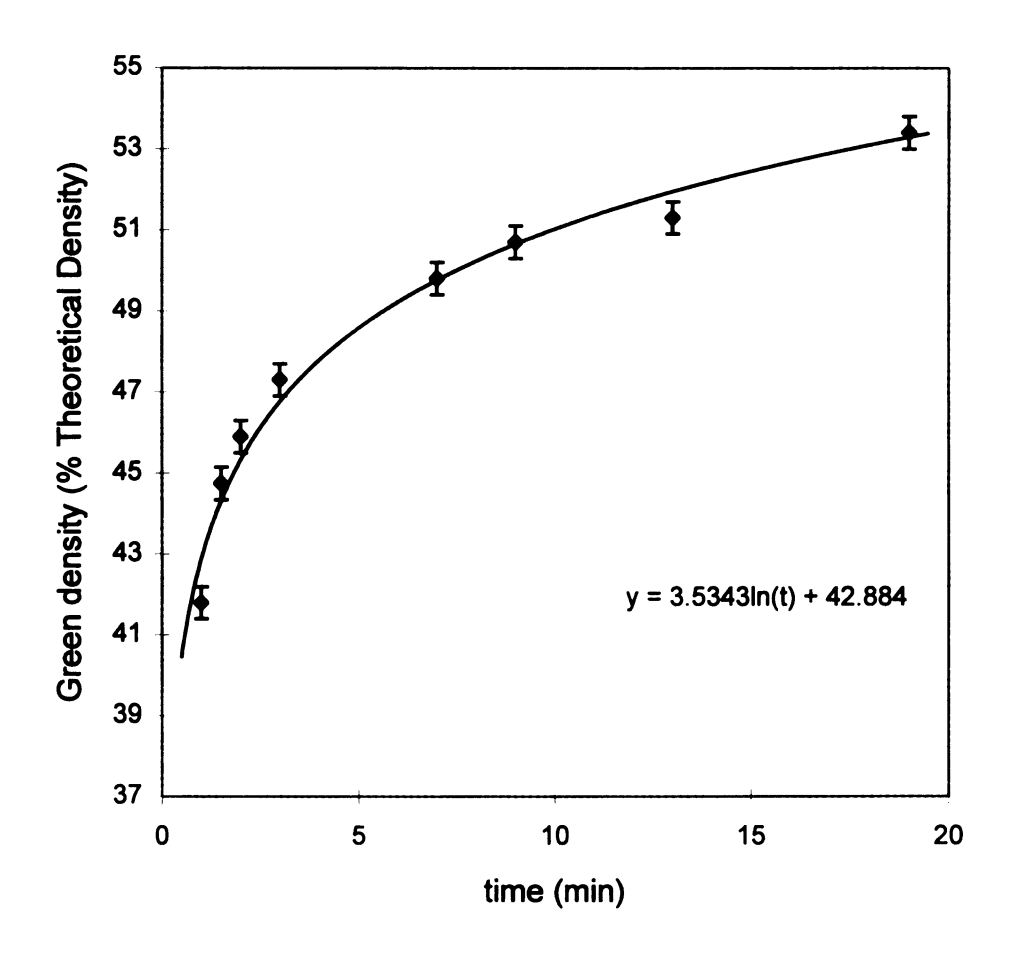


Figure 3.13 Ultrasonication time effect on slip casting green density of Si_3N_4 .

ultrasonication times (~10 min.) and reached a maximum after 20 minutes of ultrasonication. From these results, it is believed that the soft agglomerates were broken up in the first few minutes of ultrasonication. Subsequently, particles were gradually removed from the hard agglomerates, slowing the deagglomeration process. After 20 minutes of ultrasonication, all that remained were hard agglomerates called "aggregates" [92], which could not be eliminated by ultrasonication.

3.3.2 Effect of Ball Milling

Ball milling can be used to break up the hard agglomerates that ultrasonication failed to eliminate. During ball milling, the mechanical forces on the particles are much stronger than the ultrasonication-created "cavity forces". However, extensive ball milling will cause particles to be pressed together, forming new agglomerates bonded by van der Waals forces [5] as the particles move between the grinding media and the container wall. The slip cast green density of a Si₃N₄ compact which was ball milled is shown in Figure 3.14. The slip cast green density of the ball milled suspension is lower than that of an identically prepared suspension which was ultrasonicated. Density increases were only found when the suspension was ultrasonicated after ball milling (Figure 3.14). Two scenarios are possible for this increase. One is that the hard agglomerates were broken up by ball milling while the soft agglomerates, joined by van der Waals forces, were eliminated by ultrasonication. The second possibility is that ball milling broke the particles, changing the size distribution which led to the increases in packing in the green bodies. Figure 3.15 (a) and (b) show the Si₃N₄ particle size does not have obvious change after the ball milling, indicating the second possibility is probably insignificant.

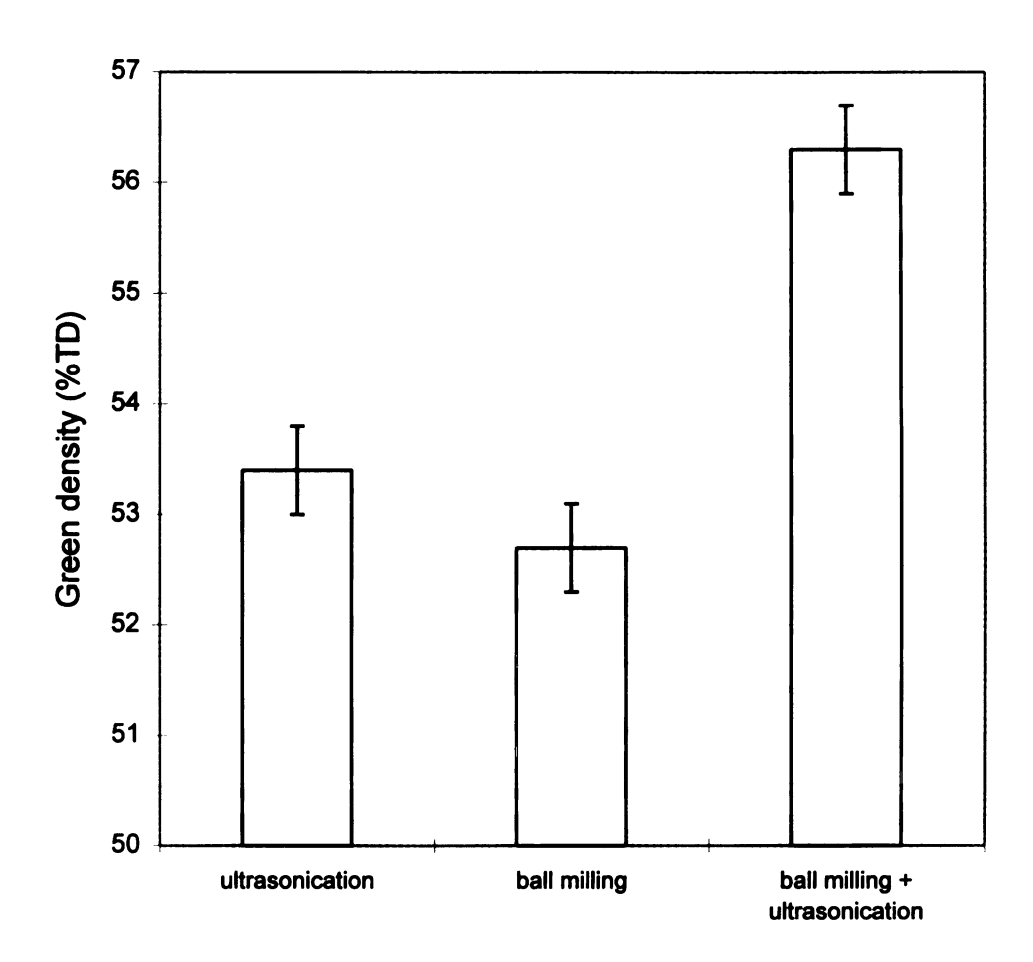


Figure 3.14 Effect of ultrasonication and ball milling on slip casting green density of Si_3N_4 .

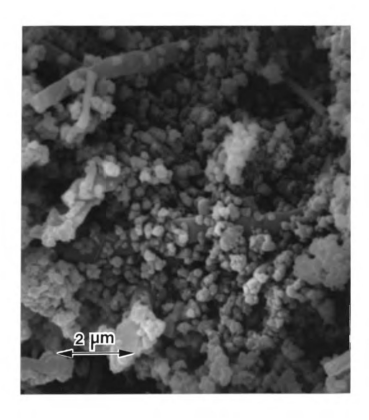


Figure 3.15 (a) SEM micrograph of $\mathrm{Si}_3\mathrm{N}_4$ composite green compact with 30 vol% SiC whiskers. Both materials were not ball milled.

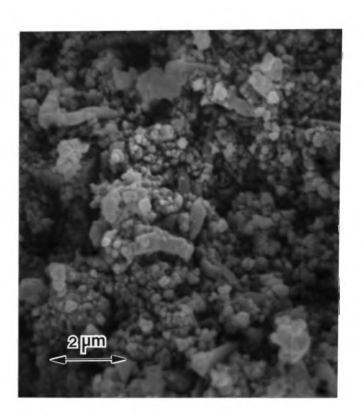


Figure 3.15 (cont'd)

(b) SEM micrograph of ${\rm Si_3N_4}$ composite green compact with 30 vol% SiC whiskers. Both materials were ball milled.

3.3.3 Effects of Ultrasonication and Ball Milling on SiC_{(w}/Si₃N₄ System

The micrograph of a diluted SiC whisker suspension (Figure 3.16) showed that SiC whisker agglomerates were broken down after only a few minutes of ultrasonication while the aspect ratio of the whiskers were maintained since there was no ball milling. The SiC whisker agglomerates are assumed to be softer than the Si_3N_4 agglomerates since they look like loose "nets" which may not represent bonding so much as physical entanglement, while the Si_3N_4 particles are joined by van der Waals forces or in some cases, reaction bonded, due to high temperature calcination used in the preparation of the α - Si_3N_4 powder [93].

Therefore, when Si₃N₄/SiC_(w) suspensions were created, SiC whiskers were added to the suspension after the Si₃N₄ was ball milled, followed by 20 minutes of ultrasonication to the mixed suspensions before slip casting as shown in the flow diagram of Figure 3.17. The results, shown in Figure 3.18 indicated that this method, combining ball milling and ultrasonication was effective in increasing green density.

3.3.4 Effect of Whisker Loading on Green Density

As noted by other researchers [49], green density decreases as whisker loading exceeds 30 $^{\text{V}}$ /_o because whisker "nets" form, which reduce particle packing efficiency. For SiC_(w)/Si₃N₄ suspensions prepared in this study, this expected decrease in density at >30 $^{\text{V}}$ /_o was observed for samples which were only ultrasonicated (Figure 3.18). However, when ball milling was combined with ultrasonication, the predicted density decrease at



Figure 3.16 SEM micrograph of diluted SiC whisker suspension.

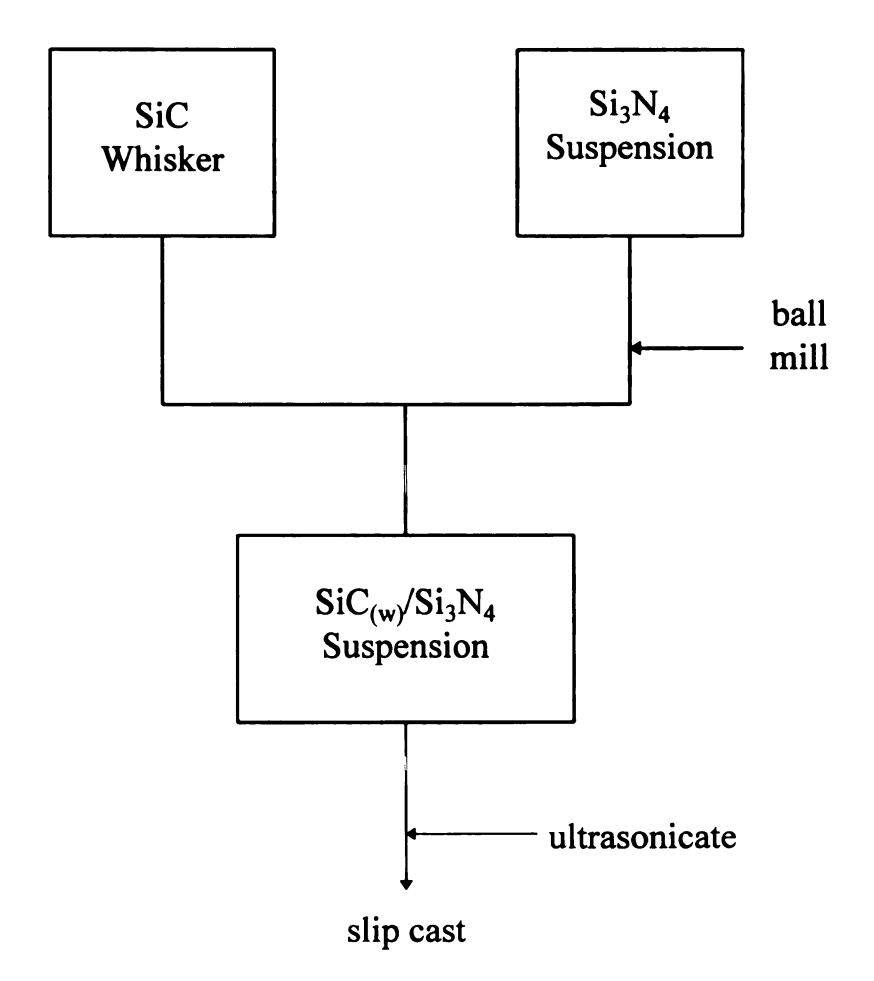


Figure 3.17 Flow chart of the method combining ball milling and ultrasonication.

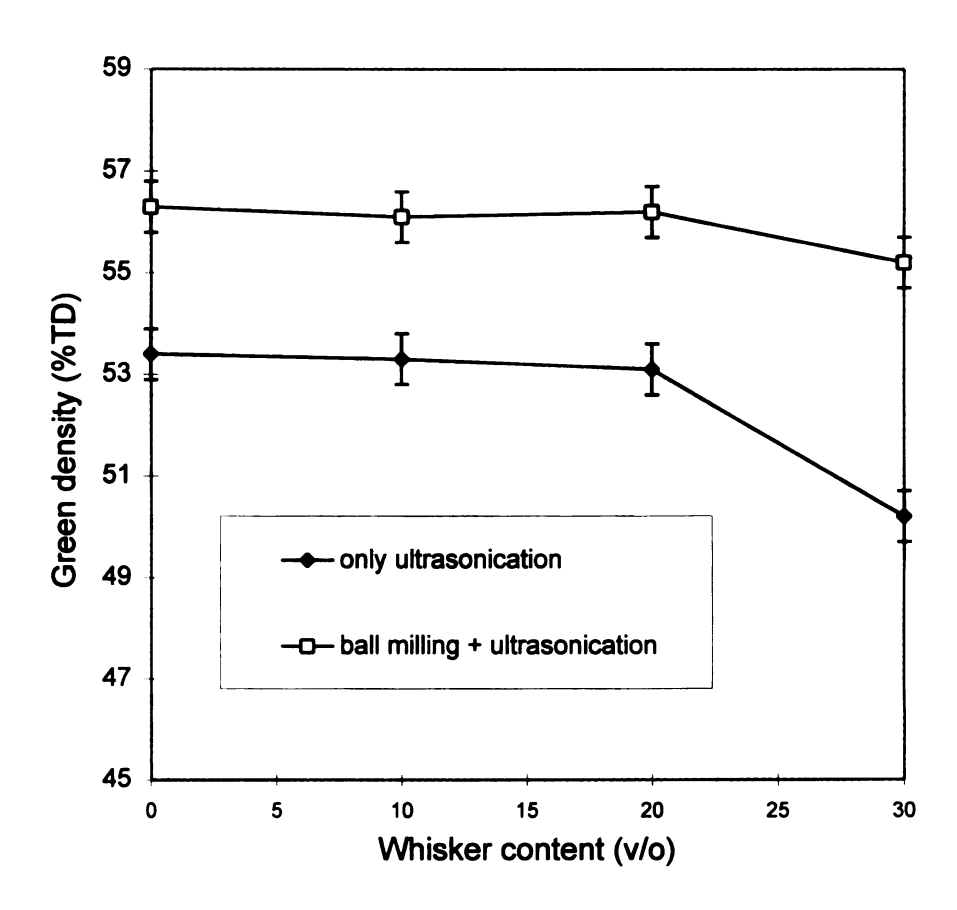


Figure 3.18 Slip cast green density as a function of whisker loading.

 $30^{\text{v}}/_{\text{o}}$ was not observed. Because agglomerates were kept out of the whisker nets in non-ball-milled suspensions, while fine Si_3N_4 particles in the agglomerate-free suspensions which are very small compared to the size of voids in whiskers nets could somehow fill in. This resulted in a reduction of the whisker "nets" effect in those specimens fabricated by the proposed method.

3.3.5 Effect of Reducing Whisker Aspect Ratio

Reduction of the whisker aspect ratio will play an important role in increasing green density and sintered density. The aspect ratio of the ball-milled whiskers were significantly reduced from ~25 to ~15, which is still relatively high, as shown in Figure 3.19 (a) and (b). The addition of whiskers to a green compact actually has two side effects on the green density. (1) It increases the green density because the fully dense whiskers replace certain amounts of powder in the green bodies. (2) It decreases the green density since more voids will be introduced by "whisker nets". In Figure 3.20, the reduction of the whisker aspect ratio resulted in improvements on the slip cast green density compared to the non-ball-milled whiskers especially when the whisker loading was high. It should be noticed that the densities of 20 vol% whisker samples were higher than that of 10 vol% whisker samples because of the contribution of factor (1), whereas factor (2) is still not significant at 20 vol% level. The effect of the whisker aspect ratio on the sintered density and mechanical properties will be discussed later.

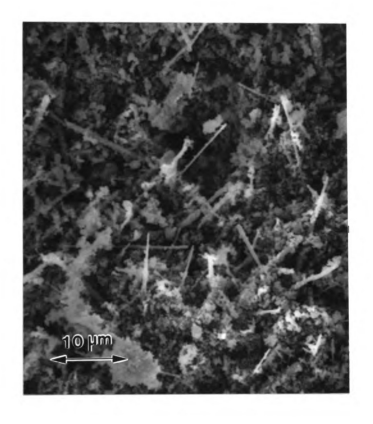


Figure 3.19 (a) SEM micrograph of $\mathrm{Si}_3\mathrm{N}_4$ composite green compact with 30 vol% SiC whisker. Both materials were prepared without ball milling.

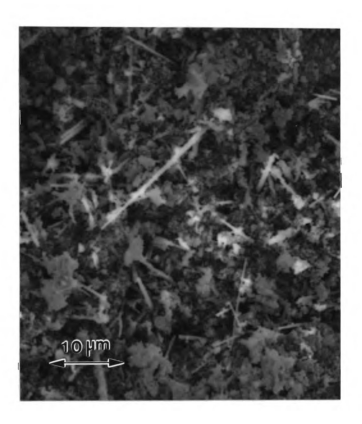


Figure 3.19 (cont'd)

(b) SEM micrograph of Si₃N₄ composite green compact with 30 vol% SiC whisker. Both materials were ball milled.

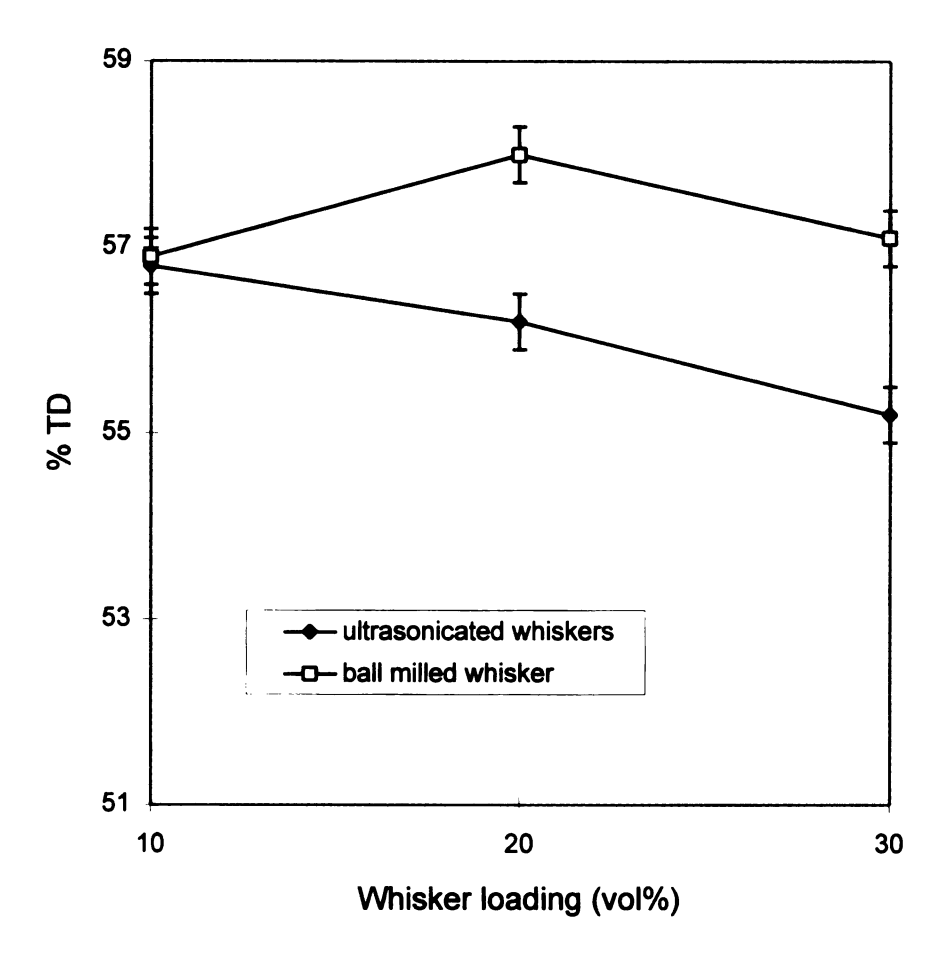


Figure 3.20 Effect of ball milling SiC whiskers on slip cast green density.

3.4 Sintering Additives

Y₂O₃ and Al₂O₃ have been widely used as sintering additives in the manufacturing of Si₃N₄ ceramics. Commercial Si₃N₄ powders contain oxygen as an impurity, present as SiO₂ on the Si₃N₄ powder particles. Additions of Y₂O₃ and Al₂O₃ will react with the SiO_2 to form a glassy grain boundary phase which promotes densification and the α - to β -Si₃N₄ transformation. It has been stated that there is no significant error if the formation of the grain boundary phase in the sintering of Si₃N₄ is estimated from the Y₂O₃-Al₂O₃-SiO₂ phase diagram [94]. It was reported by Weaver and Lucek [95] that 8 wt% would be the optimized Y₂O₃ content. Small amounts of Al₂O₃ are used to lower the eutectic temperature and 8Y2A was finally chosen as the composition of the additives. SN-E10 powder initially contains 1.2 wt% oxygen with 0.3 wt% oxygen introduced during the fabrication process [84]. 1.5 wt% oxygen corresponds to ≈2.8 wt% SiO₂. Therefore, the glass forming point can be shown as in the Y₂O₃-Al₂O₃-SiO₂ phase diagram [94] in Figure 3.21. The glassy phase will be formed when the temperature is above 1600°C. Choosing the composition in the lower temperature region will improve sinterability, but at the cost of high temperature properties, which are important for Si₃N₄ ceramics.

3.5 Sintered Density

The effect of ball milling Si_3N_4 on the sintered density is not clearly shown (Figure 3.22) in monolithic Si_3N_4 samples, since the monolithic Si_3N_4 already reached nearly full density without ball milling. But the effect can be seen on the 10 vol% whisker samples where deagglomeration by ball milling Si_3N_4 increased the density from 2.65 g/cm³ to

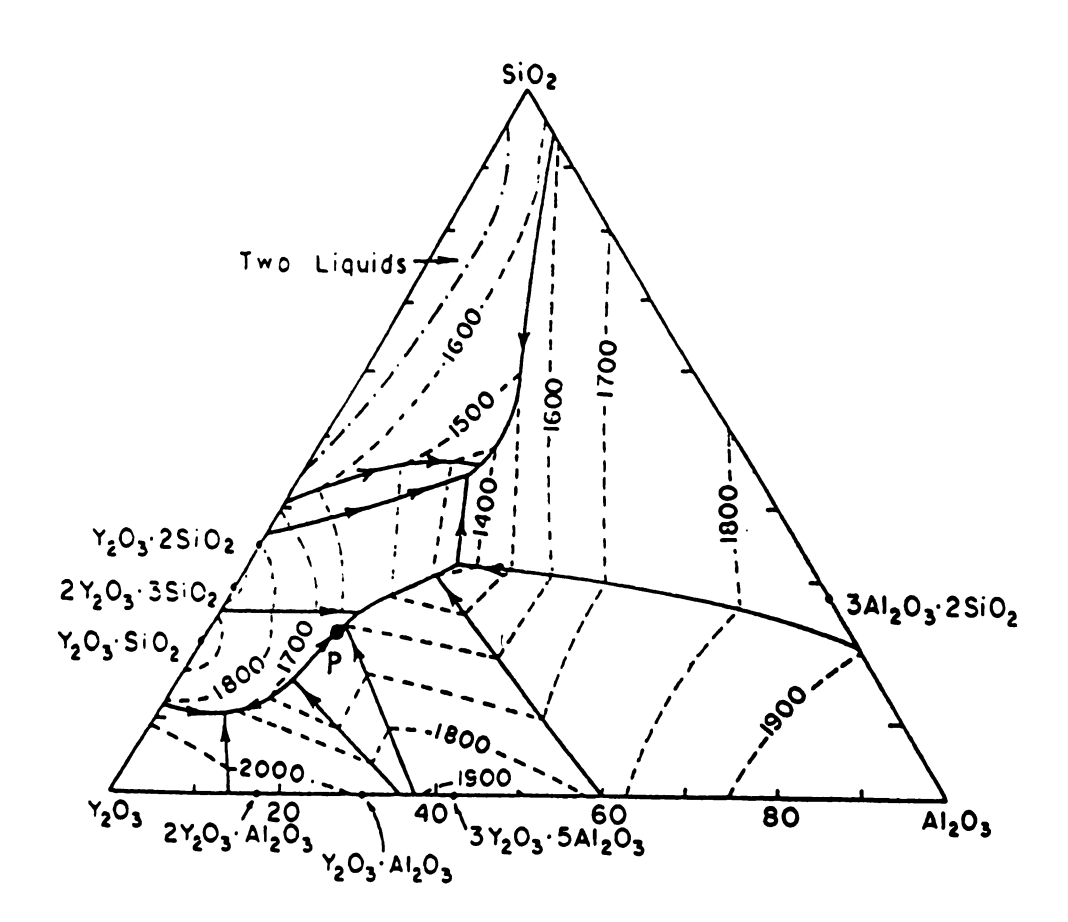


Figure 3.21 Al₂O₃-Y₂O₃-SiO₂ phase diagram (taken from [94]). *P* denotes the grain boundary phase composition.

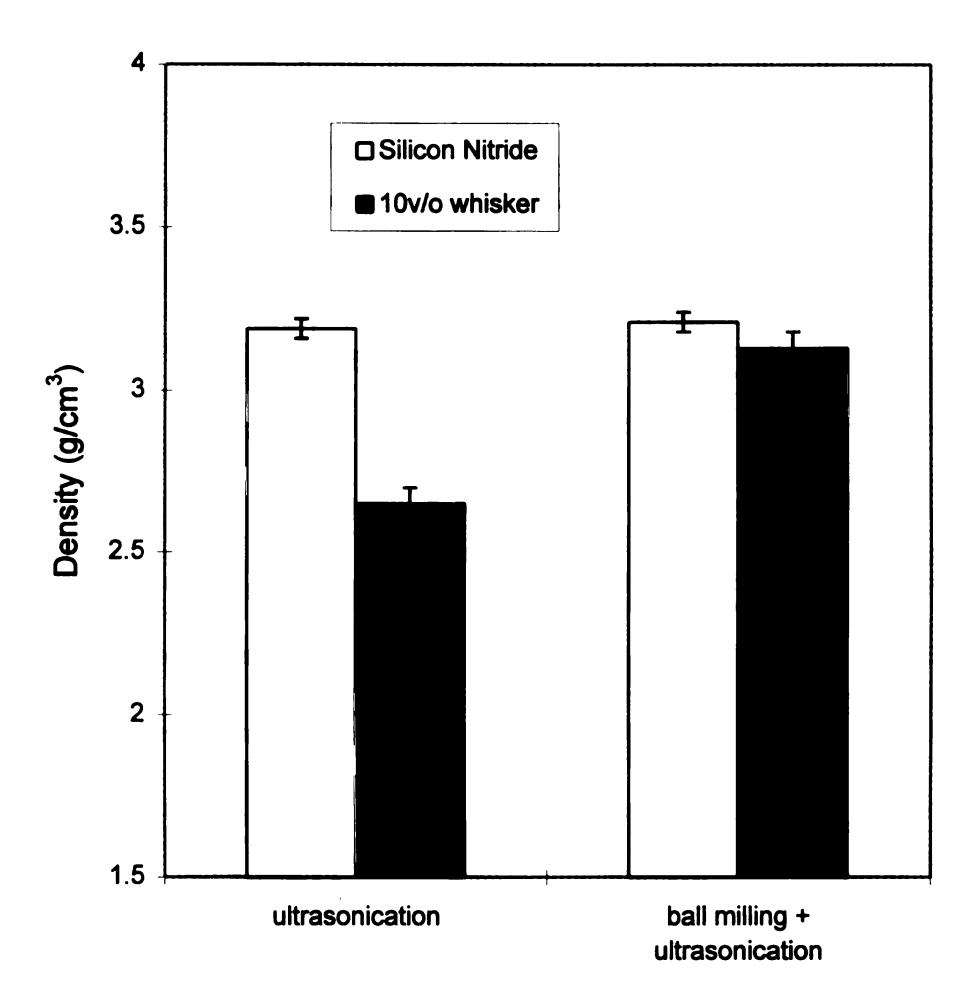


Figure 3.22 Effect of ball milling Si_3N_4 on the sintered density. Whiskers were added to the suspensions after ball milling.

3.13 g/cm³, corresponding to an increase from 80% to 95% of theoretical density.

Samples sintered at 1800°C had higher densities than those sintered at 1750°C. 4 hours of sintering produced samples having higher densities than samples sintered for 2 hours (Figure 3.23 and Figure 3.24).

The addition of SiC whiskers inhibits densification, as can be seen in both Figure 3.23 and Figure 3.24 where the density decreases while the content of SiC whisker increases. As Lange [52] proposed in his constrained network model for predicting densification behavior of composite powders, transient stresses will be developed during sintering when one region of the powder compact, in our case, SiC whisker, shrinks differently from its surroundings. As the Si₃N₄ matrix shrinks, a SiC whisker generates a shear stress in the matrix and tensile hoop stresses at the particle-matrix interface. Until this shear stress can be relaxed by shear flow in the matrix or by viscous flow of the liquid phase, the hoop stress will act to inhibit sintering and to reduce densification. Further more, the shrinkage of the fine powder matrix causes the SiC whiskers to touch, preventing the shrinkage of the composite powder compacts. The sinterability of the composites also decreases with the aspect ratio of the whiskers [96]. When non-ballmilled whiskers were used as in Figure 3.23, the density dropped when whisker content reached 20 vol%. But in Figure 3.24, the sharp drop in density happened only when the whisker content reached 30 vol%, because the whisker aspect ratio was reduced by ball milling.

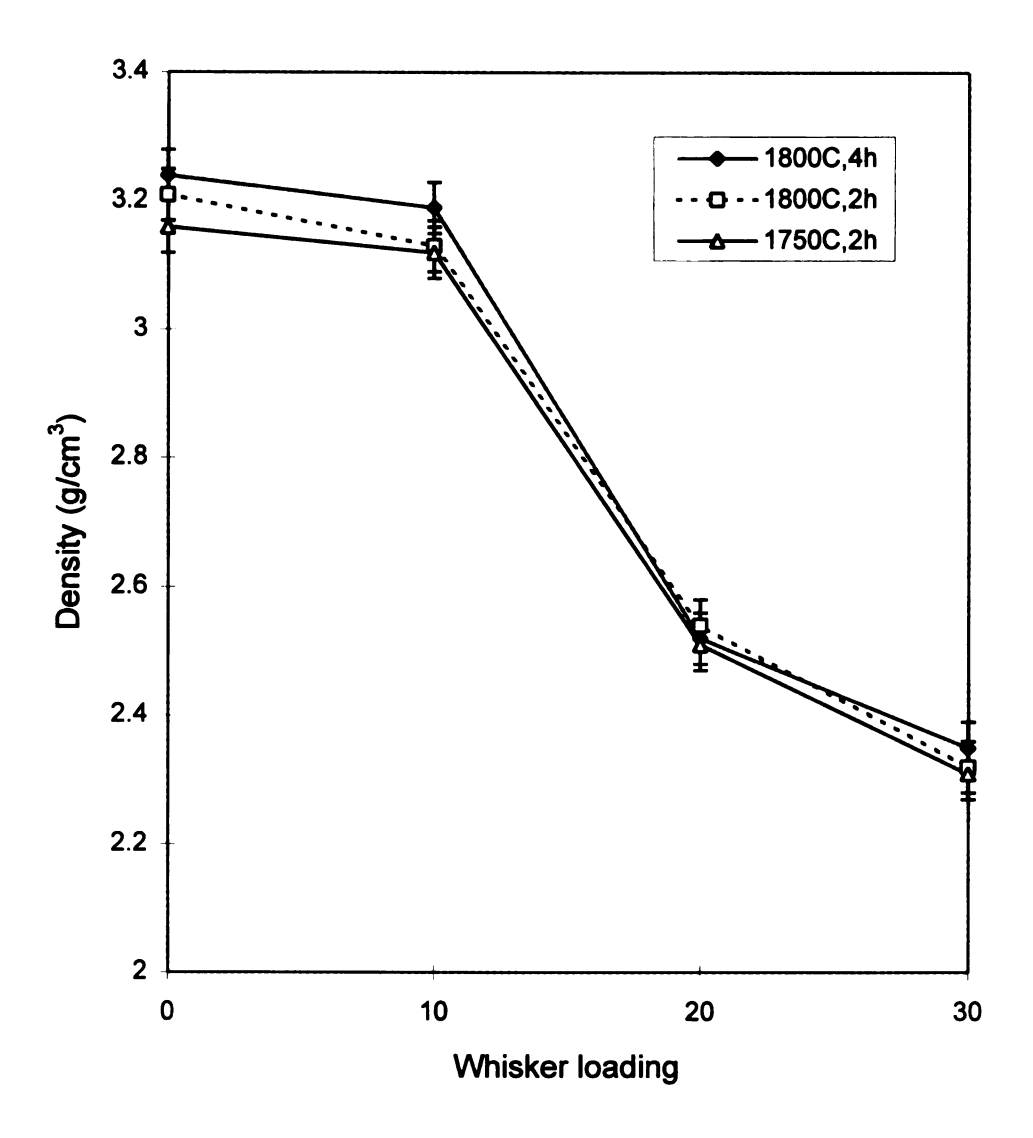


Figure 3.23 Sintered density as a function of SiC whisker loading. Whiskers were only ultrasonicated.

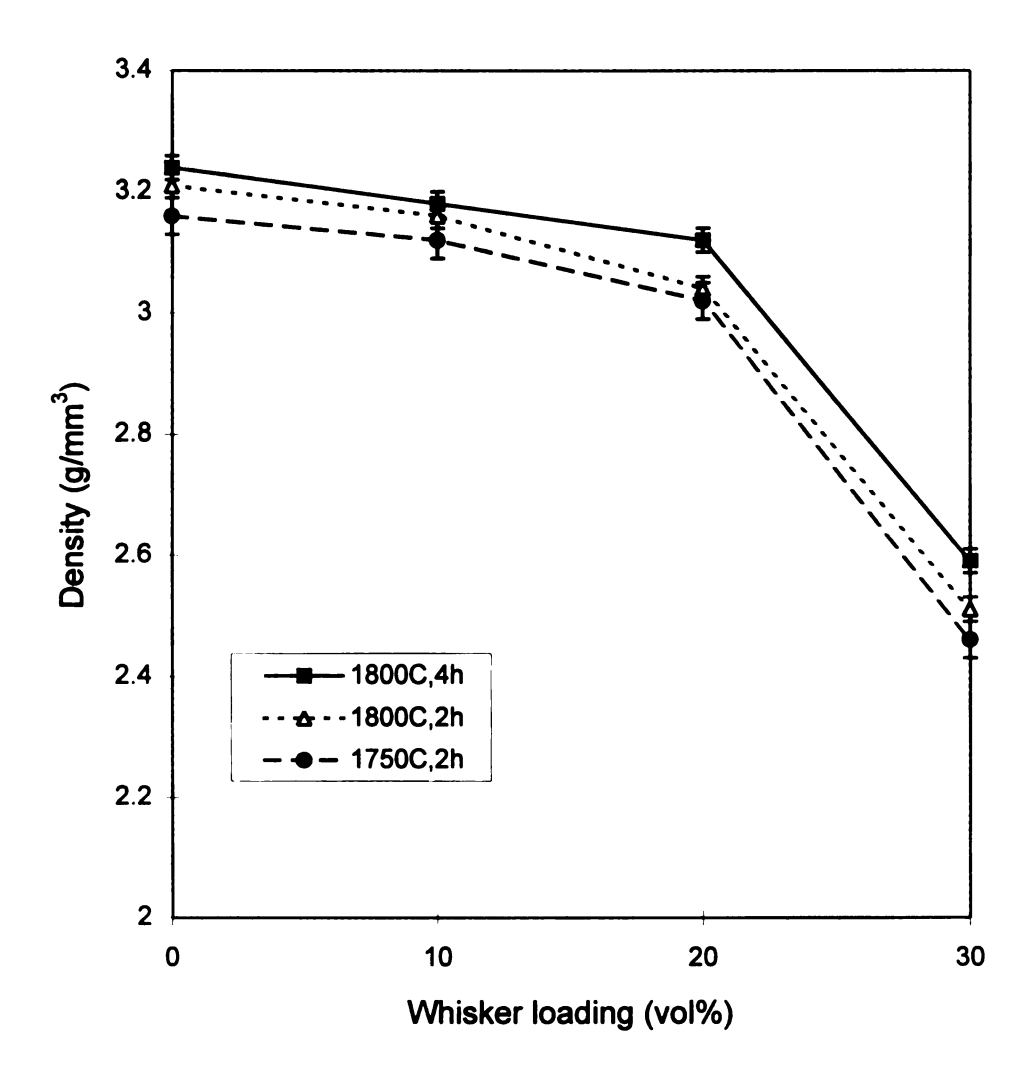


Figure 3.24 Sintered density as a function of whisker loading. Whiskers were ball milled.

3.6 Microstructure of the Composites

The microstructure of the $SiC_{(w)}/Si_3N_4$ composites is characterized by acicular β - Si_3N_4 grains, SiC whiskers and grain boundary phases. SiC whiskers are hard to distinguish from β -Si₃N₄ grains since there are no obvious differences between their diameters and aspect ratios. But they do exist in the sintered products and are still β -type. This will be verified later by the X-ray diffraction data, in which β -SiC peaks are sharp and no peak broadening was observed. β -grains, which usually have a hexagonal cross-section (Figure 3.25) are formed by a solution-diffusion-reprecipitation mechanism and have a narrow size-distribution since large grains are rarely observed.

The ultrasonication and ball milling of the Si_3N_4 suspensions seemed to have had no effect on the final microstructure (Figure 3.25 (a) (b) (c)), as they only broke the agglomerates, and did not change the particle size in the green compacts. Samples sintered at 1750° C and 1800° C have the same microstructure as shown in Figure 3.26 and Figure 3.28 (a), which suggestes that the α -to- β transformation can be completed at both sintering temperatures. But the sintered densities are slightly higher at 1800° C (Figure 3.23 and Figure 3.24) because at higher temperatures the glassy phases have a lower viscosity, which improves the redistribution of liquid phases during sintering. Increase of the sintering time from 2 hours to 4 hours resulted in little increase in density (Figure 3.23 and Figure 3.24), but there was no obvious change on the final grain size (Figure 3.27 and Figure 3.25 (a)). This suggestes that the α -to- β transformation is completed, a small rearrangement of β -grain is still possible.

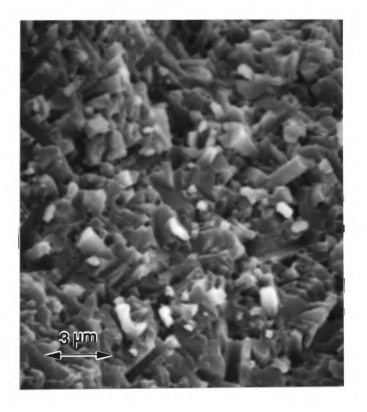


Figure 3.25 (a) Fracture surface of monolithic ${\rm Si_3N_4}.$ Ultrasonicated only. Sintered at 1800°C for 2 hours.

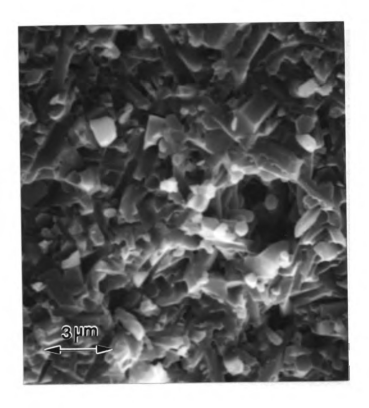


Figure 3.25 (cont'd)

(b) Fracture surface of monolithic Si₃N₄. Ball milled only. Sintered at 1800°C for 2 hours.

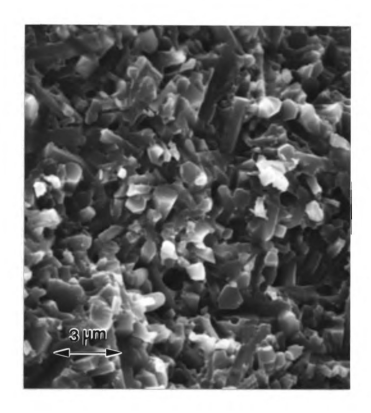


Figure 3.25 (cont'd)

(c) Fracture surface of monolithic Si₃N₄. Ultrasonicated and ball milled. Sintered at 1800°C for 2 hours.

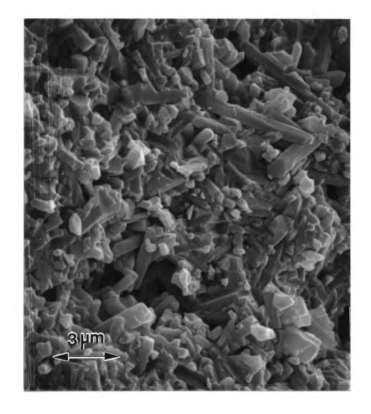
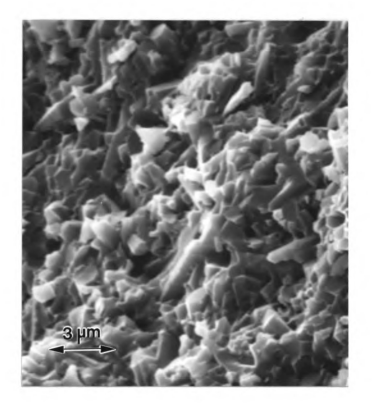


Figure 3.26 Fracture surface of Si₃N₄ composite with 10 vol% non-ball-milled SiC whiskers. Sintered at 1750°C for 2 hours.



 $\begin{tabular}{ll} \textbf{Figure 3.27} & Fracture surface of monolithic Si_3N_4. Ultrasonicated only. \\ & Sintered at 1800°C for 4 hours. \\ \end{tabular}$

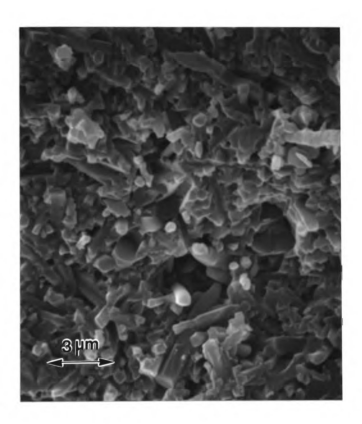


Figure 3.28 (a) Fracture surface of ${\rm Si}_3N_4$ composite with 10 vol% non-ball-milled SiC whiskers. Sintered at 1800°C for 2 hours.

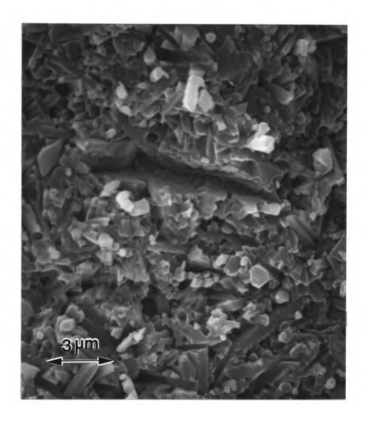
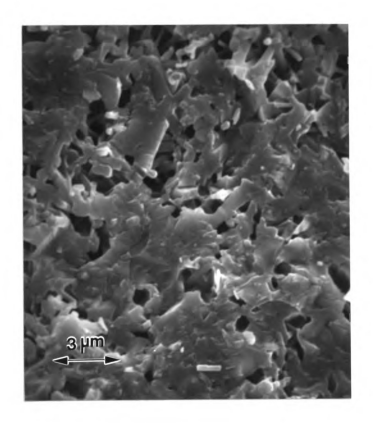


Figure 3.28 (cont'd)

(b) Fracture surface of ${\rm Si_3N_4}$ composite with 10 vol% ball-milled SiC whiskers. Sintered at $1800^{\circ}{\rm C}$ for 2 hours.

The addition of SiC whiskers to monolithic Si₃N₄ inhibits grain growth. This can be seen by comparing the fracture surface of monolithic Si₃N₄ and 10 vol% whisker composites in Figure 3.25 (c) and Figure 3.28 (a), the composites have a smaller average grain size than the monolithic products. The addition of SiC whiskers also inhibits the redistribution of glassy phase. 20 vol% of non-ball-milled SiC whiskers resulted in a microstructure (Figure 3.29 (a)) characterized by glass-enriched regions and voids, which correspond to only 77% of theoretical density. The ball-milling of whiskers did not change the microstructure when whisker loading was 10 vol% as shown in Figure 3.28 (a) and (b). 20 vol\% whisker composites can still be sintered to 95\% of theoretical density and have a similar microstructure (Figure 3.29 (b)) as that of 10 vol% samples. The porous and glass-enriched type microstructure (Figure 3.30 (b)) occurred when whisker loading reached 30 vol%. Ideally, SiC whisker should be easy to find on a fracture surface of a 30 vol% whisker sample. This was not true as seen in Figure 3.30 (a) and (b), which suggestes that most of the SiC whiskers were enwrapped in glassy phases, preventing the movement of liquid and resulting in large amount of voids left between whiskers.

The composition of the grain boundary phases also plays an important role in the development of β -Si₃N₄. Figure 3.31 showed that an additive composition of 4Y2A resulted in a smaller grain than that of 8Y2A (Figure 3.25 (a)), which would change the mechanical properties of the final products.



 $\begin{tabular}{ll} Figure~3.29~(a) Fracture surface of Si_3N_4 composite with 20 vol\% non-ball-milled SiC whiskers. Sintered at 1800°C for 2 hours. \\ \end{tabular}$

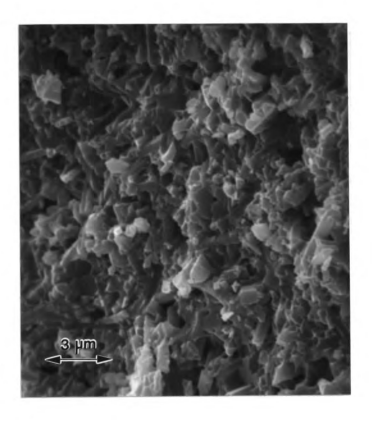


Figure 3.29 (cont'd)

(b) Fracture surface of Si₃N₄ composite with 20 vol% ball-milled SiC whiskers. Sintered at 1800°C for 2 hours.

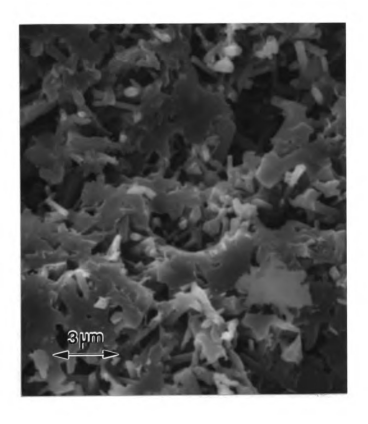


Figure 3.30 (a) Fracture surface of ${\rm Si_3N_4}$ composite with 30 vol% non-ball-milled SiC whiskers. Sintered at 1800°C for 2 hours.

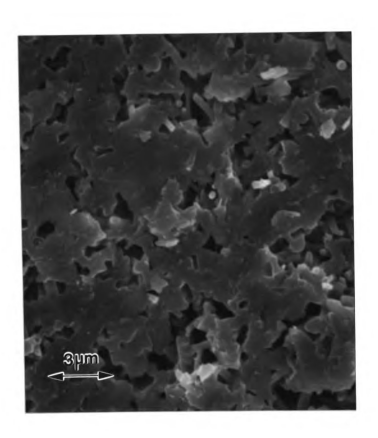


Figure 3.30 (cont'd)

(b) Fracture surface of Si₃N₄ composite with 10 vol% ball-milled SiC whiskers. Sintered at 1800°C for 2 hours.

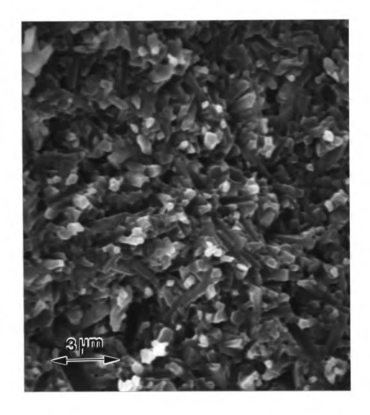


Figure 3.31 Fracture surface of monolithic Si₃N₄ having 4Y2A additive. Sintered at 1800°C for 2 hours.

Crack-like voids were found in composites (Figure 3.32) but not found in monolithic products. Lange [52] proposed that when tensile stresses develop in the matrix during sintering of composites, disruptive processes, e.g. the development of crack-like voids, may occur to relieve the stresses and allow the matrix to densify.

3.7 Mechanical Properties of SiC_(w)/Si₃N₄ composites

Monolithic Si_3N_4 has a relatively high fracture toughness of around 7~8 MPa·m^{1/2} (Figure 3.33) due to the high fracture energy caused by the formation of elongated β -grains, which produce a rough fracture surface (Figure 3.25) with a higher specific area than that of an equiaxed microstructure. The existence of the grain boundary phase is considered to be one of the important factors for improving the fracture toughness, because it leads to the situation in which cracks propagate along a grain boundary and $SiC_{(w)}/Si_3N_4$ interfaces in the composites. The toughening mechanism by crack deflection, branching and bridging may be induced if the grain boundary phases have suitable strengths.

The deagglomeration processes were very helpful in increasing density, but did not change the grain morphology and therefore have little effect on the fracture toughness of the matrix as shown in Figure 3.33. But the addition of whiskers will affect the mechanical properties of the composites.

Figure 3.34 shows that the addition of 10 vol% non-ball-milled whiskers increased the fracture toughness, but 20 vol% whiskers resulted in a sharp drop in toughness. This can

Figure 3.32 Crack like void was observed in fracture surface of $Si_3N_4/SiC_{(w)}$ composite.

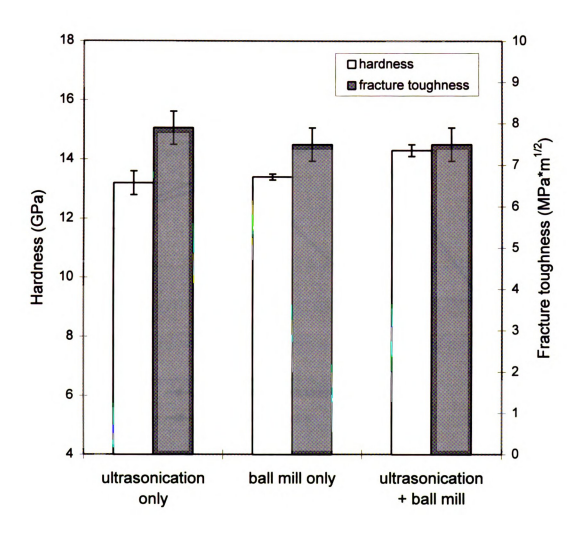


Figure 3.33 The effect of ultrasonication and ball milling on the mechanical properties of monolithic Si₃N₄. Sintered at 1800°C for 2 hours.

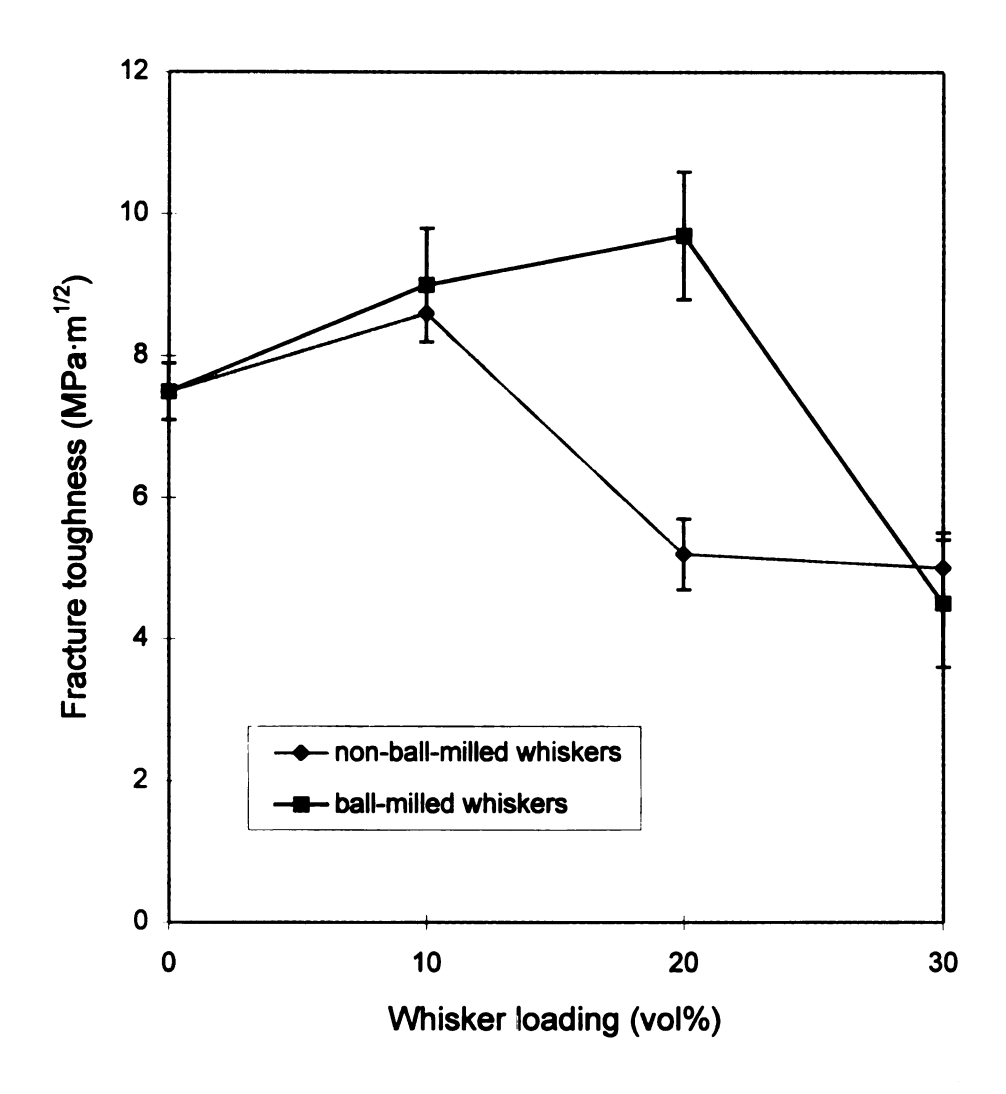


Figure 3.34 Fracture toughness as a function of whisker loading. Sintered at 1800°C, 2 hours.

be seen in the microstructure of this material which was characterized with voids and glass-enriched regions (Figure 3.29 (a)). Ball-milled whiskers continuously increased the fracture toughness of the composites until the whisker content reached 30 vol%. The materials with the highest fracture toughness of ~10 MPa·m^{1/2} was found to have 20 vol% ball-milled whisker reinforcement. The addition of whiskers, regardless of whether ball-milled or not, decreased the hardness of the composites as shown in Figure 3.35 because of the increase in porosity.

Becher and Hoffmann et al. [74] reported that the fracture toughness of Si₃N₄ ceramics having elongated grain structures increases with increases in grain diameter. The addition of whiskers inhibits not only the densification, but also the grain growth, as discussed previously. It suggests that the toughness of the matrix is not constant and decreases with the amount of whiskers. Therefore, the increase in fracture toughness in composites must be attributed to the presence of whiskers. Both SiC whiskers and β-Si₃N₄ have elongated shapes and high aspect ratios, the differences between their contributions to fracture toughness are probably (1) a compressive residual stress produced in the radial direction on the whiskers caused by differences in the thermal expansion coefficients between SiC and Si₃N₄, and (2) the surface roughness of SiC whiskers increased the pull-out resistance. Based on the HREM observation by Lee and Hiraga [97] that SiC whiskers having internal defects such as twins and stacking faults, which are similar to our case (Figure 3.4a), have rough surfaces resulting in the increase of interfacial bonding by the increase of contact area.

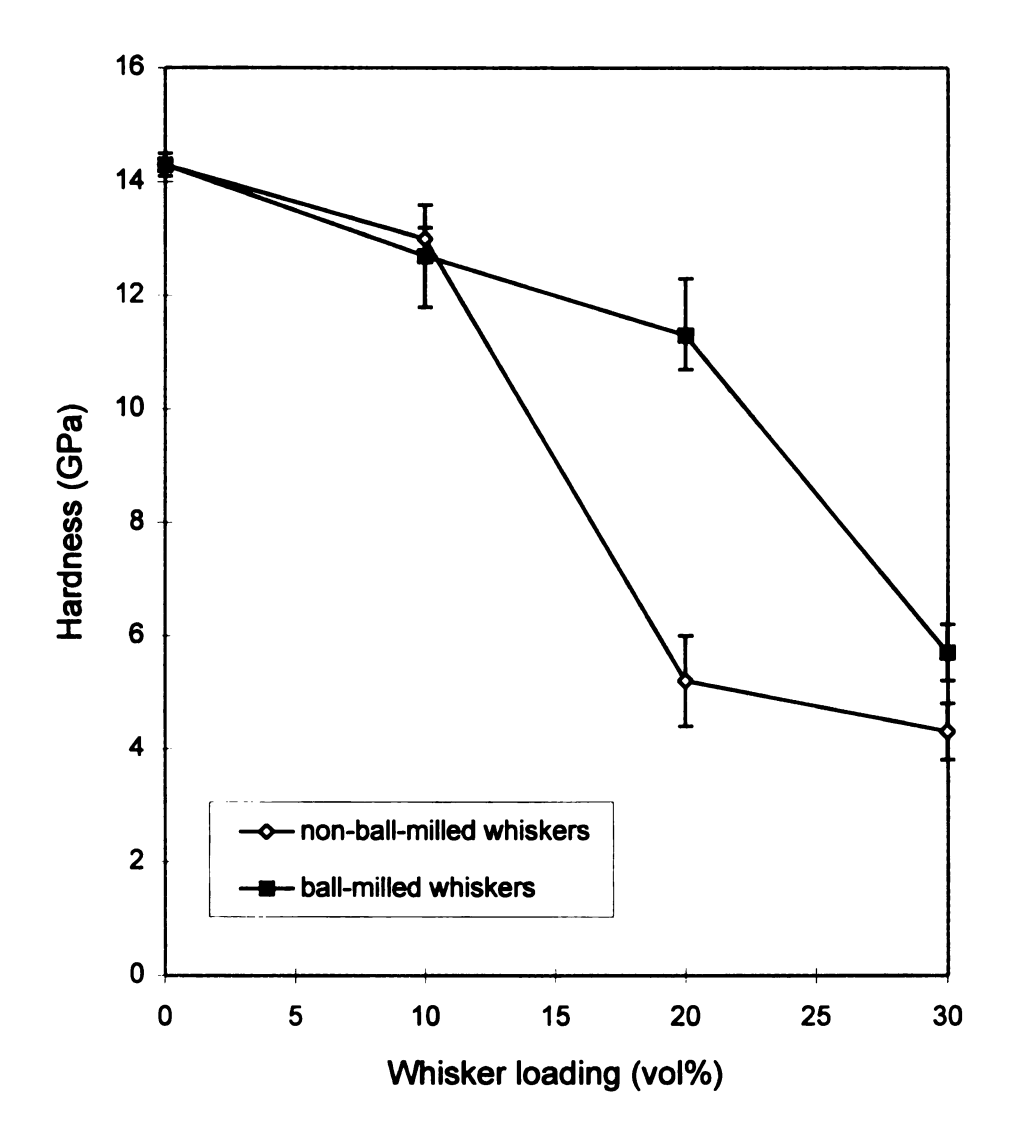


Figure 3.35 Hardness as a function of whisker loading. Sintered at 1800°C, 2 hours.

Sintering temperature and time did not have a significant effect on the mechanical properties of the composites as shown in Figure 3.36 and Figure 3.37. Sintering at 1800°C increased the fracture toughness slightly compared with sintering at 1750°C, which might be due to the possible increase in grain size.

3.8 X-ray Diffraction Analysis

The diffraction patterns of SiC whiskers and Si_3N_4 starting powder are shown in Figure 3.38 and Figure 3.39, respectively. SiC is β -type and has the FCC structure. Si_3N_4 powder is α -type, but has a small amount of β -grains.

In monolithic Si_3N_4 and 10 vol% whisker composites, the α - β transformation is completed, since there is no β peak found in the diffraction patterns shown in Figure 3.40 and Figure 3.41. For 20 vol% whisker composites, the whisker aspect ratio influenced the transformation. In ball-milled whisker samples (Figure 3.42), the transformation was completed while there was still 30 mol% α left in the non-ball-milled whisker samples (Figure 3.43). Similarly, 39 mol% and 32 mol% α remained in the 30 vol% non-ball-milled whisker (Figure 3.44) and ball-milled whisker samples (Figure 3.45), respectively. These samples with residual α all correspond to low sintered densities and porous microstructure. It suggested that some α particles did not have a liquid phase surrounding them and could not complete the solution-precipitation process, because glassy phases were "held" by SiC whiskers and could not be distributed homogeneously through out the sample.

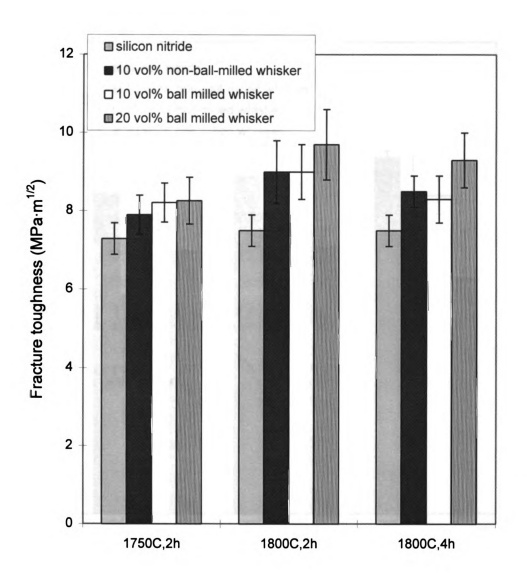


Figure 3.36 The effect of sintering temperature and time on the fracture toughness of composites.

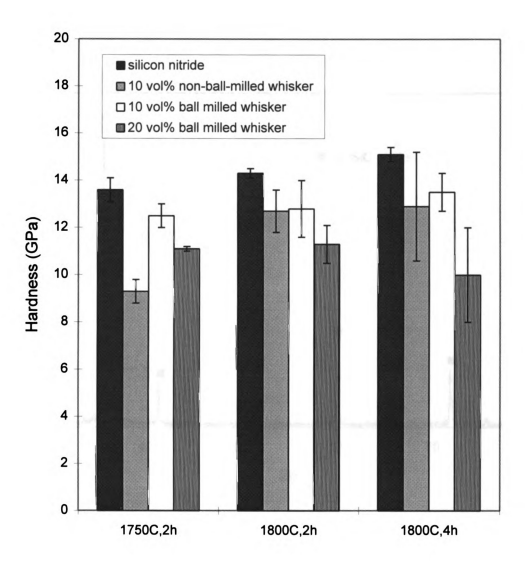


Figure 3.37 The effect of sintering temperature and time on the hardness of composites.

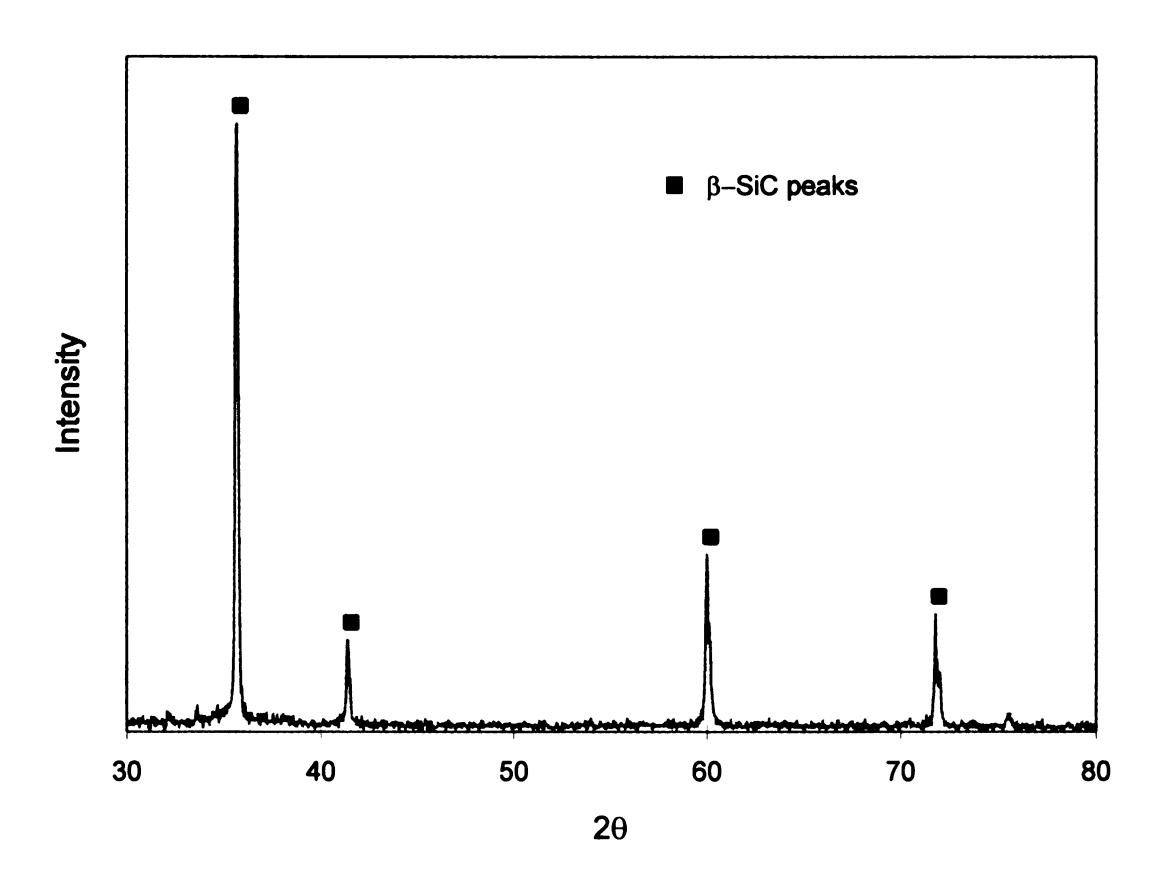


Figure 3.38 Diffraction pattern of SiC whiskers.

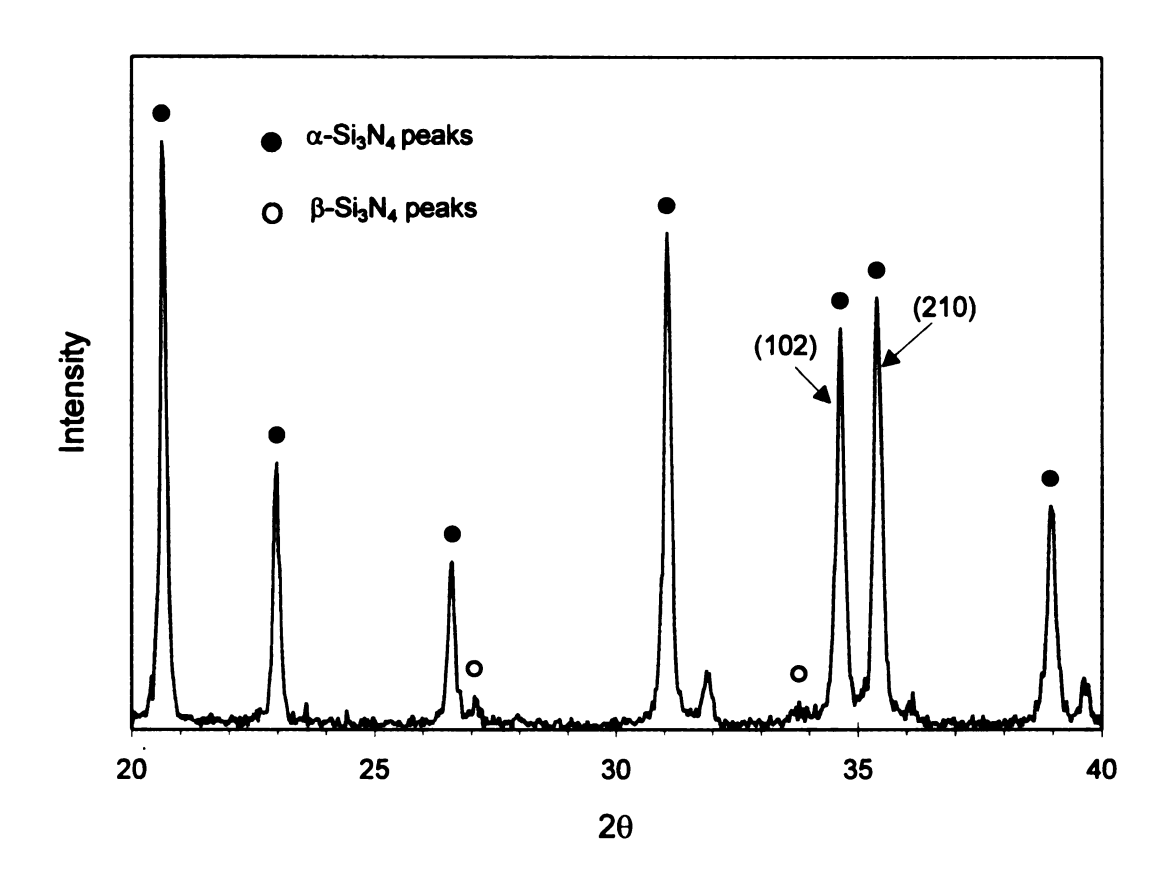


Figure 3.39 Diffraction pattern of silicon nitride starting powder.

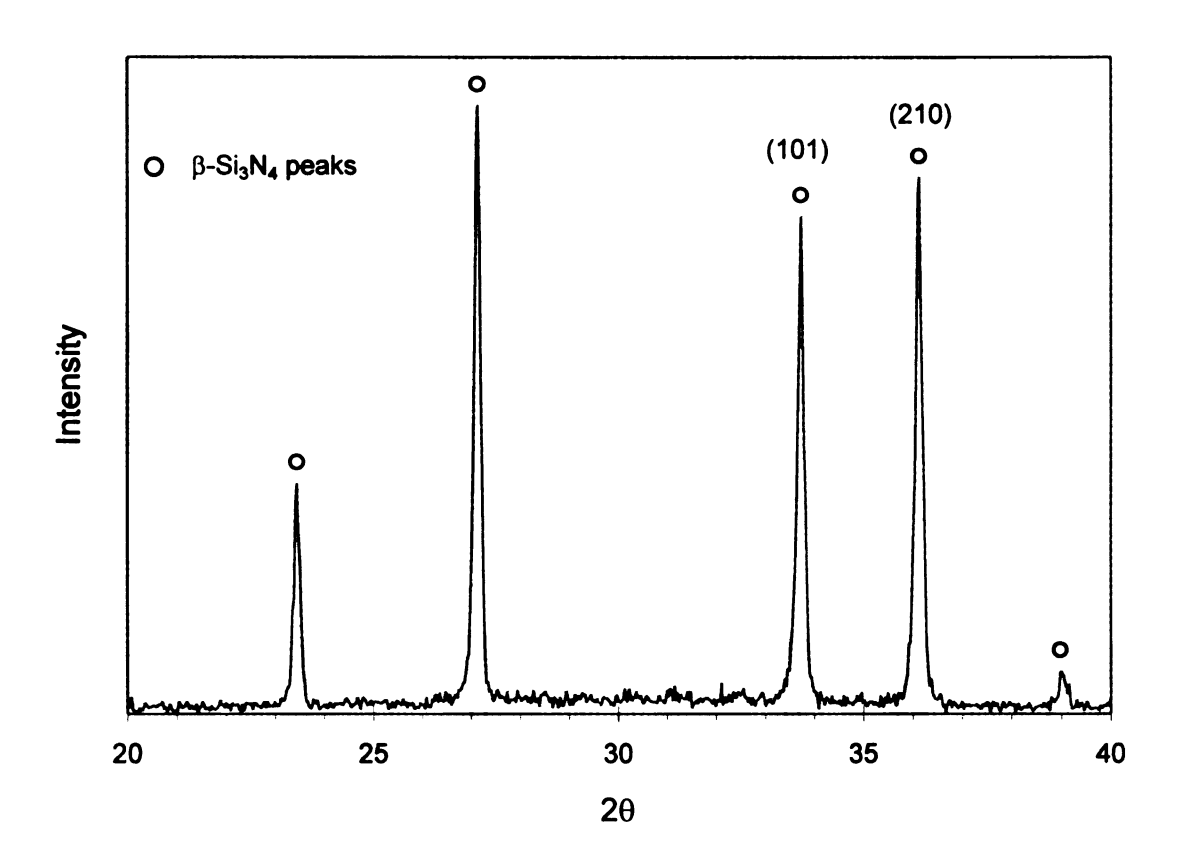


Figure 3.40 Diffraction pattern of monolithic silicon nitride ceramic.

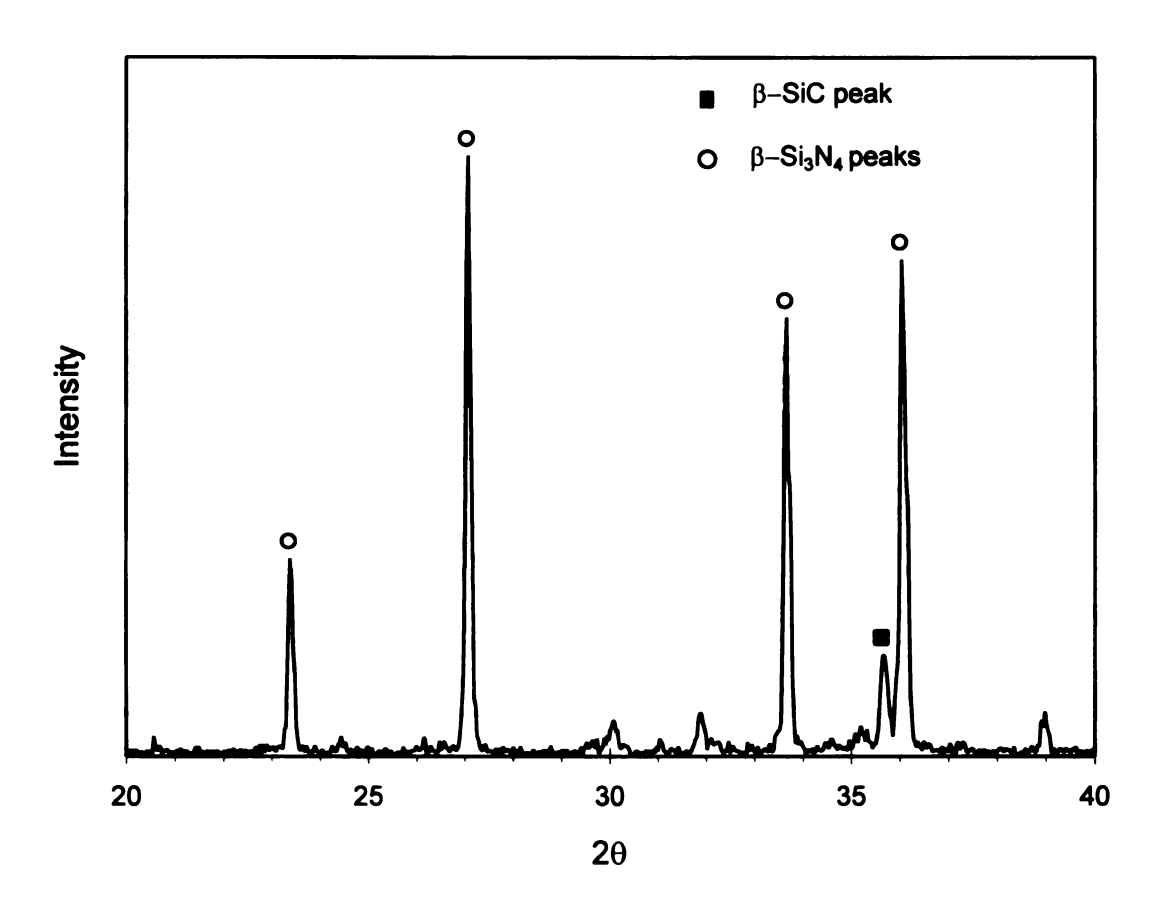


Figure 3.41 Diffraction pattern of silicon nitride composite with 10 vol% ball-milled SiC whiskers.

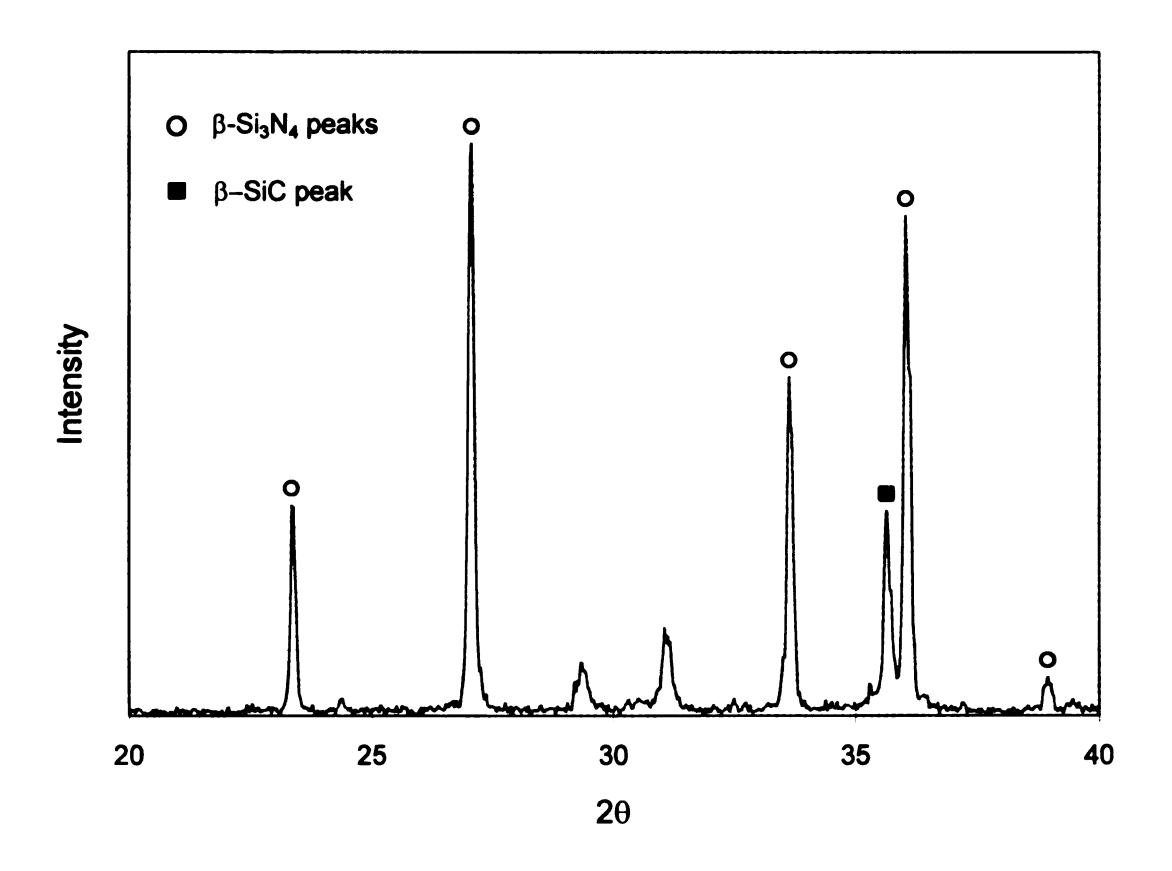


Figure 3.42 Diffraction pattern of silicon nitride composite with 20 vol% ball-milled whiskers.

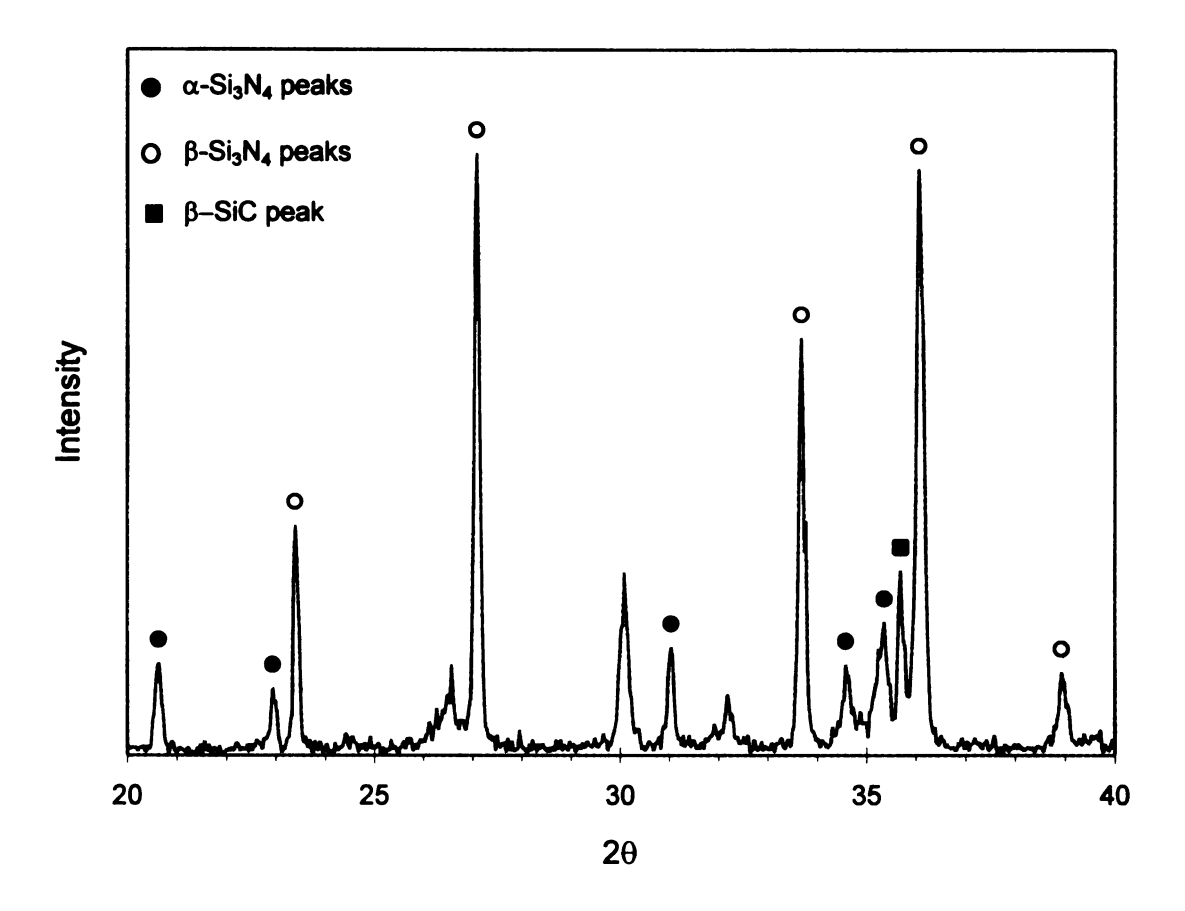


Figure 3.43 Diffraction pattern of silicon nitride composite with 20 vol% non-ball-milled SiC whiskers.

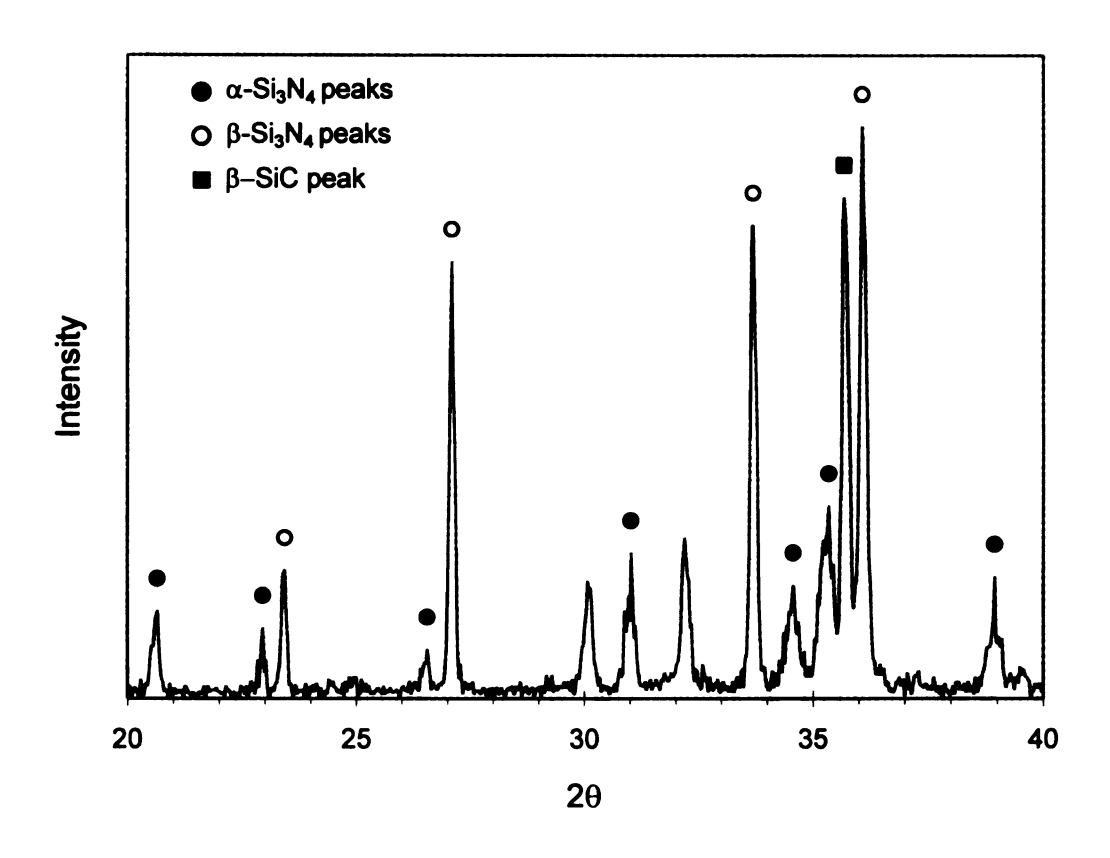


Figure 3.44 Diffraction pattern of silicon nitride composite with 30 vol% non-ball-milled SiC whiskers.

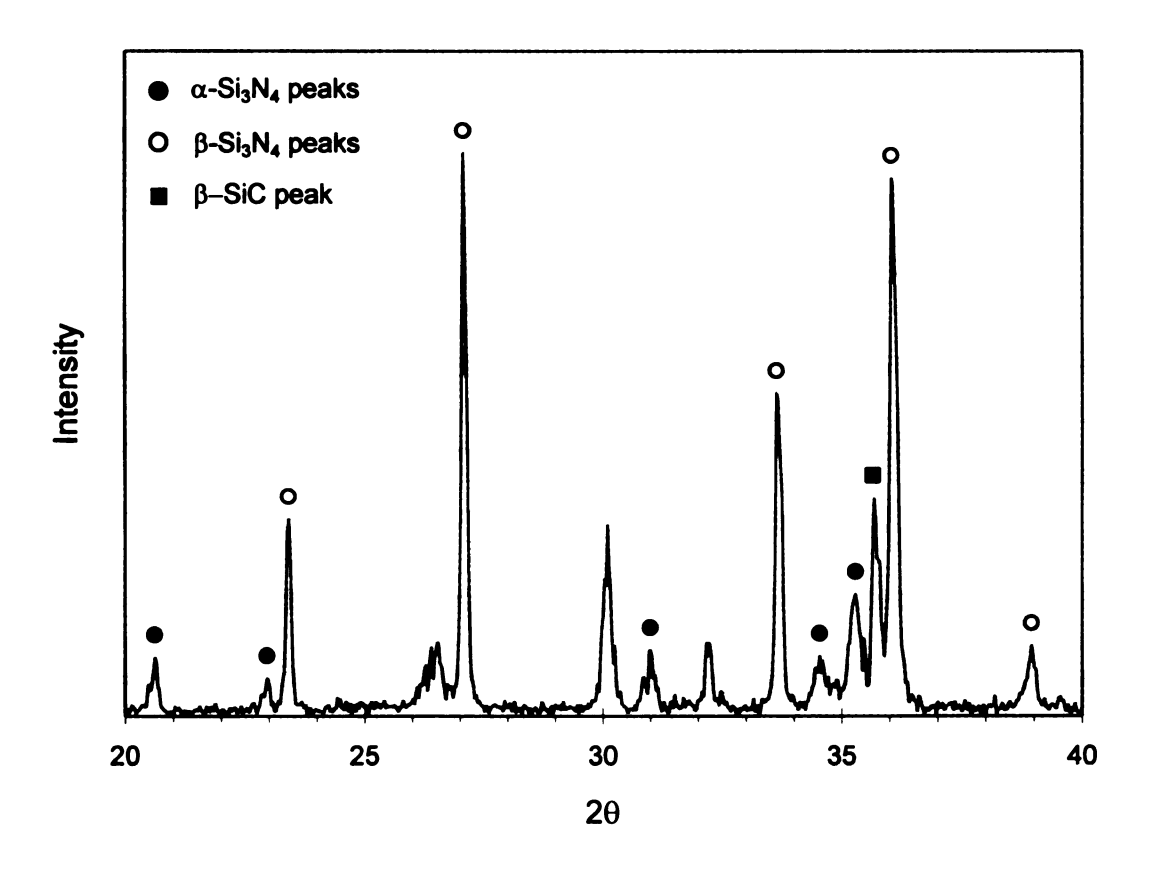


Figure 3.45 Diffraction pattern of silicon nitride composite with 30 vol% ball-milled whiskers.

4. CONCLUSIONS

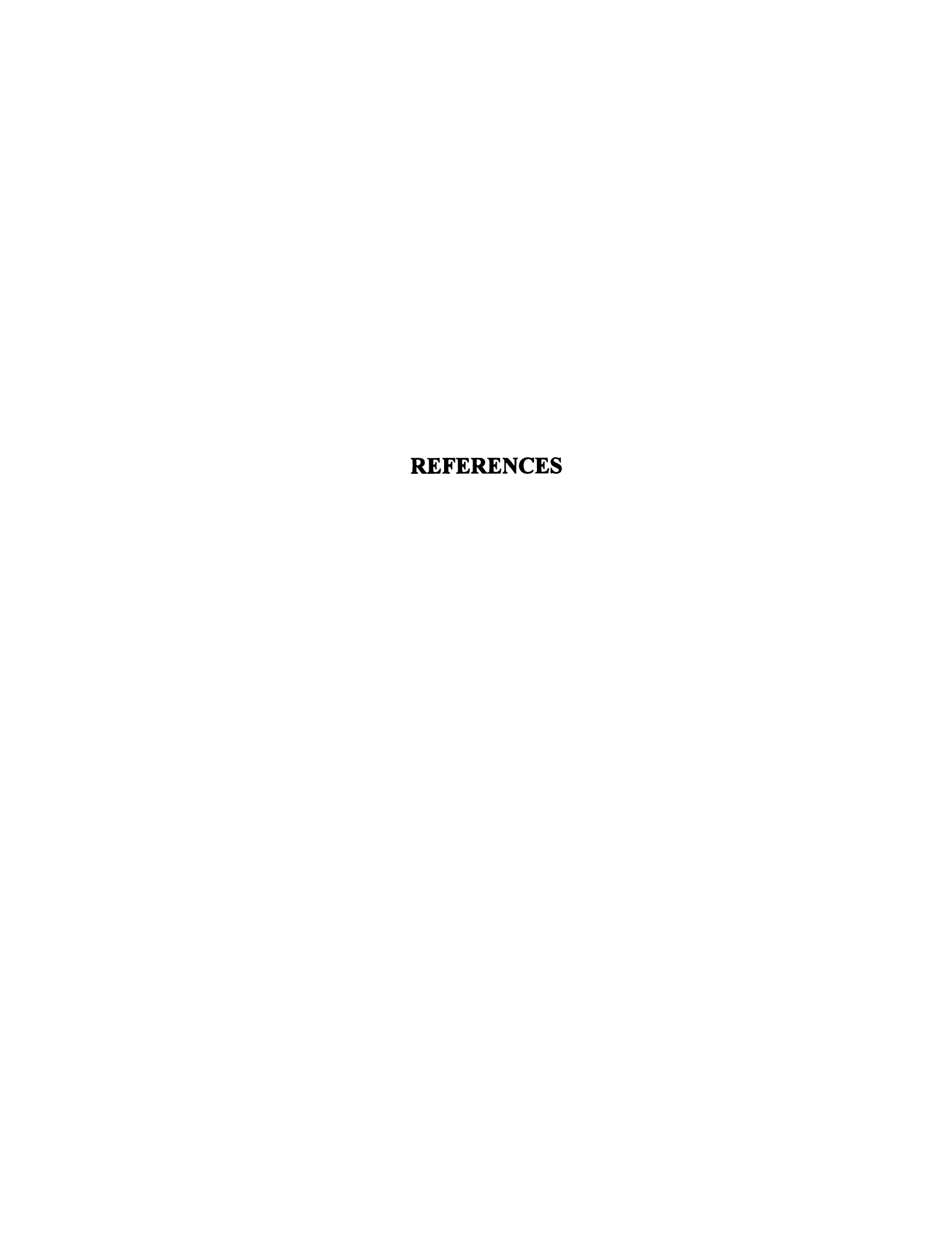
The computer program Suspension Stability® was effective in predicting optimum suspension conditions for colloidal processing of ceramic composites. For SiC_(w)/Si₃N₄ composites system, the predicted pH value of 11 was suitable for slip casting and reduced the extent of agglomeration, providing a good suspension environment for further deagglomeration processes.

Both ultrasonication and ball milling are useful methods for deagglomeration. Soft agglomerates like SiC whisker agglomerates can be broken-up by ultrasonication while hard Si_3N_4 agglomerates can not. Therefore, more attention should be paid to the deagglomeration of Si_3N_4 powders in $Si_3N_4/SiC_{(w)}$ systems than that of the SiC whiskers. A combination of ball milling and ultrasonication is recommended to achieve nearly agglomerate-free, ceramic suspensions. This method also reduces whisker "nets" effect when whisker loading exceeds 30 $^{\rm v}/_{\rm o}$. Deagglomeration processes do not affect the microstructure and mechanical properties of composites directly, they improve the properties of composites by providing an agglomerate-free matrix.

The ball milling of SiC whiskers reduces, but still maintains a relatively high whisker aspect ratio. The ball milling of the SiC whiskers increased the packing efficiency in green compacts and enhanced the sinterability of the composites, and thus allowed more whiskers to be added to composites. Although addition of whiskers in composites

inhibited grain and glassy phase redistribution, small amounts of whiskers still increase the fracture toughness of the composites. The highest fracture toughness value of ~ 10 MPa·m $^{1/2}$ was found in 20 vol% ball-milled-whisker composites. Higher volume fraction of whiskers in composites resulted in porous microstructure with glass-enriched regions.

The microstructure of composites is characterized by elongated grains of β -Si₃N₄ and SiC whiskers and glassy phases. For low whisker content composites, all α -Si₃N₄ was transformed into the β , while there was still large amount of residual α in the sintered products when whisker content was high.



REFERENCES

- [1] T. W. Chou, R. L. McCullough and R. B. Pipes, Scientific American, 254 (1986) 193.
- [2] M. J. Hoffmann and G. Petzow, <u>Silicon Nitride Ceramics</u>, <u>Scientific and Technological Advances</u>, MRS Proceedings, **287** (1993).
- [3] F. F. Lange, J. Am. Ceram. Soc. 72 (1989) 3.
- [4] L. M. Sheppard, Am. Ceram. Soc. Bull., 68 (1989) 979.
- [5] R. J. Hunter, Foundations of Colloid Science, Volume 1, Clarendon Press, Oxford, 1987.
- [6] A.L. Smith, "Electrical Phenomena Associated With The Solid-Liquid Interface," <u>Dispersion of Powders in Liquids</u>, G. D. Parfitt ed., Elsevier Publishing Company Limited, London (1969).
- [7] Duncan J. Shaw, <u>Introduction to Colloid and Surface Chemistry</u>, third edition, Butterworth Inc., Boston (1980).
- [8] G. Gouy, J. Phys. Chem., 9 (1910) 457.
- [9] D.L. Chapman, *Phil. Mag.*, **25** (1913) 475.
- [10] O. Stern, Z. Elektrochem., 30 (1924) 508.
- [11] Deryagin, B. V. and Landau, L., Acta Phys. Chim. URSS, 14 633 (1941).
- [12] Verwey, E. J. W. and Overbeek, J. Th. G., <u>Theory of the Stability of Lyophobic Colloids</u>, Elsevier (1948).
- [13] Hamaker, H. C., Physica, 4 (1937) 1058.
- [14] D. Tabor, <u>Colloidal Dispersions</u>, The Royal Society of Chemistry, London, 1981.
- [15] A. Bleier, J. Am. Ceram. Soc., 66 (1983) C79.

- [16] B. V. Derjaguin, Kolloid-Z., 69 (1934) 155.
- [17] B. V. Derjaguin, Acta physicochim., 10 (1939) 333.
- [18] G. R. Wiese, and T. W. Healy, Trans. Faraday Soc., 66 (1970) 490.
- [19] J. Lyklema, Colloid and Interface Science Volume 1, Academic Press, New York, 1976, pp257.
- [20] N. Z. Fuchs, Physik, 89 (1934) 736.
- [21] R. Hogg, T. W. Healy, and D. W. Fuerstenau, *Trans. Faraday Soc.*, 62 (1966) 1638.
- [22] B. A. Wilson and M. J. Crimp, Langmuir, 9 [11] (1993) 2836.
- [23] R. K. McGeary, J. Am. Ceram. Soc., 44 [10] (1961) 513.
- [24] F. F. Lange, J. Am. Ceram. Soc., 67 [2] (1984) 83.
- [25] D. W. Johnson, D. J. Nitti, and L. Barrin, Am. Ceram. Soc. Bull., 51 [12] (1972) 896.
- [26] K. A. Kusters, S. E. Pratsinis, S. G. Thomas and D. M. Smith, *Chemical Engineering Science*, 48 [24] (1993) 4119.
- [27] S. Dutta, Key Engineering Materials, **56-57** (1991) 99.
- [28] F. Rossignol, P. Goursat and J. L. Besson, *Journal of the European Ceramic Society*, 13 [4] (1994) 299.
- [29] T. Fukasawa, Y. Goto and A. Tsuge, Journal of the Ceramic Society of Japan, Int. Edition, 101 (1993) 607.
- [30] S. Koh, D. Kim and C. Kim, J. Mater. Sci. Lett. 12 (1993) 237.
- [31] G. C. Wei and P. F. Becher, Amer. Ceram. Soc. Bull. 64 (1985) 298.
- [32] S. T. Buljan, J. G. Baldoni and M. L. Hukabee, Amer. Ceram. Soc. Bull. 66 (1987) 347.
- [33] P. D. Shaleck, J. J. Petrovic, G. F. Hurley and F. D. Gac, ibid. 65 (1986) 351.
- [34] R. Lundberg, L. Kahlman, R. Pompe, R. Carlsson and R. Warren, *ibid*. **66** (1987) 330.

- [35] M. Rühle, B. J. Dalgleish, and A. G. Evans, Scr. Metall., 21 [5] (1987) 681.
- [36] P. F. Becher and G. C. Wei, J. Am. Ceram. Soc., 67 [12] (1984) C-267--C-279.
- [37] P. Becher, C. H. Hsueh, P. Angelini, and T. N. Tiegs, *Mater. Sci. Eng.*, A107 (1989) 257.
- [38] K. T. Faber and A. G. Evans, Acta Metall., 31 [4] (1983) 565.
- [39] P. Angelini and P. F. Becher, in <u>Proceedings of the Electron Microscopy Society of America</u>. Edited by G. W. Bailey, San Francisco Press, San Francisco, CA, (1987) pp148.
- [40] G.H. Campbell, M. Rühle, B.J. Dalgleish and A.G. Evans, J. Am. Ceram. Soc., 73 [3] (1989) 461.
- [41] T. N. Tiegs and P. F. Becher, ibid 66 (1987) 339.
- [42] G. Pezzotti, and I. Tanaka, and T. Okamoto, J. Am. Ceram. Soc., 73, (1990) 3033.
- [43] G. Pezzotti, I. Tanaka, T. Okamoto, M. Koizumi, and Y. Miyamoto, J. Am. Ceram. Soc., 72 [8] (1990) 521.
- [44] Brook, R. J., Materials Science and Engineering, 71 (1985) 305.
- [45] T. Yonezawa, S. Saito, M. Minamizawa and T. Matsuda, in "New Materials and Processes for the Future", Edited by N. Igata, I. Kimara, T. Kishi, E. Nakata, A. Okura and T. Uryu (The Nikkan Kogyo Shimbun, Japan, 1989) pp.1131.
- [46] C. Olagnon, E. Bullock, Journal of the European Ceramic Society, 7 (1991) 265.
- [47] M. Mitomo, S. Saito, T. Matsuda and T. Yonezawa, J. Mater. Sci., 28 (1993) 5548.
- [48] J. V. Milewski, Advanced Ceramic Materials, 1 [1] (1986) 36.
- [49] J. XinXiang and R. Taylor, British Ceramic Transactions, 93 [1] (1994) 11.
- [50] T. N. Tiegs and D. M. Dillard, J. Am. Ceram. Soc., 73 [5] (1990) 1440.
- [51] P. D. Shalek, J. J. Petrovic, G. F. Hurley, and F. D. Gac, Am. Ceram. Soc. Bull., 65 [2] (1986) 351.
- [52] F. F. Lange, J. Mater. Res., 2 [1] (1987) 59.
- [53] G. W. Scherer, J. Am. Ceram. Soc., 70 [10] (1987) 719.

- [54] R. K. Bordia and R. Raj, J. Am. Ceram. Soc. Commun., 69 [3] (1986) C55-C57.
- [55] M. R. Freedman, J. D. Kiser, and W. A. Sanders, <u>NASA Techical Memorandum</u>, n101336 (1988) pp18.
- [56] E. Yasuda, T. Akatsu and Y. Tanabe, Journal of the Ceramic Society of Japan, Int. Edition, 99 (1991) 51.
- [57] T. Matsui, O. Komura and M. Miyake, Journal of the Ceramic Society of Japan, Int. Edition, 99 (1991) 1063.
- [58] P. F. Becher, C.-H. Hsueh, P. Angelini and T. N. Tiegs, *J. Am. Ceram. Soc.*, 71 (1990) 521.
- [59] F. F. Lange, J. Am. Ceram. Soc., 62 (1979) 428.
- [60] K. Matsuhiro and T. Takashashi, Ceram. Eng. Sci. Proc., 10 (1989) 807.
- [61] D. Hardie and K. H. Jack, *Nature*, **180** (1957) 332.
- [62] S. Wild, P. Grieveson and K. H. Jack, Special Ceram. 5 (1972) 385.
- [63] K. R. Lai and T. Y. Tien, J. Am. Ceram. Soc., 76 (1993) 91.
- [64] G. Ziegler, J. Heinrich and G. Wötting, J. Mater. Sci. 22 (1987) 3041.
- [65] K. Kijima and S. Shirasaki, J. Chem. Phys. 65 (1976) 2668.
- [66] H. Wada, M. Wang, and T. Tien, J. Am. Ceram. Soc., 76 [10] (1988) 837.
- [67] F. L. Riley (ed.), Progress in Nitrogen Ceramics, Martinus Nijhoff, 1983.
- [68] G. Wötting and G. Ziegler, Ceramurg. Int. 10 (1984) 18.
- [69] W. D. Kingery, J. Appl. Phys. 30 (1959) 301.
- [70] L. J. Bowen, R. J. Weston, T. G. Carruthers and R. J. Brook, J. Mater. Sci., 13 (1978) 341.
- [71] P. Drew and M. H. Lewis, J. Mater. Sci., 9 (1974) 261.
- [72] O. Abe, J. Mater. Sci., 25 (1990) 4018.
- [73] C. D. Greskovich and C. O'Clair, Am. Ceram. Soc. Bull. 57 (1978) 1055.

- [74] P. F. Becher, H. T. Lin, S. L. Hwang, M. J. Hoffmann, I-W. Chen, in <u>Silicon Nitride Ceramics</u>, <u>Scientific and Technological Advances</u>, ed. I-W. Chen, P. F. Becher, M. Mitomo, G. Petzow and T-S, Yen, Pittsburgh, Mater. Res. Soc., 1993, pp147.
- [75] G. Wöetting, B. Kanka and G. Ziegler, Non-Oxide Technical and Engineering Ceramics, London/New York: Elsevier, 1986.
- [76] S. Hampshire, M. Leigh, V. J. Morrissey, M. J. Pomeroy and B. Saruhan, <u>Ceramic Materials and Components For Engines</u>, ed. V. Tennery, Westermille, Am. Ceram. Soc., 1989.
- [77] W. A. Sanders and D. M. Mieskowski, Ceram. Bull. 64 (1985) 304.
- [78] S. Hampshire, The Sintering of Nitrogen Ceramics, Lancashire, England: Parthenon, 1986.
- [79] A. J. Pyzil, D. F. Carroll, C. J. Hwang and A. R. Prunier, <u>Proc. 4th Int. Symp. Ceramic Materials and Composites for Engines</u>, ed. R. Carlsson, T. Johansson, L. Kahlman, London/New York: Elsevier, 1992.
- [80] M. Mitomo, S. Uenosono, J. Am. Ceram. Soc., 75 (1992) 103.
- [81] G. Wöetting, and G. Ziegler, Fortschrittsber. Dkg 1 (1985) 33.
- [82] D. C. Larsen and J. W. Adams, "Evaluation of Ceramics and Ceramic Composites for Turbine Engine Applications", <u>IIT-Research Institute</u>, <u>Semiannual Interim</u>
 <u>Technical report No. 13</u>, June 1983: Contract F 33615-82-C-5101.
- [83] T. Yamada, Y. Kanetsuki, K. Fueda, T. Takahashi, Y. Kohtoku and H. Asada, Key Engineering Materials, 89-91 (1994) 177.
- [84] K. Takatori, S. Wada and N. Kobayashi, Journal of Ceramic Society of Japan, Int. Edition, 101 (1991) 470.
- [85] J. C. Mittl, R. L. Tallman, P. V. Kelsey Jr. and J. G. Jolley, J. Non-Cryst. Solids, 71 (1985) 287.
- [86] I. Tanaka, G. Pezzotti, T. Okamoto and T. Miyamoto, J. Am. Ceram. Soc., 72 (1989) 1656.
- [87] J. P. Singh, K. C. Goretta, K. S. Kupperman, J. L. Routbourt and J. F. Rhodes, Adv. Ceram. Materials, 3 [4] (1988) 357.
- [88] S. K. Dutta, A. K. Mukhopadhyay, D. Chakrarboty, J. Am. Ceram. Soc., 71 [11] (1988) 942.

- [89] J. M. Desmarres, P. Goursat, J. L. Besson, P. Lespade and B. Capdepuy, *Journal of the European Ceramic Society* 7 (1991) 101.
- [90] P. C. Hiemenz, <u>Principles of Colloid and Surface Chemistry</u>, second edition, Marcel Dekker, New York, 1986, pp780.
- [91] S. G. Thoma, M. Ciftcioglu and D. M. Smith, Powder Technology, 68 (1991) 53.
- [92] M. Ciftcioglu, M. Akinc, and L. Burkhart, Am. Ceram. Soc. Bull., 65 [12] (1986) 1591.
- [93] Japanese Patent 1139881, Ube Industries, Ltd., Ube, Japan.
- [94] E. M. Levin, C. R. Robbins and H. F. McMurdie, <u>Phase Diagrams for Ceramists</u>, 1969. Edited by M. K. Reser. American Ceramic Society, Columbus, OH: Fig. 2586.
- [95] G. O. Weaver and J. W. Lucek, Am. Ceram. Soc. Bull., 57 [12] (1978) 1131.
- [96] E. A. Holm and M. J. Cima, J. Amer. Ceram. Soc. 72 (1989) 303.
- [97] B. Lee and K. Hiraga, Materials Transactions, JIM, 34 [10] (1993) 930.

MICHIGAN STATE UNIV. LIBRARIES
31293014051886